Aus der Medizinischen Klinik mit Schwerpunkt Rheumatologie und
Klinische Immunologie der
Medizinischen Fakultät Charité – Universitätsmedizin Berlin

DISSERTATION

Establishment and evaluation of a human three-dimensional *in vitro* model for the study of osteoarthritis

zur Erlangung des akademischen Grades
Doctor medicinae (Dr. med.)

vorgelegt der Medizinischen Fakultät
Charité – Universitätsmedizin Berlin

von

Marie-Christin Weber

aus Bitburg

Datum der Promotion: 04.06.2021

PREFACE

Partial results of this theses have been published in the following publications:

- Weber MC, Fischer L, Damerau A, Ponomarev I, Pfeiffenberger M, Gaber T, Gotschel S, Lang J, Roblitz S, Buttgereit F, Ehrig R, Lang A. Macroscale mesenchymal condensation to study cytokine-driven cellular and matrix-related changes during cartilage degradation. Biofabrication. 2020;12(4):045016.

- Weber M-C, Fischer L, Damerau A, Ponomarev I, Pfeiffenberger M, Gaber T, Götschel S, Lang J, Röblitz S, Buttgereit F, Ehrig R, Lang A. In vitro and in silico modeling of cellular and matrix-related changes during the early phase of osteoarthritis. bioRxiv. 2019:725317. (Preprint)

- Weber MC, Ponomarev I, Gaber T, Buttgereit F, Lang A. Simulating osteoarthritis in vitro with human scaffold-free 3D cartilage transplants. Osteoarthritis and Cartilage. 2018;26:S103. (Conference abstract)

TABLE OF CONTENTS

LIST OF TABLES

LIST OF FIGURES

ABBREVIATIONS

AB	Alcian blue
ACAN	Aggrecan
ACL	Anterior cruciate ligament
ACR	American College of Rheumatology
ADAMTS	A disintegrin and metalloproteinase with thrombospondin motifs
BLAST	Basic Local Alignment Search Tool
BCRT	Berlin Brandenburg Centre for Regenerative Therapies
BIH	Berlin Institute of Health
BSA	Bovine serum albumin
cDNA	Complementary DNA
COL1(2,10)A1	Collagen type I (II, X) alpha 1 chain
COX	Cyclooxygenase
Ct-value	Cycle threshold value
DAB	3,3′-Diaminobenzidin
DAMP	Damage-associated molecular pattern
DMEM	Dulbecco’s modified eagle’s medium
DNA	Deoxyribonucleic acid
ECM	Extracellular matrix
EDTA	Ethylenediaminetetraacetic acid
EF1A	Elongation factor 1 alpha 1
EULAR	European League Against Rheumatism
GAG	Glycosaminoglycan
HE	Hematoxylin Eosin
hMSC	Human mesenchymal stromal cell
HRP	Horseradish peroxidase
IGF	Insulin-like growth factor
IL	Interleukin
IL-1R	Interleukin-1 receptor
IL-1RA	Interleukin-1 receptor antagonist
IFN	Interferon
iPSC	Induced pluripotent stem cells
LIF	Leukemia inhibitory factor

MMP	Matrix metalloproteinase
MRI	Magnetic resonance imaging
mRNA	Messenger RNA
MSC	Mesenchymal stromal cell
NCBI	National Centre for Biotechnology Information
NF-κB	Nuclear factor-kappaB
NSAID	Nonsteroidal anti-inflammatory drug
ns	not significant
OA	Osteoarthritis
OARSI	Osteoarthritis Research Society International
PBMC	Peripheral blood mononuclear cell
PFA	Paraformaldehyde
PBS	Phosphate-buffered saline
PCM	Pericellular matrix
qPCR	Quantitative polymerase chain reaction
rh	recombinant human
RIN	RNA integrity number
RGB	Red Green Blue
RNA	Ribonucleic acid
ROI	Region of interest
SD	Standard deviation
SEM	Standard error of the mean
SFCC	Scaffold-free cartilage-like constructs
SYSADOA	Symptomatic slow-acting drugs in osteoarthritis
TGF	Transforming growth factor
TNF	Tumor necrosis factor
TNF-R	Tumor necrosis factor receptor
TLR	Toll-like receptor
VEGF	Vascular endothelial growth factor
3D	Three-dimensional

ABSTRACT

Introduction: Osteoarthritis (OA) is one of the predominant joint diseases worldwide, impacting the quality of life of a large percentage of patients and causing a high socioeconomic burden. OA is characterized by the degradation of articular cartilage and pathological changes in the whole joint, leading to pain and loss of joint function. To date, there is no clinically approved treatment option available that could modify the disease progression or even cure OA. As OA is a chronic disease developing over decades in humans, model systems such as *in vivo* animal models and *in vitro* cell culture models are needed in OA research to be able to investigate which pathophysiological changes lead to the osteoarthritis phenotype, and to evaluate potential diagnostic and therapeutic options. *In vitro* models have the advantage that they can be based on human cells and the number of animals used in experiments can be reduced.

Methods: In this thesis, a human three-dimensional *in vitro* model of OA was established and evaluated. The model system was based on scaffold-free tissue-engineered cartilage-like constructs (SFCCs) that only consisted of human mesenchymal stromal cells (hMSCs) and their extracellular matrix (ECM). Firstly, the SFCCs were cultured for three weeks under normal conditions in standard culture medium and samples taken weekly to show their cartilage-like phenotype. To simulate the pro-inflammatory environment of OA, SFCCs were cultured for three weeks in a medium substituted with Interleukin-1 beta (IL-1β) and Tumor necrosis factor alpha (TNFα), which are considered as the main pro-inflammatory cytokines in OA. Histology and histomorphometry were used to evaluate the microscopic structure and cell distribution, quantitative polymerase chain reaction was performed to analyze gene expression patterns of ECM molecules, cytokines and proteases, and immunohistochemistry and proteomics were used for protein expression analysis.

Results: The cartilage-like phenotype of the SFCCs has been demonstrated, including the expression of aggrecan and type II collagen as specific markers for hyaline cartilage. Pro-inflammatory stimulation with IL-1β and TNFα demonstrated an increase of pro-inflammatory cytokines and proteases, as well as histological changes and a decrease in cell count similar to cartilage degradation observed in osteoarthritic joints.

Conclusion: Using tissue-engineered cartilage-like constructs based on human cells as *in vitro* model systems for the study of OA could improve translation of research results into the human condition, yield a better understanding of OA pathophysiology and find new therapeutic options for OA.

ZUSAMMENFASSUNG

Einleitung: Arthrose ist eine der häufigsten Gelenkerkrankungen weltweit, beeinträchtigt die Lebensqualität einer hohen Anzahl an Patienten und ist mit hohen sozioökonomischen Kosten verbunden. Arthrose ist gekennzeichnet durch die allmähliche Zerstörung von Gelenkknorpel und pathologischen Veränderungen des gesamten Gelenks und führt schließlich zu Schmerzen und einem Verlust der Gelenkfunktion. Bisher existiert noch keine klinisch zugelassene Therapieoption, die das Fortschreiten der Erkrankung modifizieren oder sogar aufhalten kann. Da Arthrose einen chronischen, über Jahrzehnte voranschreitenden Verlauf hat, werden Modellsysteme wie *in vitro* Tiermodelle und *in vitro* Zellkulturmodelle benötigt um die pathophysiologischen Veränderungen, die zu dem Phänotyp einer Arthrose führen zu untersuchen und potentielle diagnostische und therapeutische Optionen zu untersuchen. *In vitro* Modelle haben den Vorteil, dass sie auf humanen Zellkulturen basieren können und dass so die Anzahl der Tiere, die für Tierversuche verwendet werden, reduziert werden kann.

Methoden: In dieser Arbeit wurde ein humanes dreidimensionales *in vitro* Arthrose-Modell etabliert und evaluiert. Das Modellsystem basierte auf gerüstfreien, mittels Tissue Engineering hergestellten, knorpelähnlichen Konstrukten (SFCC) die ausschließlich aus humanen mesenchymalen Stromazellen (hMSC) und deren extrazellulärer Matrix bestehen. In einem ersten Schritt wurden SFCCs für drei Wochen unter normalen Bedingungen in Standardmedium kultiviert und wöchentlich Proben entnommen, um den knorpelähnlichen Phänotyp zeigen zu können. Um die inflammatorischen Bedingungen der Arthrose zu simulieren, wurden SFCCs für drei Wochen in einem Zellkulturmedium kultiviert, dem Interleukin-1 beta (IL-1β) und Tumor necrosis factor alpha (TNFα) zugesetzt waren und die als die prädominierenden proinflammatorischen Zytokine im Zusammenhang mit Arthrose angesehen werden. Histologie und histomorphometrische Auswertungen wurden genutzt, um die mikroskopische Struktur und Zellverteilung zu untersuchen, quantitative Polymerase-Kettenreaktion wurde zur Analyse der Genexpression von Molekülen der extrazellulären Matrix, Zytokinen und Proteasen durchgeführt und Immunhistochemie und Proteomics wurden genutzt, um die Proteinexpression zu bestimmen.

Ergebnisse: Es konnte der knorpel-ähnliche Phänotyp der SFCCs, inklusive der Expression der knorpelspezifischen Marker Aggrecan und Type II Kollagen, gezeigt werden. Die Stimulation der SFCCs mit IL-1β and TNFα zeigte einen Anstieg an proinflammatorischen Zytokinen und Proteasen sowie histologische Veränderungen und einen Rückgang der Zelldichte, wie sie auch in arthrotischen Gelenken zu finden sind.

Schlussfolgerungen: Die Verwendung von humanen, auf Tissue Engineering basierten knorpelähnlichen Konstrukten als *in vitro* Arthrose-Modelle könnte in Zukunft Translation von Forschungsergebnissen in die klinische Praxis verbessern und dabei helfen, die

Pathophysiologie der Arthrose besser verstehen und so neue therapeutische Möglichkeiten finden zu können.

CHAPTER 1: GENERAL INTRODUCTION

Articular cartilage covering the bone surface in joints is essential for smooth and pain-free movement of the human body. Osteoarthritis (OA) is the most common degenerative joint disease characterized by the breakdown of articular cartilage, and changes in subchondral bone structure and synovium that usually progress slowly over years or even decades. These structural changes lead to a loss of joint integrity and function, and to pain for patients affected by OA. Thus, OA is a serious disease due to its high prevalence and impact on the patients' quality of life. Multiple risk factors have been identified to contribute to the evolution of OA in humans, including age, obesity, and genetical and mechanical factors. The upregulation of pro-inflammatory cytokines within the joint as well as cartilage matrix degeneration through specialized matrix degrading enzymes are essential in OA pathophysiology. However, the exact pathways leading to the induction and maintenance of OA are not yet fully understood. Consequently, no treatment that can modify the disease progression or even heal OA has been clinically proven to date. The management of patients with OA in clinical practice thus mainly focuses on pain management, physical therapy and joint replacement surgery. In order to better understand the pathophysiology of OA, and in search of new therapeutic options for the treatment of OA, preclinical model systems including *in vivo* animal models and *in vitro* cell culture models are used. However, translatability of research outcomes into the human condition is often limited by using *in vivo* model systems, due to differences in joint anatomy, joint biomechanics, genetical factors and the immune system. *In vitro* model systems can overcome some of these limitations as they can be based on human cells or tissue. Model systems based on cell culture methods can in some cases replace animal models for certain research questions and are thus important with regard to the 3R principle (reduce, refine and replace), which aims for a more ethical use of animals in biomedical research. In this thesis, an OA *in vitro* model has been established and validated, which was based on tissue-engineered cartilage-like constructs that were generated from human mesenchymal stromal cells (hMSCs) with no scaffold involved.

CHAPTER 2: LITERATURE REVIEW

2.1 Osteoarthritis – A clinically orientated overview

2.1.1 Epidemiology

As a degenerative disease of diarthrodial joints, OA can affect every synovial joint in the human body that is equipped with articular cartilage on the joint surfaces. In humans the joints most often affected by OA are the hip, the knee, the joints of the hand and foot, the shoulder and the intervertebral joints of the spine [5]. The main features of OA pathophysiology include the degeneration of articular cartilage through matrix degrading enzymes and the upregulation of pro-inflammatory and catabolic cytokines within the joint tissues [2].

Taking all subgroups and affected joint regions together, OA is one of the most common joint disease worldwide [6]. However, studies to gain exact information about the epidemiology of OA are complicated to perform and to compare, as definitions of OA vary. Differences in location, etiology and characteristics of clinical presentation, as well as differences between radiological and clinical classification systems lead to a wide range of data describing the prevalence and incidence of OA [7]. Even so, it is estimated that around 20% of patients above the age of 60 suffer from OA [8]. Epidemiological studies in Germany based on health questionnaires conducted by the Robert Koch Institute and the Federal Statistical Office in 2010 showed a total prevalence of OA in 27.1% of women and 17.9% of men, and a 12-month-prevalence in 22.8% of women and 14.3% of men. The direct cost of OA to the German health care system was estimated to be 7.62 billion Euros in 2008 [9]. This did not include indirect costs due to inability to work or early retirement. In the 2010 Global Burden of Disease study, hip and knee OA together were identified as the 11th highest disease contributing to global disability measured by years lived with disability, with increasing prevalence compared to data from 1990 [10].

2.1.2 Clinical risk factors

OA is a complex and multifactorial condition with a variety of different risk factors. The impact of each etiological factor can differ for each joint that is affected by OA. To date, several biological, genetic and biomechanical risk factors for the development and especially the progression of OA have been identified [11].

Age is the most common risk factor for OA in all joints, mainly due to changes in tissue homeostasis and extracellular matrix (ECM) composition [12]. Obesity and increased body fat mass have been shown to increase the risk for the development and progression of OA not only in load-bearing joints like the knee, but also for hand OA [13, 14]. Structural abnormalities of the skeleton seem to be risk factors for the progression of OA, such as varus and valgus deformity of the knee, hip dysplasia and femoroacetabular impingement [15-18]. Biomechanical overload on the one hand, and joint immobilization on the other, can both lead to a loss of cartilage volume and the progression of OA under certain circumstances [19]. Genetics play another important part in the development of OA. Genome-wide association studies and epigenetic studies have identified several genetic loci and methylation patterns that are associated with late-onset OA [20]. Contrary to common genetic polymorphisms, each of which has only a rather small impact on OA pathogenesis, there are rare single gene defects, mainly of genes that are directly involved in the development of articular cartilage, that can cause severe early-onset OA [21]. Posttraumatic OA originates from joint trauma such as intraarticular fractures, rupture of the anterior cruciate ligament (ACL) of the knee, meniscus injury or ruptures of ligaments that lead to joint instability. In certain joints, such as the ankle, posttraumatic OA is responsible for most cases of OA as its idiopathic form is rare in these joints [22].

2.1.3 Clinical features and symptoms

The main symptoms of OA include pain, impaired range of motion, joint stiffness and joint instability, with pain being the most common one [23]. The clinical presentation of patients with OA differs in early and late stages of the disease. There is a high percentage of people with radiographic features of OA who do not experience any symptoms [24]. However, if OA becomes symptomatic, pain and loss of joint function can lead to psychological distress and loss of quality of life for these patients [25]. In the early phase of symptomatic OA, patients mostly suffer from pain during movement of the joint, especially during the beginning of specific movements and when using the full range of movement of the joint. Stress-induced pain after longer periods of moving or forced movements are also common. Episodical flare-ups of symptoms are typical for OA. Pain at night and persistent pain are common at late stage osteoarthritis [23]. While the range of motion is usually not impaired during the early phases of OA, it becomes more prevalent in later stages when bone remodeling is present [26]. Apart

from joint stiffness, joint instability is another symptom that is associated with OA, especially with regard to knee OA [27].

2.1.4 Diagnosis and classification systems

Diagnosis of OA is based on two major parts, clinical examination and radiology. Firstly, patient management includes clinical evaluation and medical history taking with a focus on pain, functional losses, quality of life and possible risk factors and the physical examinations [28]. As there are no clinically used biomarkers for OA yet, blood tests can be performed to rule out a differential diagnosis like rheumatoid arthritis by measuring markers for inflammation or antibodies associated with autoimmune disease that affect the joints [29]. Radiography is used to identify signs for OA like joint space narrowing, osteophytes, sclerosis and bone deformity, although these changes usually occur later in the progression of OA and do not always correlate to the severity of clinical symptoms [3, 24]. Magnetic resonance imaging (MRI) can be used to identify

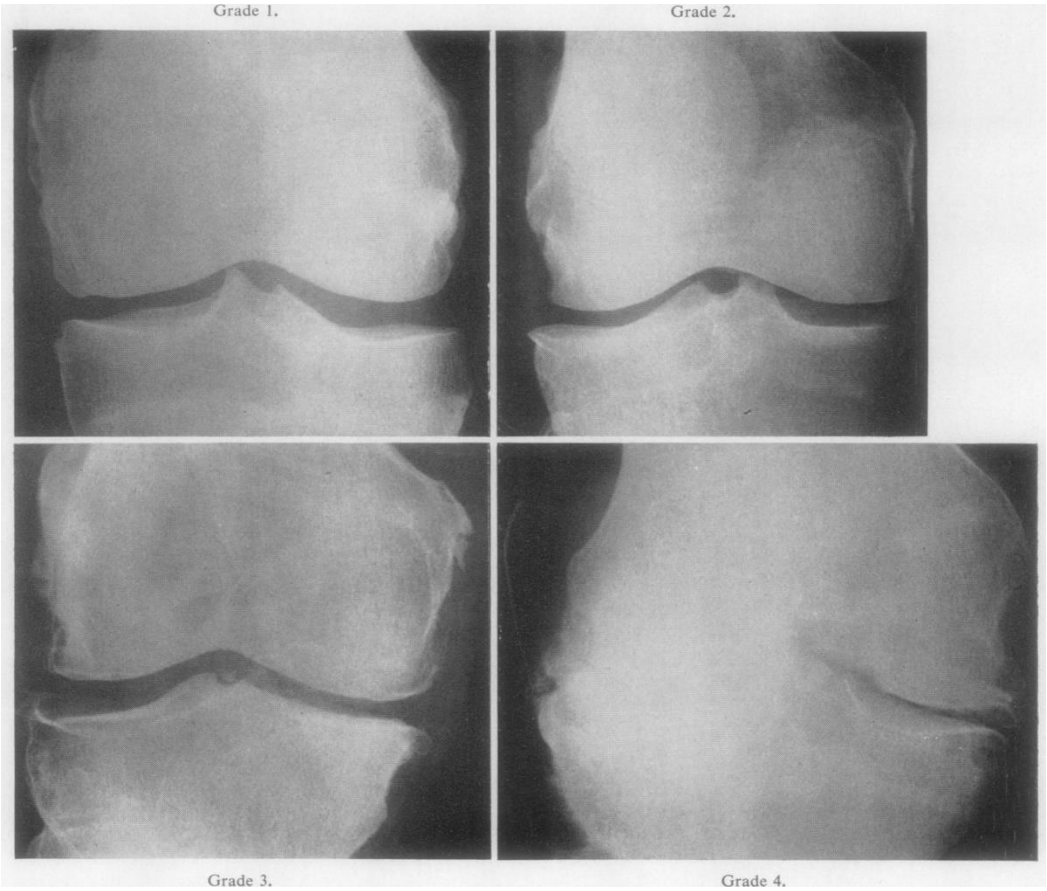

Figure 1: The Kellgren-Lawrence grading system for osteoarthritis
Figure and legend reproduced from [3]. Radiographic images from the original work of Kellgren and Lawrence show the radiological grading system for OA on the example of the knee joint. Radiographic features typical for OA defined by Kellgren and Lawrence include osteophyte formation, periarticular ossicles, narrowing of the articular cartilage, sclerosis of the subchondral bone, pseudocysts and altered shape of bone ends.

cartilage defects and other potential causes for joint pain, for example meniscal or ligamental injuries of the knee or osteonecrosis of the femoral head [30].

International associations involved in OA research have identified criteria for a clinical and/or radiological classification of OA to improve the sensitivity and specificity of diagnostic tools and provide standardized definitions of OA for clinical research. The most common classification systems were introduced by the European League Against Rheumatism (EULAR) for hand and knee OA, and the American College of Rheumatology (ACR) for OA of the hip, knee and hand [31-35].

The radiography classification system introduced by Kellgren and Lawrence in 1957, as shown in Figure 1, is still used in clinical practice and research although it only takes into account late stages of OA where bone lesions and remodeling are already present [3]. To date, there is no method to diagnose early stages of OA that are mainly characterized by degradation of the ECM. Standard MRI is already used to detect focal lesions of articular cartilage, and specialized MRI sequences seem to be a promising method to detect early changes in ECM composition and to monitor potential OA therapies [36].

2.1.5 Treatment

An ideal treatment regime for symptomatic OA would be able to reduce pain, slow down or stop the progression of joint degeneration, sustain joint function and mobility, and improve the patients' quality of life. However, there has been no clinically approved treatment option developed that can modify the disease progression to date [37]. Current clinical management of patients with symptomatic OA includes non-pharmacological, pharmacological and surgical options that mainly target the reduction of pain and the improvement of joint function.

In non-pharmacological OA treatment, health education is important in the setting of OA as a chronic disease especially with regard to patient compliance. Lifestyle modification such as weight loss, strength training and low impact aerobic exercise have been shown to not only alleviate symptoms but also to possibly slow down the progression of cartilage loss, especially in the knee joint [38, 39]. Since pain is the predominant symptom in OA patients, pain management is important in the therapeutic

regime. It can be distinguished between non-pharmaceutical pain relief through physical therapy or orthopedic braces and other tools, and pharmaceutical pain management. Pharmacological options include topical or oral non-selective non-steroidal anti-inflammatory drugs (NSAIDs), selective cyclooxygenase (COX)-2 inhibitors, paracetamol and opioids, but adverse effects of these drugs are common. Another group of pharmaceuticals, known as symptomatic slow-acting drugs for osteoarthritis (SYSADOA) that include glucosamine and chondroitin sulfate, were shown in two Cochrane meta-analysis to have small therapeutic effects on OA [40, 41]. As some joints such as the knee are easily accessible for intraarticular injections, application of several intraarticular pharmaceuticals such as hyaluronic acid, corticosteroids and platelet-rich plasma is routinely used in OA management when oral pharmacological treatment becomes insufficient but a surgical intervention is not yet indicated [42-44].

Surgical interventions for the treatment of OA can be categorized into joint-preserving surgery, joint-replacement and arthrodesis. Joint-preserving surgical procedures are mainly performed on the knee and hip and include corrective osteotomies around the joints, especially tibial condylar valgus osteotomy for OA of the medial knee compartment, and pelvic osteotomies for OA associated with hip dysplasia or Perthes disease and the arthroscopic debridement of femoroacetabular impingement [45, 46]. The most widely used surgical procedure for advanced OA, however, is joint replacement. Hip and knee replacement are predominant in orthopedic surgery, but joint replacement of other joints such as the shoulder, elbow, ankle and finger joints is possible but performed less frequently. Joint replacement surgery is efficient in relieving pain and improving joint function. However, the direct surgical risks and the risk of needing revision surgery due to implant wear or infection need to be considered when indicating surgery [47, 48]. As pain in OA usually occurs during movement, arthrodesis is another surgical treatment option for some joints affected by OA such as the ankle or the first metatarsophalangeal joint [49, 50].

Treatment guidelines from international societies involved in OA research such as the ACR and EULAR, have been developed to bring these various therapeutic modalities together and help identify an adequate option for each patient [51-53].

2.2 Cartilage

Skeletal bone and its connective tissues, cartilage, tendons and ligaments provide the human body with a skeletal structure that enables the human body to move. In embryonic development cartilaginous structures are formed through the clustering of mesenchymal cells that differentiate to chondroblasts and finally to chondrocytes [54]. The perichondrium is a layer of fibrous connective tissue which contains blood vessels and mesenchymal precursor cells that can differentiate into chondrocytes to allow partial cartilage regeneration. The perichondrium surrounds all cartilage tissues except for adult articular cartilage and fibrous cartilage. There is only one cell type present in cartilage, the chondrocyte. Chondrocytes are embedded into the ECM, consisting mainly of collagen fibrils, proteoglycans and glycosaminoglycans (GAGs). Cartilage is free of blood vessels and chondrocytes are provided with nutrients by diffusion through the ECM from the surrounding perichondrium or synovial fluid [55]. There are different types of cartilage - elastic, hyaline and fibrous cartilage, with articular cartilage being a subtype of hyaline cartilage. The differences between each type of cartilage is mainly based on the relation of cells to the ECM, and the composition of the ECM. Fibrous cartilage is the type of cartilage with the least cells per amount of ECM. The main collagen found in the ECM is type I collagen, which is arranged in fibers making this type of cartilage elastic to pressure and giving it high tensile strength. Fibrous cartilage can be found, for example, in the menisci of the knee, the intervertebral discs and the articular surfaces of the mandibular joint. Elastic cartilage has the highest cell density. Elastic fibers enable this type of cartilage to be highly elastic to pressure as well as to bending. It is found in the epiglottis, the small bronchial tubes and the outer ear. Hyaline cartilage is the most important cartilage in the human body. Most of the airways, the larynx, the trachea and the big bronchia, the growth plate of most bones, the articular cartilage and the embryonic precursor of the bony skeleton consist of hyaline cartilage [56].

Articular cartilage is a subtype of hyaline cartilage. It does not have a perichondrium, and is thus being mostly supplied with nutrients through diffusion from the synovial fluid of the joint. Chondrocytes of articular cartilage are usually arranged in groups of a few cells, called chondrons [57]. They are surrounded by a thin pericellular matrix (PCM) that consists of type VI and type IX collagen amongst others [58]. The chondrocytes and their PCM are embedded within the ECM, containing mainly type II collagen,

proteoglycans and GAGs. The components of the ECM are arranged in a highly distinct order within articular cartilage, enabling the absorbance and distribution of pressure over the whole articular surface of the joint. Collagen fibrils of articular cartilage are mostly made of type II collagen together with type IX and type XI collagen. The main proteoglycan in articular cartilage is aggrecan, which forms large, negatively charged aggregates with the GAG hyaluronic acid. Due to its ability to bind water, water makes up about 80% of the wet weight of articular cartilage [59]. Within a layer of articular cartilage, which can be up to 5 mm thick, collagen fibrils and cells are arranged in four different zones. The first is the superficial zone where collagen fibrils are aligned

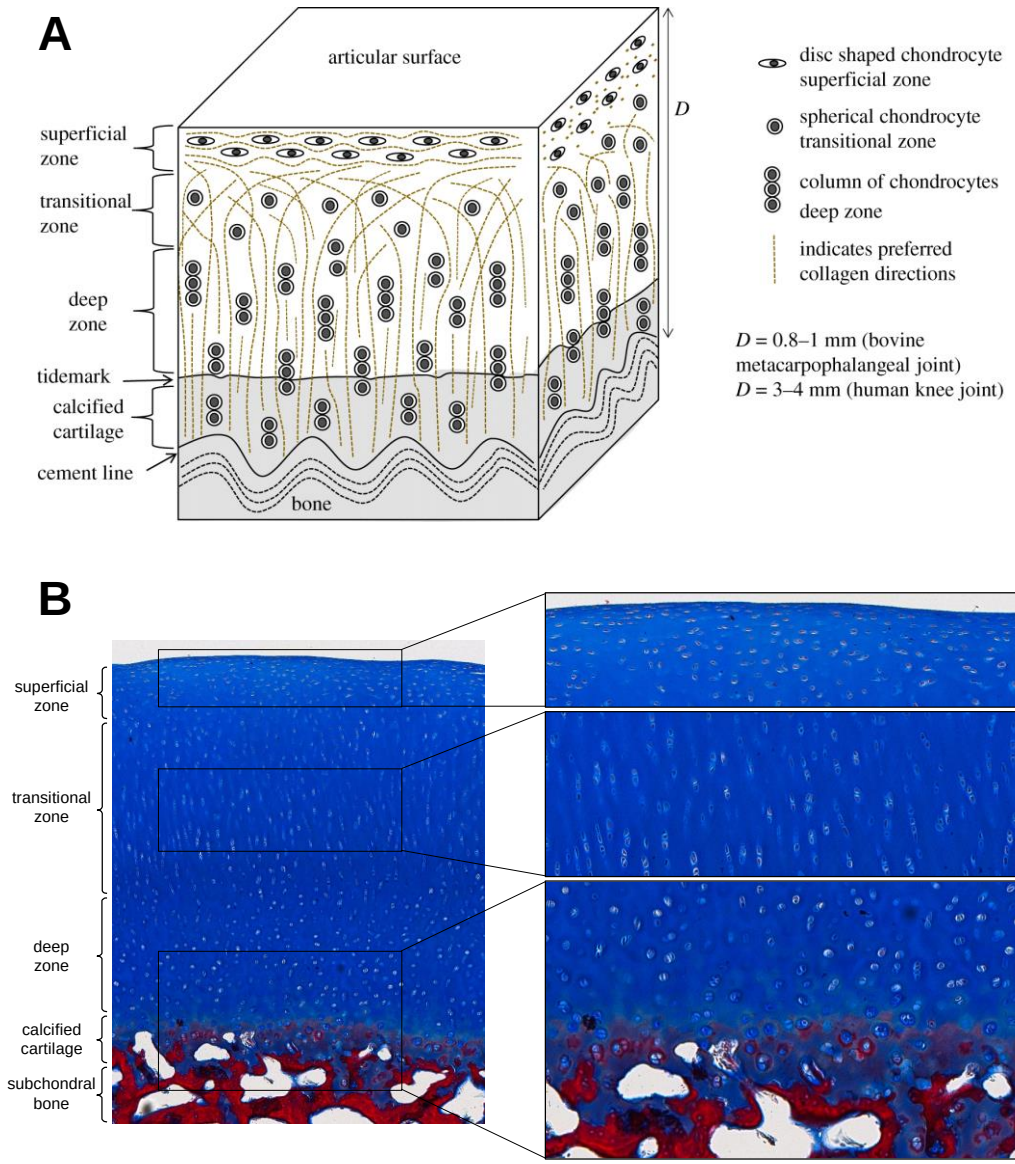

Figure 2: Histological structure of articular cartilage

(A) Figure and legend reproduced from [4]. Zonal structure of articular cartilage with the preferred arrangement of collagen fibrils and chondrocyte shape. **(B)** Equine articular cartilage from the fetlock joint stained with azan staining. Equine articular cartilage shows a similar histological and zonal structure to human articular cartilage. The slice was kindly provided by Gabriela Korus (Julius-Wolff-Institute, Charité – Universitätsmedizin Berlin).

tangential to the surface, allowing tensile strength and protection of the deeper layers. Underneath the superficial zone lies the transitional zone which makes up about half of the total cartilage volume. This is followed by the deep zone, where the collagen fibrils are arranged vertically to the articular surface and chondrocytes are clustered in columns parallel to the collagen fibrils, allowing this zone to be highly resistant to compressive forces. Just above the subchondral bone lies a layer of calcified cartilage providing a strong fixation through anchoring of collagen fibrils in the bone. Between the calcified and non-calcified cartilage layers is the so-called tidemark (Fig. 2A) [60, 61]. Figure 2B shows a histological section of equine articular cartilage that has a similar microscopic anatomy to human articular cartilage. The complex anatomy of articular cartilage, the missing ability of chondrocytes to proliferate, the lack of a perichondrium providing chondrocyte progenitor cells, and the absence of blood supply make articular cartilage one of the most susceptible tissues toward micro- and macro-injury in the human body.

2.3 Osteoarthritis – Current understanding of its pathophysiology

As a predominant joint disease worldwide, OA is characterized by the degeneration of articular cartilage leading to microscopic and macroscopic alterations of the whole joint including the subchondral bone and synovium, which causes pain and loss of joint function for the patients affected by OA. The main characteristics of the disease progression in OA can be summarized as an imbalance of repair and destruction of joint tissues after macro- or micro-injuries, which is caused by a variety of different pathophysiological principles such as local and systemic inflammation, genetic predisposition, ageing and metabolic factors [28]. In this chapter, some of the main findings on OA pathophysiology are summarized.

2.3.1 Microscopic and macroscopic morphological changes in OA cartilage

Pathological changes within cartilage are characterized by the alteration of ECM composition and chondrocyte homeostasis [62, 63]. During early stages of OA, the highly organized collagen-proteoglycan matrix within the ECM loses its structure due to proteolytic activity within the joint, leading to the loss of the structural and functional integrity of the cartilage [64, 65]. As described above, around 80% of the wet weight of cartilage is water which is held inside the tissues due to the high GAG content of

cartilage. Anionic GAGs hold a high number of cations for charge balancing which then attract water molecules, providing the cartilage with compression strength. The negative charge of GAGs also prevents compression due to electrical repulsion. Proteoglycans are connected to the collagen fibrils by link proteins within the ECM network of articular cartilage. They therefore cannot use their full solubility, which leads to their tendency to expand again after compression. The presence of proteoglycans and GAGs thus allows healthy cartilage to regain its original volume after compression [56]. These features of articular cartilage are important in understanding the impact that disturbances of ECM integrity can have on its biomechanical properties and its susceptibility for further damage. As a consequence of ECM disruption in early stages of OA, tissue swelling and an increase in water content occur [66]. Further on, the changes in the composition of the ECM lead to morphological changes of the cartilage architecture. A histological classification system has been established to classify these morphological changes within the articular cartilage during disease progression of OA into 6 grades [60]. Classification criteria include fibrillation of the superficial layer, discontinuity of the surface, fissures, cell proliferation or cell death, erosion and denudation leading to the total loss of uncalcified cartilage, and morphological changes in the subchondral bone such as microfractures, bone remodeling and osteophyte formation. These morphological changes of the articular cartilage lead to altered mechanical properties, making it even more susceptible to biomechanical overload and injuries [67].

2.3.2 OA as an inflammatory disease

The exact events that play a role in the onset of OA have not yet been fully understood, and there might be different phenotypes of OA, all leading to similar morphological changes in OA cartilage as described in the previous section. Therefore, it is known that the reasons for the continuous breakdown of ECM are not predominantly biomechanical forces but the development of a pro-inflammatory and catabolic environment within the joint. This leads not only to pathological changes of the cartilage, but also of the subchondral bone and synovium or *vice versa*. It has been corroborated by evidence that OA can be seen as an inflammatory disease and not only a solely mechanical deterioration of articular cartilage [68].

Many pro-inflammatory cytokines are known to play an important role in the pathogenesis of OA, with interleukin 1 beta (IL-1β) and tumor necrosis factor alpha (TNFα) being the predominant ones [69, 70]. IL-1β and TNFα have both been shown to suppress the synthesis of ECM molecules, to induce the expression of proteases and to initiate an inflammatory cascade by stimulating the expression of a variety of other pro-inflammatory and catabolic factors [71-75]. IL-1β acts upon binding on the IL-1 receptor (IL-1R), of which two isoforms are known. The type 1 IL-1R was shown to be expressed on chondrocytes and synovial cells, and even as being at a higher level in osteoarthritic cells compared to normal cells [76, 77]. IL-1β stimulation of chondrocytes leads the expression of a natural IL-1R antagonist which might be able to protect the chondrocytes against excessive IL-1β signaling [78]. The tumor necrosis factor receptor 1 (TNF-R1), also known as p55 TNF-R, has been shown to be the receptor for pro-inflammatory signaling of TNFα in chondrocytes [79, 80]. One of the major downstream biochemical pathways that is induced by both IL-1β and TNFα, is the Nuclear factor-kappaB (NF-κB) signaling cascade. Initiation of the NF-κB pathway results in the release of the transcription factor NF-κB from its inhibitor, and the transcription of genes for the major proteases and pro-inflammatory cytokines in OA [81].

Other pro-inflammatory and catabolic cytokines that seem to play an important role during the initiation and progress of OA are interleukin 6 (IL-6), interleukin 8 (IL-8), leukemia inhibitory factor (LIF), and interleukin 17 (IL-17). Furthermore, anti-inflammatory and anabolic factors such as interleukin 4 (IL-4), interleukin 10 (IL-10), interleukin 13 (IL-13), IL-1R antagonist (IL-1RA) and interferon gamma (IFNγ) were found to be differentially expressed in OA compared to healthy joints [69, 70]. It has been shown that cytokines in osteoarthritic joints derive not only from chondrocytes, but also from cells within the synovium and subchondral bone [82, 83]. Interestingly, fragments of ECM molecules that are formed during cartilage degradation in the form of damage-associated patterns (DAMPs) were shown to be able to activate pro-inflammatory pathways, especially in the synovial membrane [84].

2.3.3 The role of chondrocytes in OA pathophysiology

As the chondrocyte is the only cell type within articular cartilage, it plays a specific role in OA pathophysiology through its role in ECM production, its expression of different

surface markers, and its evolutionary features and differentiation properties. Under normal conditions, chondrocytes do not proliferate and preserve the cartilage homeostasis through very low turnover of ECM molecules in adaptation to mechanical loading. In early phases of OA, however, this homeostasis is disrupted, and chondrocytes exhibit a higher metabolic activity in the attempt to repair structurally damaged cartilage matrix [85]. Besides upregulating the expression of ECM proteins, chondrocytes themselves have been shown to be able to produce both pro- and anti-inflammatory cytokines and matrix degrading proteases [86]. Pro-inflammatory cytokines not only contribute to the ECM degradation in osteoarthritis cartilage, but they also seem to be important for maintaining a balance between anabolic and catabolic processes within joint tissues as studies on knock-out mice for IL-6 have shown [87]. Nevertheless, an overexpression of pro-inflammatory cytokines by chondrocytes contributes to the progression of OA. Activation of the chondrocytes in OA has been shown to not only be mediated through pro-inflammatory cytokines, but also through mechanisms involving different kinds of surface receptors [88]. As such, a subset of receptors belonging to the innate immune system have been shown to be expressed on chondrocytes. One type of these receptors are toll-like receptors (TLRs). They belong to the group of pattern recognition receptors and can be activated by DAMPs which are molecular fragments of ECM components [84]. Other surface receptors that are assigned to the innate immune system and have been identified on chondrocytes include receptors of the complement pathway and receptors for advanced glycation end products which are known to accumulate in tissues during ageing [89, 90]. Mechanosensitive ion channels on chondrocytes have been shown to be activated through abnormal biomechanical stress on the cartilage leading to an overexpression of pro-inflammatory mediators or chondrocyte apoptosis [91, 92].

A feature of chondrocytes that arises from their developmental function in the growth plate of long bones seems to contribute to the morphological changes in late phases of OA. Chondrocytes have been shown to switch to gene expression patterns and morphological changes that are associated with hypertrophy, especially in the deep zone of the articular cartilage [93].

Recent findings on OA pathogenesis have put cell senescence into focus [94]. Cell senescence is a phenotypic state characterized by the inability of cells to further divide,

which can be caused by a combination of growth and arrest signals. In OA cartilage these signals originate from mechanical stimulation and growth factors on the one hand, and a pro-inflammatory environment and DNA damage on the other. Features of cell senescence have been identified in OA chondrocytes, including the expression of $p16^{INK4A}$ and senescence-associated β-galactosidase, and the ability to express an altered secretory profile, including the secretion of higher levels of pro-inflammatory cytokines and proteases [95-98].

2.3.4 The role of subchondral bone and synovium in OA pathophysiology

Morphological changes in osteoarthritic joint include not only the loss of articular cartilage but also alterations in subchondral bone and the synovium of the joint. Therefore, it is important to consider these tissues as part of OA pathophysiology.

Subchondral bone is the first layer of bone underneath the cartilage, located between calcified cartilage below the tidemark and trabecular bone. It can be morphologically divided into the subchondral bone plate and subchondral trabecular bone. In the early phase of OA, a loss of subchondral bone mass with decreased mineralization and bone stiffness was observed in several *in vivo* OA models, probably due to increased bone turnover initiated by pro-inflammatory and catabolic factors [83]. The loss of subchondral bone mass can be histologically described as the thinning of the subchondral bone plate and rarefication of trabecular structure. In the later phases of OA, features of subchondral bone change. Thickening of the subchondral bone plate (also known as sclerosis) increased bone volume and the formation of osteophytes occurs. Bone marrow edema-like lesions and subchondral bone cysts are changes within the subchondral bone that can often be seen in radiological images of patients with OA [99]. It has been shown that osteoblasts can react to mechanical overload similar to chondrocytes by expressing pro-inflammatory cytokines and matrix degrading proteases [100].

The synovial membrane is a specialized connective tissue that forms the inner layer of the joint capsule. It does not contain endothelial cells but two specialized types of synovial cells. Type A synovial cells are macrophages responsible for phagocytosis of joint debris from the synovial fluid [101]. Type B synovial cells are specialized fibroblasts that secrete components of the synovial fluid such as GAGs, especially

hyaluronic acid and proteoglycans like lubricin. Observations of osteoarthritic joints highlight clinical, histological and molecular features of the synovium and their contribution to the OA phenotype [102]. Synovitis is a common feature of OA, with clinically relevant joint effusion and swelling, as well as increased pain [103]. Synovial cells have been shown to release pro-inflammatory cytokines and matrix degrading enzymes into the joint space. Consequently, they contribute, like osteocytes and chondrocytes, to the inflammatory environment in OA joints [104]. Histological features of OA synovium include hyperplasia and hypertrophy, as well as increased vascularity and infiltration with macrophages and T-cells [82].

2.3.5 Biochemical pathways leading to cartilage destruction

The progressive cartilage destruction in OA is a result of two essential mechanisms: (I) the inhibition of the expression of ECM molecules by pro-inflammatory and catabolic cytokines; and (II) the proteolytic breakdown of ECM components.

Both, IL-1β and TNFα have been shown to be responsible for the downregulation of ECM molecule expression in chondrocytes. Amongst others, type II collagen, proteoglycans such as aggrecan and link protein have been shown to be downregulated by IL-1β and TNFα in several OA model systems [105-109].

Two major groups of proteases have been identified in osteoarthritic cartilage and seem to play an important role in OA pathogenesis: matrix metalloproteinases (MMPs) and a disintegrin and metalloproteinase with thrombospondin motifs (ADAMTS). MMPs are calcium-dependent zinc-containing endopeptidases that are responsible for the remodeling of the ECM in a variety of different tissues. In osteoarthritic cartilage MMP-1, MMP-3, MMP-8 and MMP-13 were identified to be upregulated and are responsible for the degeneration of collagen molecules, as well as other ECM components [110-112]. ADAMTS are also zinc metallo-endopeptidases, and ADAMTS-4 and ADAMTS-5 are the predominant members of this protease family in OA pathogenesis. They have been shown to degrade aggrecan at different molecular sites than MMPs [113, 114]. Due to its highly crosslinked secondary structure and the presence of proteoglycans and GAGs, the collagen network in articular cartilage is highly resistant to unspecific proteolytic activity. It seems that in initial ECM changes during early OA, ADAMTS

break down aggrecan molecules, which makes the ECM matrix susceptible to MMP-dependent collagen degradation and continuing aggrecan breakdown [115].

As MMPs and ADAMTS are upregulated through pro-inflammatory and catabolic signaling in OA joints, this process of matrix degradation and inflammation is perpetuated through positive feedback loops of cytokine, protease and ECM breakdown product release within the joint, involving all major tissues, cartilage, subchondral bone and synovium, as mentioned above. Some of the exact mechanisms in cartilage homeostasis and in OA pathophysiology have not been revealed yet, especially regarding the disease onset. However, it is evident that OA is not a uniform disease. Each individual patient presents with a different subset of etiological factors leading to a similar phenotypical outcome [116]. The commonly described morphological changes and signaling molecules are summarized in Figure 3.

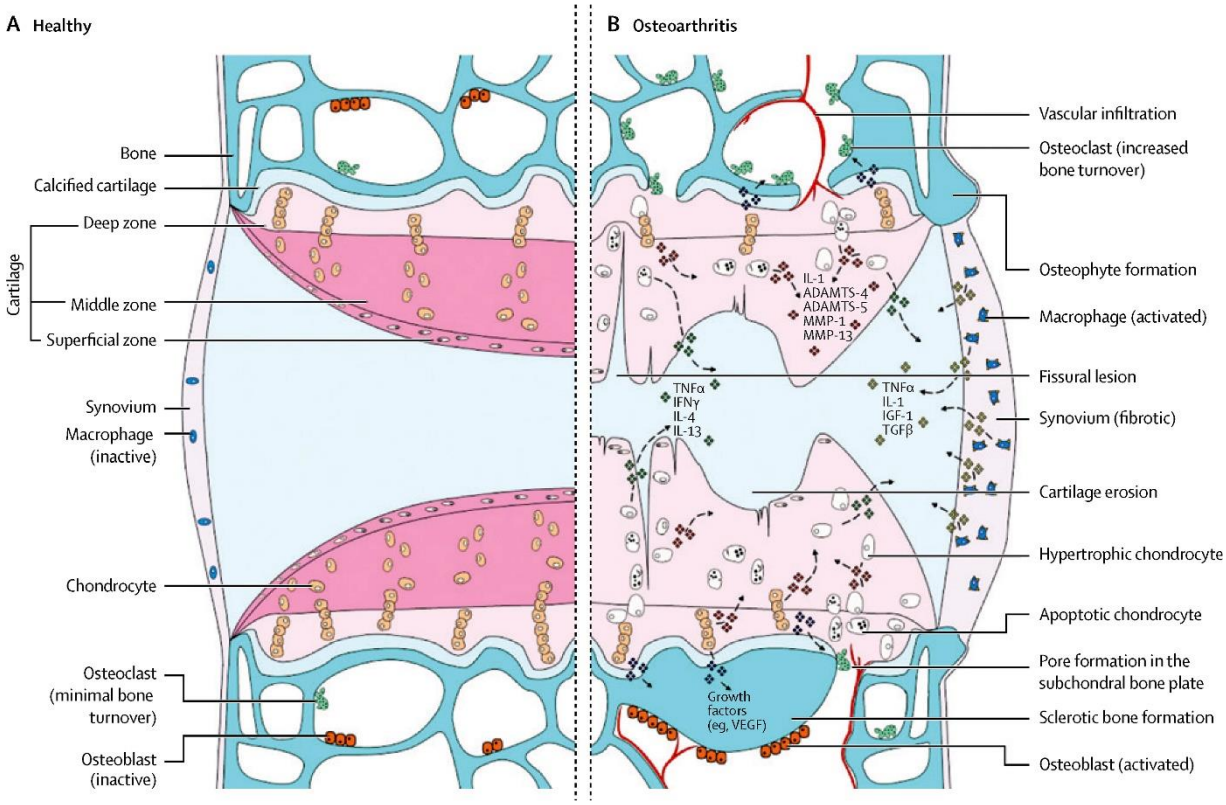

Figure 3: Morphological changes and signaling molecules in OA pathophysiology
Figure reproduced from [2]. The left side shows healthy articular cartilage, synovium and subchondral bone of a diarthrodial joint. The left side shows morphological changes of these tissues as observed in osteoarthritic joints with the important pro-inflammatory cytokines, proteases and growth factors involved in OA pathophysiology. Abbreviations: IL = interleukin, MMP = matrix metalloproteinases, ADAMTS = a disintegrin and metalloproteinase with thrombospondin motifs, VEGF = vascular endothelial growth factor, IGF = insulin-like growth factor, TNF = tumor necrosis factor, TGF = transforming growth factor.

2.4 Disease models in OA research

Similar to other fields in biomedical research, disease models are of great importance in the study of OA pathogenesis. *In vivo* and *in vitro* models build the foundation for findings on pathophysiology, discovery of potential therapeutics and toxicity testing. In OA research, disease models are particularly important as OA is a chronically evolving and multifactorial condition. In the following, the main reasoning for the need for OA disease models in preclinical research is described.

(I) OA is a chronic disease that often progresses over decades in humans and symptoms usually only occur in late stages of the disease, making it difficult to investigate early processes of the disease in humans. Disease models have helped to reveal characteristics of the early phases of the disease, helping to develop diagnostical tools for early detection of the disease in humans.

(II) OA is a multifactorial disease in humans, making it difficult to elucidate single risk factors, the biochemical pathways they influence and the contribution they make to the full phenotype of the disease.

(III) The management and diagnostic procedures in humans with OA usually only include history taking, physical examination and plain radiographs. Patients mostly seek medical advice in later stages of the disease and only if symptoms occur. Differently to other conditions, there are usually no blood tests, biopsies or other biological samples taken routinely from patients with OA. Tissue sampling can only occur, if at all, during joint replacement operations of the end-stage disease. This lack of human samples and diagnostic procedures leads to a high demand for disease models, not only for the study of OA pathophysiology and the development of therapeutics, but also to find new diagnostic tools.

Since OA is such a heterogeneous disease, there is no gold standard disease model for either *in vitro* or *in vivo*. The following sections will give an overview of the two main types of models, i.e. *in vivo* and *in vitro* models, their use in OA research and their advantages and disadvantages.

2.4.1 *In vivo* animal models of OA

Animal species that serve as *in vivo* animal models for OA research include mice, rats, rabbits, guinea pigs, dogs, sheep and goats, as well as horses. In most cases, the knee is the target joint for OA induction and analysis [117]. Smaller animals such as small rodents, rabbits and guinea pigs are cost-effective, management and handling are easy, and histological analysis can often be performed with the whole joint on one slice. Their lifespan is naturally short, making the experiments less time consuming. The mouse as a model organism is of particular interest as a variety of different gene knockout strains have been established to investigate the effect of single genes on the development of cartilage and OA [118]. However, the histology of the articular cartilage and joint loading condition in small animals differs greatly from human cartilage, which limits the translatability into the human condition [117].

Bigger animals such as sheep, goats, dogs and horses have larger-sized joints that allow for the application of MRI and arthroscopy. Their cartilage histology is similar to human cartilage. Consequently, they can be used in preclinical pharmaceutical studies and in the evaluation of surgical therapeutic options. However, the use of larger animals as OA models involves higher costs and longer experimental periods. They are also more diverse regarding genetic and phenotypic features, making comparability between studies more difficult [119, 120].

The development of OA in model organisms can be classified into spontaneously occurring and chemically- or physically-induced OA. Spontaneously occurring OA models, for example, include naturally occurring OA in some animals such as dogs and horses, or OA that develops through a genetic knockout or through age and obesity [87, 121-123]. OA can be chemically induced through the injection of substances that are toxic, pro-inflammatory or have enzymatic activity. Substances used for chemically-induced OA include collagenases, papain, monosodium iodoacetate and amphotericin-B [118, 124-126]. Another way to trigger the development of OA in the model organisms is through causing physical injury that leads to joint instability or cartilage defects. These physically-induced OA models include the surgical destabilization of the medial meniscus model and the ACL rupture model [127, 128]. Cartilage defects can also be manually created, a method that is often used for the evaluation of possible regenerative therapies [129].

The variety of species and methods for inducing an OA phenotype allows for the study of different etiological factors within the pathophysiology of OA. However, the diversity of *in vivo* models leads to problems regarding the comparability of study outcome measurement, reproducibility and standardization. Some efforts have been made in OA research to be able to better compare *in vivo* study results. For example, the Osteoarthritis Research Society International (OARSI) has introduced standardized classification systems for the evaluation of histology for most animal models used in OA research. Furthermore, when using animal models for OA research, it is important to find the appropriate model organism and method of OA induction that fit the research question, to improve the translatability of results by obtaining valuable outcome measures [130].

Nevertheless, the main issues causing a deficit of translatability into clinical praxis are that: (I) no animal model can fully represent all aspects of the phenotype of human OA; (II) rodents are mainly used, which have different loading conditions on joints, and factors like pain and fatigue are not easily measurable; (III) there are differences between the joints in animal models and humans, mainly cartilage thickness and anatomy as well as immunological differences.

2.4.2 *In vitro* cell culture models of OA

There is a wide variety of different *in vitro* models that are used in OA research. *In vitro* models for the study of OA are designed by a combination of different variables: the source of the cells used within the model, the type of culture procedure such as monolayer of 3D culture, and the method of inducing OA, with cytokine-induced and load-based OA being the two most common ones [131]. *In vitro* models are commonly used in OA research because model parameters are easy to manipulate, and they can be used for high throughput experimental set-ups. Furthermore, *in vitro* models contribute to refine, reduce and replace the use of animals in biomedical research, known as the 3R principle. Russell and Burch first introduced this principle in 1959 with their book *"The principles of humane experimental technique"* [132]. As one of the main symptoms of OA is pain, the induction of OA in animals will always be associated with pain, thus making OA research an area where the application of the 3R principles is of particular importance. While *in vitro* models do not directly contribute to the reduction

of pain in experiments using animal models, they help to reduce the number of animals used.

There are different sources of cells used in *in vitro* models of OA. They include immortalized chondrocyte cell lines, primary chondrocytes and stem cells that are differentiated into the chondrogenic lineage [119]. Chondrocyte cell lines are often used to gain a better understanding of the chondrocytes themselves - particularly their metabolism and their subset of cell surface receptors. One example of an immortalized chondrocyte cell line is the ATDC5 cell line. It can differentiate similarly to primary chondrocytes, and be cultured in monolayer as well as in 3D culture systems. It is therefore used as an *in vitro* model to study influences on chondrogenesis and chondrocytes hypertrophy [133]. Another common source of cells used in *in vitro* OA models are primary chondrocytes which can be isolated from animal or human articular cartilage. One important disadvantage of primary chondrocytes is that they dedifferentiate rapidly after only a few passages, and only keep their chondrogenic phenotype for longer when cultured in 3D conditions such as pellet cultures or on scaffolds like agarose [134, 135]. Stems cells or multipotent cells used in OA models are mostly mesenchymal stromal cells (MSCs) and induced pluripotent stem cells (iPSCs) that can be isolated from different tissues in animals and humans. They are mainly of interest due to their usage in tissue engineering and other potential regenerative therapeutic options in OA treatment. The difficulties of using stem cells in OA *in vitro* models are that stem cells are not differentiated into the final cell type yet, that the cell populations have donor specific features, and that cell populations are often not homogeneous [119, 136].

Different types of culture systems for *in vitro* models exist. Monolayer cultures are the simplest culture form of *in vitro* models. They are cost-effective, but do not take into account effects of other factors such as the interaction with the ECM and other tissues of the joint. 3D culture systems include pellet culture and spheroids or cell aggregates with or without the use of scaffolds to provide a 3D basis for the cells. Growth in a 3D state allows cell-cell and cell-matrix interactions, which are especially important in an avascular tissue like cartilage. It also provides the system with structural strength which allows for the analysis of mechanical load on the system [137]. However, the characteristics of 3D culture systems highly depend on the scaffold and its composition

which is used to provide the 3D structure. With a variety of different cell types, culture sizes and scaffolds used to create 3D cultures, and no existing standard method, comparability between each system is limited [136]. As there are different joint tissues, cartilage, bone and synovium contributing to the pathogenesis of OA, co-cultures of different cell lines are used to study their interactions and the contribution of each tissue and cell type to the OA phenotype [138]. The different joint tissues are highly dependent on movement, mechanical forces and dynamic conditions that naturally occur *in vivo* and specialized culture methods have been developed to mimic these dynamics. Bioreactors and dynamic cultures allow a constant flow of culture medium or the application of mechanical stimulation, simulating the *in vivo* environment within the joint more accurately [139]. Explant-based cultures are a special subgroup of *in vitro* models as the cells are not extracted from the tissue, but the tissue explants are directly used as *ex vivo* cultures. These model systems use whole tissue samples of cartilage or cartilage and bone, mostly chondral or osteochondral plugs. They are then further cultured *in vitro* similarly to 3D culture systems, with the advantage that the cells stay within their natural ECM structure. However, there is high intra- and inter-experimental variability, partly due to the differences in cell and ECM features in different regions of the joint and the different sources and techniques for tissue acquisition [136].

Like in the case of *in vivo* OA models, it is important to choose the appropriate *in vitro* model system for each research question to get reliable and translatable experimental outcomes. After choosing the appropriate cell source and culture system, the method of inducing OA in the system needs to be adapted to both the research questions and the outcome measures. Two main possibilities exist for OA induction, load- or injury-based as well as cytokine-induced OA [131]. Mechanical load and the mechanosensitive pathways are essential for cartilage to maintain its metabolic phenotype [140]. However, an overload of mechanical force onto cartilage in form of a single impact or repetitive overload can lead to tissue injuries or the activation of pro-inflammatory and catabolic pathways similar to those initiated by pro-inflammatory cytokines [91]. Thus, 3D- and explant-based *in vitro* culture systems are ideal for studying the impact of different load- and injury-stimuli on cartilage homeostasis and the development of an OA phenotype. As IL-1β and TFNα are the most important pro-inflammatory cytokines in the pathogenesis of OA, they are commonly used in their

recombinant form in cytokine-induced OA models [131]. Another possibility to induce a pro-inflammatory response *in vitro* is to use the synovial fluid of patients with OA in the culture medium [141].

The different cell types, culture procedures and methods of OA-induction that are used for creating OA *in vitro* models are listed and summarized in Table 1.

Table 1: Components of *in vitro* models for the study of OA

<table>
<tr><th>1. Cell type</th><th>2. Culture procedure</th><th>3. OA-induction</th></tr>
<tr><td>□ Cell lines
- normal clonal cell lines
- transformed clonal cell lines</td><td>□ Monolayer culture</td><td rowspan="3">□ Physically induced
→ only in 3D- or explant culture systems
- mechanical overload
- injury

□ Chemically induced
- cytokine-induced (IL-1, TNFα)
- synovial fluid-induced</td></tr>
<tr><td>□ Primary chondrocytes
→ isolated from post-operative or post-mortem cartilage tissue</td><td>□ 3D culture
- scaffold-free
- with scaffold</td></tr>
<tr><td>□ Stem cells
- MSCs
- iPSCs</td><td>□ Co-culture
- chondrocyte + osteoblasts
- chondrocytes + synoviocytes
- chondrocytes + synoviocytes + osteoblasts

□ Explant culture
- chondral plug
- osteochondral plug</td></tr>
</table>

2.5 An overview of tissue engineering of articular cartilage

Tissue engineering of articular cartilage not only provides therapeutic options in regenerative medicine, but tissue engineering methods also represent a possibility for the development of sophisticated 3D culture systems for *in vitro* OA models [142]. Great efforts have been undertaken over the past few decades to develop tissue engineered cartilage for regenerative therapies treating clinically relevant cartilage defects, mainly in load-bearing joints such as the knee. Advances have been made with regard to the different components of tissue engineered cartilage like 3D culture systems, bioreactors, scaffolds, stem cells and their differentiation protocols [143]. Many clinical trials are testing possibilities for cartilage repair using cell-based tissue-engineered cartilage products. However, challenges remain, such as the mechanical properties of tissue-engineered cartilage-like constructs as well as their long-term

integration in the *in vivo* tissue surrounding the cartilage defect [144]. Cell sources for articular cartilage tissue engineering include chondrocytes from non-articular or articular cartilage or MSCs from different tissue sources. Scaffold-based tissue engineering approaches are based on a wide variety of polymeric materials including natural polysaccharides such as starch and alginate, proteins such as collagens or silk, and synthetic polymers such as polylactic acid and polyglycolic acid [145]. Although scaffolds provide the 3D structure in tissue engineered constructs, there are some disadvantages, especially with regard to the lack of long-term studies regarding the safety and degradation of scaffolds [146]. Thus, scaffold-free tissue engineering approaches are emerging with the aim of creating cartilage-like tissue engineered constructs that are made without a supporting scaffold. Scaffold-free approaches are based on developmental processes of cartilage formation. The formation of cartilage is initiated by mesenchymal condensation in embryonic development [147]. Based on this principle, in scaffold-free cartilage tissue engineering, the self-assembly and self-organization capacities of stem cells are used to generate cell sheet or aggregates as a base for tissue-engineered cartilage-like constructs, which then develop further through cell differentiation, proliferation and the formation of ECM [148]. Several tools have been examined to enhance the properties of the resulting neocartilage. Growth factors, for example the transforming growth factor (TGF) family, as well as dynamic compression have been shown to enhance the formation of ECM in tissue engineered cartilage [149, 150].

In summary, tissue-engineered cartilage constructs, whether scaffold-based or scaffold-free, resemble sophisticated 3D cartilage models that are designed to optimally imitate the features of *in vivo* articular cartilage [142]. However, research on OA pathophysiology and cartilage tissue engineering are still approached from different communities within the field of cartilage research. However, there are great possibilities to improve *in vitro* model systems for the study of OA pathophysiology with the help of recently developed advances in articular cartilage tissue engineering. The understanding of OA pathophysiology and its translation into clinically relevant treatment options to modify the disease progression of OA or heal cartilage defects could be furthered with better *in vitro* model systems.

CHAPTER 3: AIMS AND OBJECTIVES

There is still a lack of knowledge regarding OA pathophysiology. With scaffold-free approaches in cartilage tissue engineering emerging, new possibilities for sophisticated 3D *in vitro* models to study OA pathophysiology can be developed. *In vitro* models based on human cells give the possibility of reducing the number of animals used in experiments, and to enhance the translatability of research findings into the human condition, in particular regarding the identification of regenerative therapeutic options and disease modifying drugs for OA.

Consequently, the aim of this thesis was to evaluate and validate an *in vitro* OA model based on tissue-engineered 3D cartilage-like constructs, sourcing from human mesenchymal stromal cells alone with no scaffold involved (scaffold-free cartilage-like constructs = SFCCs). In the first step, the cartilage-like phenotype of the SFCCs had to be evaluated. In the second step, OA was simulated by stimulating the SFCCs with the predominant pro-inflammatory cytokines in OA, IL-1β and TNFα. To validate the model system, the aim was to describe the major features of OA in SFCCs cultures under pro-inflammatory conditions: these are the upregulation of inflammatory pathways, and cartilage destruction through the expression of matrix degrading enzymes and the breakdown of the ECM.

The experimental work was focused on the following objectives:

(I) To characterize the features of SFCCs cultured under normal conditions and evaluate their cartilage-like phenotype using histology, immunohistochemistry and gene expression analysis.

(II) To establish a histomorphometric method based on hematoxylin and eosin stain to quantify spatial cell distribution within the SFCCs.

(III) To characterize the features of SFCCs cultured under pro-inflammatory conditions and evaluate whether OA-like changes can be measured using histology, immunohistochemistry and gene expression analysis.

(IV) To examine whether some form of regeneration or restoration occurs in SFCCs cultured with pro-inflammatory cytokines, followed by a culture under normal conditions.

CHAPTER 4: MATERIALS AND METHODS

4.1 Materials

4.1.1 Cell sources and bone marrow donors

Bone marrow was obtained from human femoral heads that were explanted during total hip replacement surgery, provided by the Centre for Musculoskeletal Surgery, Charité – Universitätsmedizin Berlin and handed out by the "Tissue Harvesting" Core Facility of the Berlin Brandenburg Centre for Regenerative Therapies (BCRT) under the ethical approval EA1/012/13. In Table 2, details regarding the bone marrow donors are listed.

Table 2: Details regarding cell sources and bone marrow donors

Donor Number	*Sex*	*Age*	*Characterization*	*Type of experiment*
1	female	71	+	Experiments under non-inflammatory conditions: Histology RNA analysis
2	female	56	+	
3	female	85	+	
4	female	59	+	Experiments under non- and pro-inflammatory conditions: Histology RNA analysis Proteomics
5	male	79	+	
6	male	66	+	

Table reproduced and modified from [1]. + = successful hMSC characterization

4.1.2 Cell culture/*in vitro* culture media and supplements

Description	*Manufacturer*	*Country*
DMEM GlutaMAX™ Medium	Thermo Fisher Scientific	Waltham, MA, USA
Gibco™ Penicillin-Streptomycin (10.000 U/mL)		
Gibco™ Trypsin-EDTA (0.05 %)		
StemMACS™ MSC Expansion Media Kit XF, human	Miltenyi Biotech	Bergisch Gladbach, Germany
Fetal Bovine Serum	PAA Laboratories	Cölbe, Germany
L-Ascorbic Acid 2-Phosphate	Sigma-Aldrich	St. Louis, MO, USA
Phosphate-Buffered Saline (PBS)	German Rheumatism Research Center (DRFZ)	Berlin, Germany
Recombinant Human Tumor Necrosis Factor-alpha (rh TNF-alpha)	ImmunoTools	Friesoythe, Germany
Recombinant Human Interleukin-1 beta (rh IL-1beta / IL1F2)		

Description	*Composition*
hMSC Expansion Medium	DMEM GlutaMAX Medium, 20 % (v/v) StemMACS, 10 % (v/v) fetal bovine serum, 100 units/ml penicillin, 0.1 mg/ml streptomycin
Standard Medium	DMEM GlutaMAX Medium, 10 % (v/v) fetal bovine serum, 100 units/ml penicillin, 0.1 mg/ml streptomycin, 9.39 mg/l ascorbic acid

4.1.3 Plasticware / Miscellaneous

Plasticware was purchased from PEQLAB Biotechnologie (Erlangen, Germany), Greiner Bio One (Frickenhausen, Germany), Sarstedt (Nümbrecht, Germany) or Eppendorf (Hamburg, Germany), except for the components in the table below.

Description	*Manufacturer*	*Country*
98 Well PCR Plates	Biozym Scientific	Oldendorf, Germany
Microseal 'B' PCR Plate Sealing Film	Bio-Rad Laboratories	Hercules, CA, USA

4.1.4 Histology and immunohistochemistry agents

Description	*Manufacturer*	*Country*
A) Tissue Embedding and Section Cutting		
16% Paraformaldehyde Aqueous Solution	Electron Microscopy Sciences	Hatfield, PA, Germany
Sucrose (Household sugar)	Südzucker	Mannheim, Germany
SCEM Embedding Medium	Sectionlab	Hiroshima, Japan
Acetone ≥ 99,5 %	Carl Roth	Karlsruhe, Germany
n-Hexane ≥ 95 %, GC Ultra Grade	Carl Roth	Karlsruhe, Germany
Tissue-Tek® O.C.T.™ compound	Sakura Finetek	Staufen, Germany
Cryofilm 2C	Sectionlab	Hiroshima, Japan
Microscopic Slides Superfrost Plus	Menzel-Gläser	Braunschweig, Germany
Microtome Blades SEC 35	Thermo Fisher Scientific	Waltham, MA, USA
B) Hematoxylin/Eosin and Alcian Blue Staining Procedures		
Harris's Hematoxylin Solution	Merck	Darmstadt, Germany
Eosin	Chroma Waldeck	Münster, Germany
Nuclear Fast Red-Aluminum Sulfate Solution		
Alcian Blue 8GX	Sigma-Aldrich	St. Louis, MO, USA

Description	*Manufacturer*	*Country*
Ethanol	Carl Roth	Karlsruhe, Germany
Xylol		
Acetic Acid (glacial) 100%	Merck	Darmstadt, Germany
Hydrochloric Acid (HCl)		
Vitro-Clud® Embedding Medium	R. Langenbrinck	Emmendingen,Germany
Microscope Coverslips 24x50mm	Menzel-Gläser	Braunschweig, Germany
C) Immunohistochemistry		
Phosphate Buffered Saline (PBS)	Biochrom	Berlin, Germany
Hydrogen Peroxide (H_2O_2) Solution	Merck Millipore	Billerica, MA, USA
Bovine Serum Albumin (BSA)	Sigma-Aldrich	St. Louis, MO, USA
Normal Horse Serum	Vector Laboratories	Burlingame, CA, USA
Primary Antibodies:		
▪ **Mouse Monoclonal Antibody to Collagen I (ab6308)** Dilution: 1:500	Abcam	Cambridge, UK
▪ **Collagen Type II Mouse (6B3)** Dilution 1:10	Quartett Immunodiagnostika	Berlin, Germany
Secondary Antibody:		
▪ **Biotinylated Horse Anti-Mouse IgG Antibody**	Vector Laboratories	Burlingame, CA, USA
VECTASTAIN® Elite® ABC HRP Kit	Vector Laboratories	Burlingame, CA, USA
DAB Peroxidase (HRP) Substrate Kit		
Mayer's Hematoxylin	Sigma-Aldrich	St. Louis, MO, USA
Aquatex® Mounting Medium	Merck	Darmstadt, Germany
Microscope Coverslips 24x50mm	Menzel-Gläser	Braunschweig, Germany

4.1.5 Gene expression analysis agents

Description	*Manufacturer*	*Country*
A) Primer Design		
Agarose	Invitrogen	Karlsruhe, Germany
UltraPure™ Ethidiumbromid		
Orange DNA Loading Dye (6X)	Thermo Fisher Scientific	Waltham, MA, USA
GeneRuler DNA Ladder Mix		
Human BioBank cDNA	Primerdesign	Camberley, UK
NucleoSpin Gel and PCR Clean-up	Macherey-Nagel	Düren, Germany
B) RNA Isolation		
RNeasy Fibarous Tissue Mini Kit	QIAGEN	Hilden, Germany
RNase-Free DNase Set		
2-Mercaptoethanol	SERVA Electrophoresis	Heidelberg, Germany
C) cDNA Synthesis		
Sensiscript® RT Kit	QIAGEN	Hilden, Germany
RNAse Inhibitor		
Oligo d(T)$_{16}$ Primer	Thermo Fisher Scientific	Waltham, MA, USA
D) qPCR		
Customized Primer	TIB Molbiol Berlin	Berlin, Germany
DyNAmo ColorFlash SYBR Green qPCR kit	Thermo Fisher Scientific	Waltham, MA, USA
RNAse-Free Water	QIAGEN	Hilden, Germany

4.1.6 Proteomics - Protein extraction and mass spectrometry

Proteomics were performed at the Berlin Institute of Health (BIH) Proteomics Core Facility by Dr. Marieluise Kirchner.

Description	*Manufacturer*	*Country*
Lysyl Endopeptidase, Mass Spectrometry Grade (Lys-C)	FUJIFILM Wako Pure Chemical Corporation	Osaka, Japan
Sequencing Grade Modified Trypsin	Promega	Fitchburg, WI, USA
MonoCap C18 HighResolution 2000	GL Sciences	Eindhoven, Netherlands
EASY-nLC II System	Thermo Fisher Scientific	Waltham, MA, USA
Q Exactive™ Plus Mass Spectrometer		

4.1.7 Instruments

Description	*Manufacturer*	*Country*
CO_2 Cell Culture Incubator	Binder	Tuttlingen, Germany
HeraSafe Cell Culture Bench	Heraeus	Hanau, Germany
Labofuge 400 Centrifuge		
Fresco 17 Microcentrifuge		
Feinwaage	Sartorius	Göttlingen, Germany
CM 1900 Cryotome	Leica Biosystems	Nußloch, Germany
Axioskop 40 Optical Microscope	Carl Zeiss	Oberkochen, Germany
TissueRuptor II	QIAGEN	Hilden, Germany
NanoDrop Spectrophotometer	PeqLab Biotechnologie	Erlangen, Germany
Agilent 2100 Bioanalyzer	Agilent Technologies	Santa Clara, CA, USA
Mx3000P qPCR System		

4.1.8 Software and online service

Description	*Manufacturer*	*Country*
AxioVision Microscopy software	Carl Zeiss	Oberkochen, Germany
FIJI ImageJ 1.52i	Open Source	n.a.
GraphPad Prism V.5	GraphPad Software	San Diego, CA, USA
Sequencing Service	LGS genomics GmbH Berlin	Berlin, Germany
Description	***URL***	
NCBI Nucleotide Database	https://www.ncbi.nlm.nih.gov/nucleotide/	
Primer Database 1	https://pga.mgh.harvard.edu/primerbank/	
Primer Database 2	http://www.rtprimerdb.org/index.php	
NCBI Primer-BLAST Online Tool	https://www.ncbi.nlm.nih.gov/tools/primer-blast/	

4.2 Methods

4.2.1 Human mesenchymal stromal cell culture

The hMSCs were isolated from human bone marrow of patients that underwent total hip replacement surgery and provided by the Center for Musculoskeletal Surgery, Charité – Universitätsmedizin Berlin. All patients gave written consent to the tissue collecting prior to surgery. All protocols and experiments were performed under the ethical approval of the Charité – Universitätsmedizin Berlin Ethics Committee and the principles of the Helsinki Declaration with the ethical approval EA1/012/13. Registration and further distribution of the sample tissues was done by the “Tissue Harvesting” Core Facility of the BCRT. Bone marrow was cultured in 175 ml cell culture flasks with MSC expansion medium containing DMEM GlutaMAX Medium which was substituted with 20 % (v/v) StemMACS, 10 % (v/v) fetal bovine serum, 100 units/ml penicillin and 0.1 mg/ml streptomycin to prevent bacterial contamination. The temperature inside the incubator was set at 37 °C in 5 % CO_2 atmosphere. After the hMSCs within the bone marrow became adherent to the cell culture flask (approximately after 3 to 4 days), medium changes and washing steps with phosphate buffered saline (PBS) were performed weekly. For each donor, the bone marrow and cells were cultured and expanded separately. Before labeling the cells as MSC, they were characterized as such by verifying their adherence to plastic in the standard culture, determining surface marker patterns and analyzing differentiation capacities following standard protocols in our laboratory [151]. Flow cytometry was used to verify the expression of CD90, CD105, CD73 and the lack of expression of CD14, CD20, CD34, CD45, and differentiation assays were performed validating the osteogenic, adipogenic and chondrogenic differentiation capacities of the cells [152]. The cells showing a phenotype characteristic for hMSCs were further cultured with weekly media changes. When cell coverage of the culture flask was high, cells were passaged to promote further expansion up until the 3rd to 5th passage, depending on the growth characteristics of the individual donor cell line. When passaging the cells, trypsin/EDTA (ethylenediaminetetraacetic acid) was used to separate the cells from the culture flask surface with an incubation time of 10 min at 37 °C, before applying DMEM with 10% (v/v) fetal bovine serum to stop the trypsin reaction. Cells were then centrifuged for 10 min at 300 *g*, washed with PBS and resuspended in hMSC expansion medium. Approximately 10^6 cells were used per flask for further expansion.

4.2.2 Scaffold-free cartilage-like constructs

The SFCCs were produced in the laboratory of our cooperation partner Igor Ponomarev at the Research Center of Medical Technology and Biotechnology in Bad Langensalza, Germany, according to a patented method (Patent no. 10 2004 001 225, German Patent and Trademark Office, 2004) [153, 154]. In total, cells of 6 different male and female donors aged between 56 and 85 were used, with each SFCC only containing cells of one single donor (see 4.1.1). Approximately 5 million hMSCs were needed to form one SFCC. The procedure included the centrifugation of cells to allow the formation of a three-dimensional structure via self-organization. A subsequent maturation process involved intermittent mechanical stimulation to promote ECM production. The mature SFCCs were then transferred back to our laboratory where they were cultured for 4 weeks ahead of experiments in a DMEM GlutaMAX Medium containing 10 % (v/v) fetal bovine serum, 100 units/ml penicillin, 0.1 mg/ml streptomycin and 9.39 mg/l ascorbic acid, which is referred to henceforth as the standard medium.

4.2.3 Experimental set-up

In the first step, an experimental set-up was implemented in which 4 SFCCs of three different donors were cultured for up to three weeks in the standard cytokine-free medium to evaluate whether changes occur within the SFCCs in a neutral environment without any pro-inflammatory stimulation. This experimental set-up will henceforth be referred to as ‘normal conditions’. At day 0, day 7, day 14 and day 21, one SFCC of each donor was taken at random and processed for further evaluation. As there was only one sample per donor and timepoint available, gene expression analysis, histology and immunohistochemistry were performed separately on every sample of this experimental set-up. In a second step, an experimental set-up was used comparing SFCCs cultured in neutral standard medium with SFCCs cultured in standard medium substituted with pro-inflammatory cytokines. 50ng/ml recombinant human IL-1β and 100 ng/ml recombinant human TNFα were added to the standard medium to simulate the pro-inflammatory environment of OA. This experimental set-up will henceforth be referred to as ‘pro-inflammatory conditions’. 9 SFCCs of three different donors were cultured for three weeks, with three SFCCs per donor being treated with neutral standard medium (CTL), and 6 SFCCs per donor being treated with standard medium plus IL-1β and TNFα (STIM, REG). After three weeks, the

Table 3: Characteristics of experimental groups

Experimental Group	*Cultivation Conditions*	*Time*
CTL	Neutral standard medium	3 weeks
STIM	Standard medium + 50ng/ml rhIL-1β and 100 ng/ml rhTNFα	3 weeks
REG	Standard medium + 50ng/ml rhIL-1β and 100 ng/ml rhTNFα + Neutral standard medium	3 weeks + 3 weeks

samples for the CTL and STIM group were taken for further analysis. Three SFCCs per donor of those being treated with cytokine-supplemented medium were cultured for three more weeks to investigate whether some form of regeneration might occur (REG). This experimental set-up generated three different sample groups that are listed in Table 3.

Allocation of SFCCs from each donor to the experimental groups was done randomly and further analysis was performed blinded by random numbering of samples. For

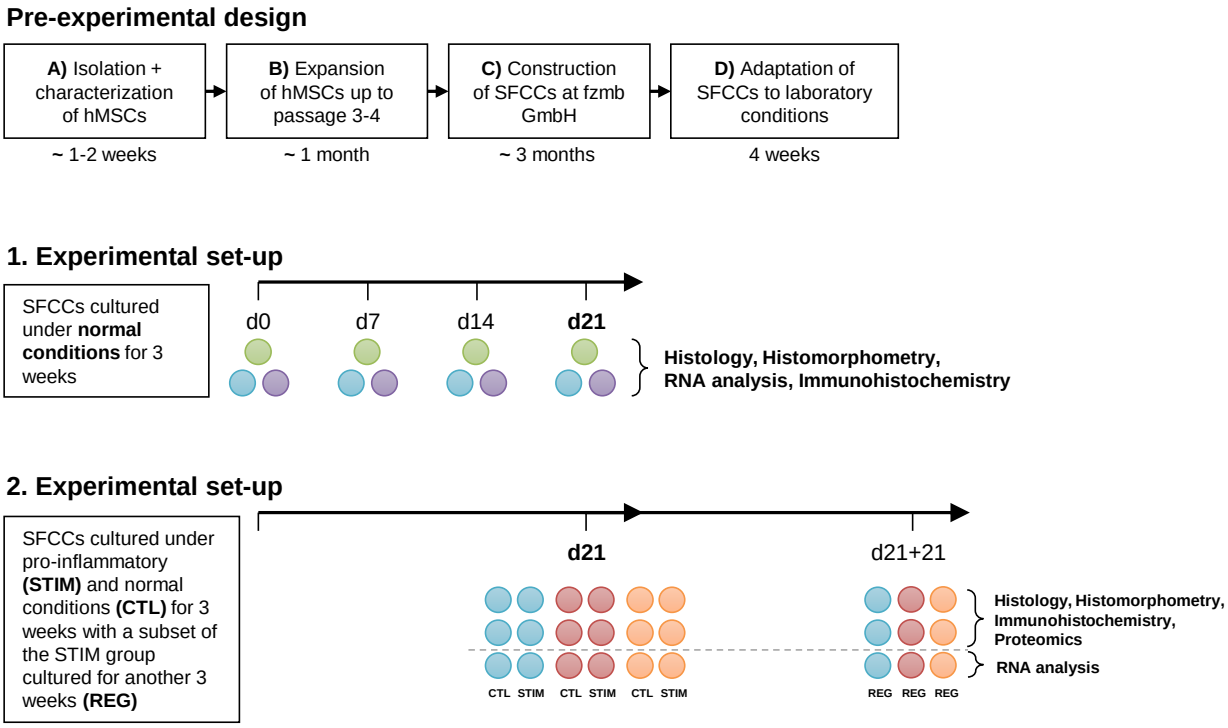

Figure 4: Overview of the experimental set-up
The graphic gives an overview of the experimental set-up including pre-experimental design, the first experimental set-up with SFCCs cultured under normal conditions for 3 weeks and the second experimental set-up with SFCCs cultured under pro-inflammatory conditions. The colored circles represent the SFCCs with each color standing for one donor. Abbreviations: hMSCs = human mesenchymal stromal cells, RNA = ribonucleic acid, d = day. Experimental groups: CTL = control, STIM = pro-inflammatory stimulation, REG = regeneration after pro-inflammatory stimulation.

every experimental group three SFCCs per donor were available, of which one was used for gene expression analysis and two for histology and immunohistochemistry. Figure 4 shows an overview of the experimental set-up.

4.2.4 Histological staining procedures

Cryosections were used for histology to be able to better compare results of the cartilage-like SFCCs with bone-like structures in other experiments as there is no decalcification needed for the cryo-sectioning method described in this paragraph.
SFCCs were either divided in half or quarters for histological analysis and processed as follows. First, the tissue had to be fixated in 4 % paraformaldehyde (PFA) for 6 hours, which was followed by a 24 h treatment with 10 %, 20 % and 30 % sucrose solution for cryopreservation. A cooling bath with dry ice and acetone was used to cool down hexane to around -78 °C to cryo-embed the samples in SCEM embedding medium. Cryo-blocks were then stored at -80 °C prior to sectioning. Cryofilms were used according to the Kawamoto et al. method to prepare cryo-sections on a cryo-microtome set at 8 µm thickness [155]. Histological sections were transported in cooling boxes on dry ice and stored at -80 °C to prevent thawing prior to the staining procedures.

- Hematoxylin/Eosin (HE) staining

Sections were air-dried for at least 20 minutes before they underwent a fixation process with 4 % PFA for 10 minutes. After a 5-minute washing step with distilled water, the first staining step was performed using Harris's hematoxylin solution for 7 minutes with two subsequent washing steps with distilled water. Since Harris's hematoxylin is a regressive hematoxylin stain, a differentiation step in an acidic solution is needed to remove excess stain. In this protocol, 0.25 ml of concentrated hydrochloric acid in 100 ml of 70 % ethanol were used, followed by two circles of washing in tap water for 10 minutes. A second staining step was performed using 0.2 % Eosin for two minutes. Since Eosin is also a regressive stain, differentiation in 96 % ethanol ensued. One washing step in 96 % ethanol and two washing steps in 100 % ethanol (2 min each) were applied, followed by fixating the staining in xylol twice for at least 2 minutes. The stained slides were then covered with Vitro-Clud and fully dried under a fume hood.

- Alcian Blue (AB) staining

Again, sections were airdried for at least 20 minutes before undergoing a fixation process in 4 % PFA for 10 minutes. Alcian blue was used to stain GAGs. It has different staining properties when used at different pH levels. Used at a pH of 2.5 it can bind to non-sulfated GAGs such as hyaluronic acid, the main GAG in cartilage. Thus, after a washing step in distilled water for 5 minutes, sections are preincubated in 3 % acetic acid for 3 minutes before being stained in a solution with 1 % Alcian Blue 8GX in 3 % acetic acid with pH 2.5 for 30 minutes. After a washing step in 3 % acetic acid and one in distilled water, a second staining step was performed using Nuclear fast red-aluminum sulfate solution for a nuclear counterstain. It followed another washing step in distilled water, before dehydrating the section in a graded ethanol series of 80 %, 96 % and 100 %. After two circles of incubation in xylol for at least 2 minutes each, slides were mounted using Vitro-Clud and fully dried under a fume hood.

4.2.5 Immunohistochemistry

Immunohistochemistry was conducted for the detection of type I and type II collagen within cryosections of the SFCCs. After airdrying, the sections were rehydrated with PBS. Firstly, endogenous peroxidase was blocked by incubating the sections with 3% hydrogen peroxide (H_2O_2) for 30 minutes to prevent non-specific background activity. After a washing step with PBS for 5 minutes, a blocking buffer containing 5 % normal horse serum and 2 % bovine serum albumin (BSA) in PBS was applied to prevent non-specific binding of the primary antibody. For the detection of type I collagen, a mouse monoclonal antibody to type I collagen (ab6308, Abcam, UK) was used in a dilution of 1:500, and for the detection of type II collagen a monoclonal antibody to type II collagen (6B3, quartett, Germany) was used in a dilution of 1:10. Incubation was performed overnight at 4 °C. After two washing steps with PBS for 5 minutes each, the sections were incubated with a secondary antibody for 30 minutes, in this case a biotinylated horse anti-mouse antibody. After another two washing steps with PBS for 5 minutes each, the sections were incubated for 50 minutes with the avidin-biotin-peroxidase complex, which was prepared 15 minutes in advance. After two final washing steps with PBS, the peroxidase substrate 3,3′-Diaminobenzidin (DAB) was applied under microscopic control to evaluate the appropriate development time. The peroxidase reaction was then stopped with PBS. After washing the section with distilled water, counterstaining in Mayer’s hematoxylin 1:2 was performed and tap water was used for

bluing of the staining. After washing the sections with distilled water, they were mounted with Aquatex medium, airdried and images were taken shortly after. The Axioskop 40 optical microscope was used to take photos of histological images at 50-, 100- or 200-times magnification with support of the AxioVision microscopy software to perform the white balance and set the scale bars.

4.2.6 RNA isolation and cDNA synthesis

SFCC samples for RNA isolation were frozen at -80 °C up until the isolation procedure. The RNA isolation kit RNeasy Fibrous Tissue Kit by QIAGEN was used to extract the RNA following the protocols provided. Prior to the actual isolation process, the tissue had to homogenized using the TissueRuptor II from QIAGEN and the ECM had to be lysed using proteinase K. RNA concentrations were measured with a NanoDrop spectrophotometer. Before proceeding to the synthesis of complementary DNA (cDNA), RNA integrity was confirmed on an automated electrophoresis Bioanalyzer system. The RNA integrity numbers (RIN) describe the degree of degradation of extracted RNA, with a RIN greater than 7 being classified as sufficient quality. RIN of RNA extracted from SFCCs ranged from RIN 8.2 to 9.1.

For cDNA synthesis, 50 ng RNA per reaction were used and transcribed using the Sensiscript RT Kit from QIAGEN with the addition of an RNase-inhibitor and an incubation time of 1 hour at 37 °C.

4.2.7 Primer design

Gene expression analysis was performed using quantitative polymerase chain reaction (qPCR). Oligonucleotide primers were designed using an online Primer-Basic Local Alignment Search Tool (BLAST) with the messenger RNA (mRNA) sequence of the gene of interest obtained from the National Centre for Biotechnology Information (NCBI) nucleotide databank. The intended length of the PCR product was set to be between around 199 to 250 bases and the estimate annealing temperature at around 60 °C. In some cases, primer databases were used to find primer sequences which were then confirmed via the Primer-BLAST. The customized primers were produced by TIB Molbiol Berlin. For primer verification, they were run on a positive test control in the form of a commercial BioBank cDNA, or a mixture of cDNA from activated human peripheral blood mononuclear cell (PBMCs) and chondrogenic differentiated hMSCs.

To evaluate primer specificity, a melt curve analysis and gel electrophoresis was performed to evaluate them for non-specific qPCR products. For final verification, qPCR products were sequenced using the sequencing service by LGS genomics GmbH Berlin. The primer sequences are listed in Table 4.

Table 4: List of primers

Gene	*Accession No.*	*for. / rev.*	*Primer Sequence*	*Position*	*Amplicon size*
EF1A	NM_001402.6	f	5‘ - GTTGATATGGTTCCTGGCAAGC - 3‘	1267 - 1288	146
		r	5‘ - TTGCCAGCTCCAGCAGCCT - 3‘	1412 - 1394	
COL1A1	NM_000088.4	f	5‘ - CTCCTGACGCACGGCC - 3‘	170 - 185	80
		r	5‘ - CCGTTCTGTACGCAGGTGATT - 3‘	249 - 229	
COL2A1	NM_001844.5	f	5‘ - GTGGGGCAAGACTGTTATCG - 3‘	4280 - 4299	238
		r	5‘ - AGGTCAGGTCAGCCATTCAG - 3‘	4517 - 4498	
COL10A1	NM_000493.4	f	5‘ - CCAGCACGCAGAATCCATCT - 3‘	70 - 89	119
		r	5‘ - TATGCCTGTGGGCATTTGGT - 3‘	188 - 169	
ACAN	NM_001135.3	f	5‘ - AACGCAGACTACAGAAGCGG - 3‘	7606 - 7625	266
		r	5‘ - GGCGGACAAATTAGATGCGG - 3‘	7871 - 7852	
MMP1	NM_002421.4	f	5‘ - CTCTGGAGTAATGTCACACCTCT - 3‘	486 - 508	199
		r	5‘ - TGTTGGTCCACCTTTCATCTTC - 3‘	684 - 663	
MMP3	NM_002422.5	f	5‘ - ATCCTACTGTTGCTGTGCGT - 3‘	79 - 98	246
		r	5‘ - CATCACCTCCAGAGTGTCGG - 3‘	324 - 305	
MMP13	NM_002427.4	f	5‘ - TCCTGATGTGGGTGAATACAATG - 3‘	321 - 343	184
		r	5‘ - GCCATCGTGAAGTCTGGTAAAAT - 3‘	504 - 482	
TNF	NM_000594.4	f	5‘ - GTCTCCTACCAGACCAAG - 3‘	658 - 675	206
		r	5‘ - CAAAGTAGACCCTGCCCAGACTC - 3‘	862 - 841	
IL1B	NM_000576.3	f	5‘ - AGCTACGAATCTCCGACCAC - 3‘	233 - 252	186
		r	5‘ - CGTTATCCCATGTGTCGAAGAA - 3‘	418 - 397	
IL8*	NM_000584.4	f	5‘ - GAATGGGTTTGCTAGAATGTGATA - 3‘	738 - 761	129
		r	5‘ - CAGACTAGGGTTGCCAGATTTAAC - 3‘	866 - 843	
IL6	NM_000600.5	f	5‘ - TACCCCCAGGAGAAGATTCC - 3‘	152 - 171	175
		r	5‘ - TTTTCTGCCAGTGCCTCTTT - 3‘	326 - 307	

Table reproduced and modified from [1]. *EF1A (EEF1A1) = eukaryotic translation elongation factor 1 alpha 1, COL1A1 = collagen type I alpha 1 chain, COL2A1 = collagen type II alpha 1 chain, COL10A1 = collagen type X alpha 1 chain, ACAN = aggrecan, MMP = matrix metallopeptidase, TNF = tumor necrosis factor, IL = Interleukin.* *******IL8 equals CXCL8 (C-X-C motif chemokine ligand 8).*

4.2.8 qPCR

For the quantification of gene expression, qPCR was performed using the qPCR kit DyNAmo ColorFlash SYBR Green at a Mx3000P qPCR System. After optimizing reaction conditions on SFCC RNA samples, a concentration of 500 nM per primer and 1.5 ng cDNA per 20 µl reaction were used. The reaction was performed under the following conditions: 7 minutes of initial denaturation at 95 °C, followed by 45 cycles of denaturation for 5 seconds at 95 °C, 7 seconds of annealing at 57 °C and 9 seconds of elongation at 72 °C. For each sample, three technical replicates were performed for the housekeeper gene *EF1A* (eukaryotic translation elongation factor 1 alpha 1), while for each gene of interest, two technical replicates were performed per sample. A melting curve analysis was performed after every qPCR run. If the melting curve showed a non-specific reaction with other PCR products, the run was repeated. If the amplification curve was below the threshold after 45 cycles, the threshold cycle value (Ct-value) was set at 45. For quantification, the Ct-value of the gene of interest was normalized to the housekeeper gene *EF1A*. The resulting data is shown using the ΔCt-value as $2^{-\Delta Ct}$.

4.2.9 Histomorphometry

A histomorphometric algorithm was developed to analyze histological sections of the SFCC for cell count per area and cell distribution within the SFCCs. The open source image analysis tool FIJI ImageJ 1.52i was used for histomorphometric analysis [156, 157]. To quantify the cell count per tissue area (cells/mm^2), a modified color deconvolution method was used to identify cells within HE stained sections of the SFCC [158].

- Identifying cell count per Total Tissue Area

In overview images of each SFCC at 50 times magnification, the section outline was defined manually using a free hand selection tool. This section outline represents the Total Area (Tt.A.) of one section (Fig. 5.1). Due to histological processing, there were areas within the sections where no tissue was present. These areas were identified manually using the Color Threshold tool, and consequently defined as the Gap Area (Gp.A.). Subtracting the Tt.A. from the Gp.A. defined the Total Tissue Area (Tt.T.A.) (Fig. 5.2). As cell nuclei are stained blue after HE staining, the Color Deconvolution plugin of ImageJ was used to separate the image into the different color layers for

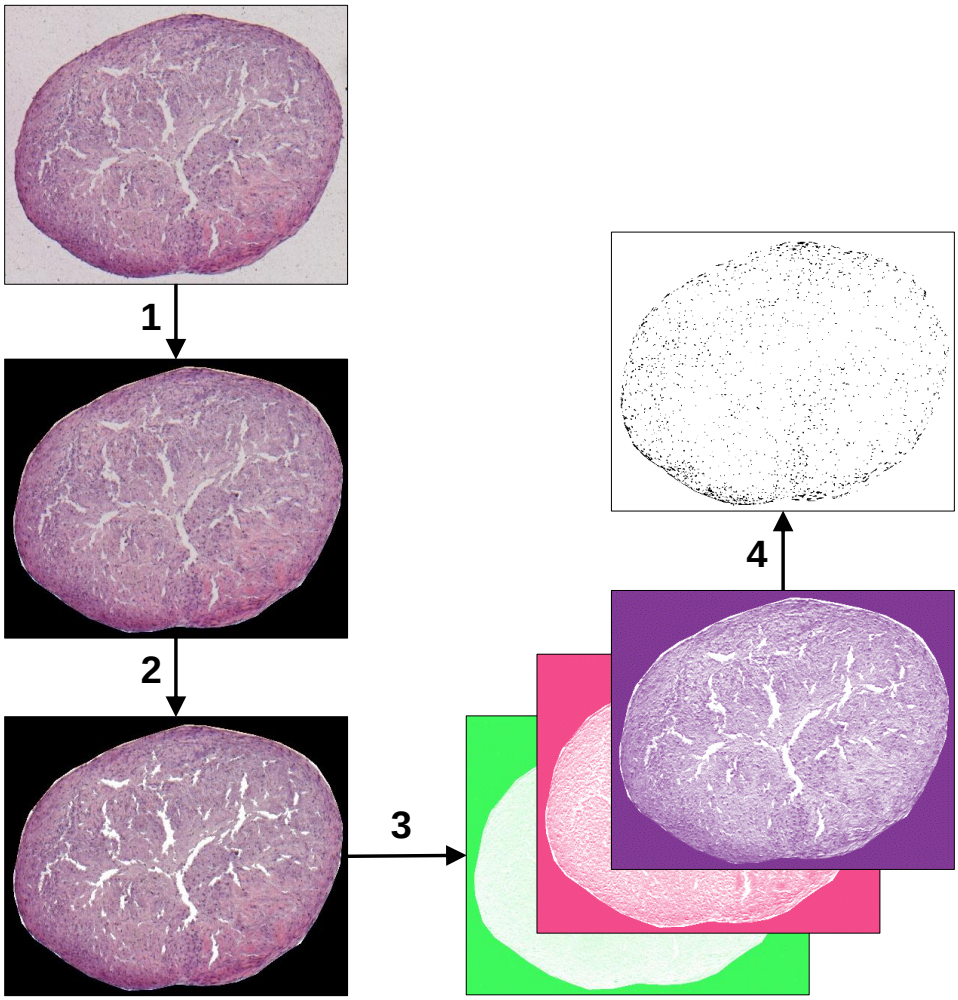

Figure 5: Histomorphometry for identifying cell count per area
Figure and legend reproduced from [1]. **1)** Firstly, the Total Area was defined using the Polygonal Selection tool in ImageJ by encircling the section outline. **2)** The Color Threshold tool of ImageJ was used to identify the areas where no tissue was present. These Gap Areas were subtracted from the Total Area to obtain the Total Tissue Area. **3)** The Color Deconvolution plugin of Fiji ImageJ was used to divide the image into the 3 color channels and the channel for hematoxylin (blue) was selected. **4)** Next, a threshold was applied on the selected color channel to obtain a binary image on which the particle analysis could be performed for the cell count per area [cells/mm2]. All analysis for cell count per area was performed exactly as described on 50x magnification overview images of HE stained sections.

further analysis. The predefined Color Deconvolution vector for HE stains in the Fiji software was applied (Fig. 5.3). The cell nuclei could then be identified with the Threshold tool based on their distinct saturation within the color layer for hematoxylin. After using the Threshold tool, a binary image in form of a black-white matrix was created (Fig. 5.4). In a final step, an approximate cell count was executed on these binary images with the Particle Analysis tool for particles of a pixel size between 5 to 250 pixels. Particles within the binary images greater than 250 did usually cover more than one cell nucleus and cells were thus quantified by manual counting. This resulted

in the cell count per Tt.T.A. which was performed identically for SFCC sections of all experiments.

- Measuring the spatial distribution of cells within SFCC sections

Due to the experimental set-up, SFCCs cultured under normal conditions from the first experimental step were quartered and SFCCs from the second experimental step with pro-inflammatory stimulation were halved before being embedded for histological processing. Thus, the regions of interest (ROIs) for spatial distribution analysis of the cells were defined differently. For SFCCs from the first experimental set-up under normal cultivation condition, the manual selection tool was used to identify an Outer Area (Ot.A.). For SFCCs from the second experimental set-up with pro-inflammatory condition, ROIs for an Outer Area (Ot.A.), an Outer Core Area (Ot.C.A.) and an Inner Core Area (In.C.A.) were defined. The ROI for Tt.A. was reduced in diameter to 0.95 for both, x- and y-axes defining a ROI representing the Ot.A. The outline of the remaining Core Area (C.A.) was then reduced in diameter to 0.5 for both, x- and y-axis defining the ROIs for the Ot.C.A. and In.C.A. The obtained ROIs could then be transferred to the binary images and the cell count was performed as described above, but for each ROI individually. For each SFCC, sections of 2 different layers were histologically stained and histomorphometrically analyzed and the mean of each value

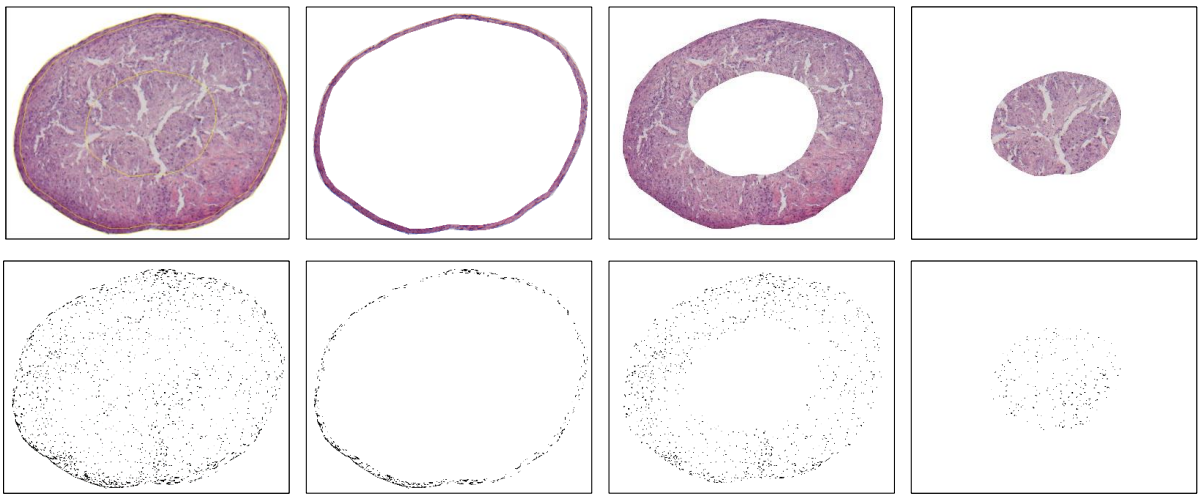

Figure 6: Definition of areas for histomorphometry

Figure and legend reproduced from [1]. To evaluate the cell distribution within different areas of the SFCCs, the 'Total Area' was further divided. The ROI for the 'Total Area' was scaled to 0.95 for x- and y-axes to obtain the 'Outer Area'. The remaining 'Core Area' was then divided into an 'Outer Core Area' and an 'Inner Core Area' by scaling the ROI for the 'Core Area' by 0.5 for the x-and y-axes. The upper row shows the different areas on the original image of the HE stained section, the bottom row shows the areas on the binary image used to identify cell nuclei.

taken for statistical analysis. The final values for cell count per area are always related to the tissue area, i.e. the area of each ROI subtracted by the corresponding gap area. The parameters defined via histomorphometry are listed in Table 5 and visualized in Figure 6.

Table 5: Histomorphometry parameters

Parameter	*Description*	*Abbreviation*	*Unit*
▪ ***Both Experimental Set-ups***			
Total Area	Total section area as determined by a polygonal selection tool in ImageJ based on overview images of full-size sections.	Tt.A.	[mm^3]
Gap Area	Gap or background area of sections determined by a color threshold in ImageJ.	Gp.A.	[mm^3]
Total Tissue Area	Total tissue area determined by the subtraction of Gap Area from Total Area (Tt.A. - Gp.A.)	Tt.T.A.	[mm^3]
Cell count per area	Number of cell nuclei identified by histomorphometry in relation to the Total Tissue Area		[cells/ mm^3]
▪ ***Experimental Set-up 1: Normal Culture Conditions***			
Outer Area	Outer border of SFCC determined by a free hand selection tool in ImageJ.	Ot.A.	[mm^3]
Core Area	Total Area subtracted by Outer Area	C.A.	[mm^3]
▪ ***Experimental Set-up 2: Pro-inflammatory Culture Conditions***			
Outer Area	Outer border of SFCC determined by a reduction of the diameter by 0.95 for x- and y-axes	Ot.A.	[mm^3]
Outer Core Area	Total Area subtracted by Outer Area, diameter reduced by 0.5 for x- and y-axes; the outer part of the remaining area represents the Outer Core Area, the inner part the inner core area.	Ot.C.A.	[mm^3]
Inner Core Area		In.C.A.	[mm^3]

Table reproduced and modified from [1]. The final values for cell count per area in the results chapter are always related to the tissue area, meaning the area of each ROI subtracted by the corresponding gap area.

- Immunohistochemistry quantification

Sections stained immunohistochemically for type I and type II collagen were also analyzed using FIJI ImageJ 1.52i in order to quantify DAB coverage. As the cryofilm method for frozen sections was used for histology, there were issues regarding the adhesions of the section on the cryofilm during the immunohistochemistry procedure. The marginal areas of the sections detached from the cryofilm in several cases, making it impossible to obtain full overview images of immunohistochemically stained sections. When this occured, two to three representative images per section at 100 times magnification were used for DAB coverage quantification and the mean was taken for further analysis. The area that was stained positive was set in relation to the Tt.T.A.,

which was determined by measuring the Tt.A. and Gp.A., as described above. In this case, the Tt.A. was equal to the whole image area and the Gp.A. was determined again using the Color Threshold tool (Fig. 7.1). The DAB positive area indicating the presence of the target antigen, type I or type II collagen, could be measured by using the Color Threshold tool as well (Fig. 7.2). The final values for relative type I/II coverage are always related to the total tissue area (Tt.T.A.), meaning the area of the ROI for Tt.A. subtracted by the Gp.A. For each set of stained sections, the thresholds were defined and validated on several sample images prior to analyzing the whole image set.

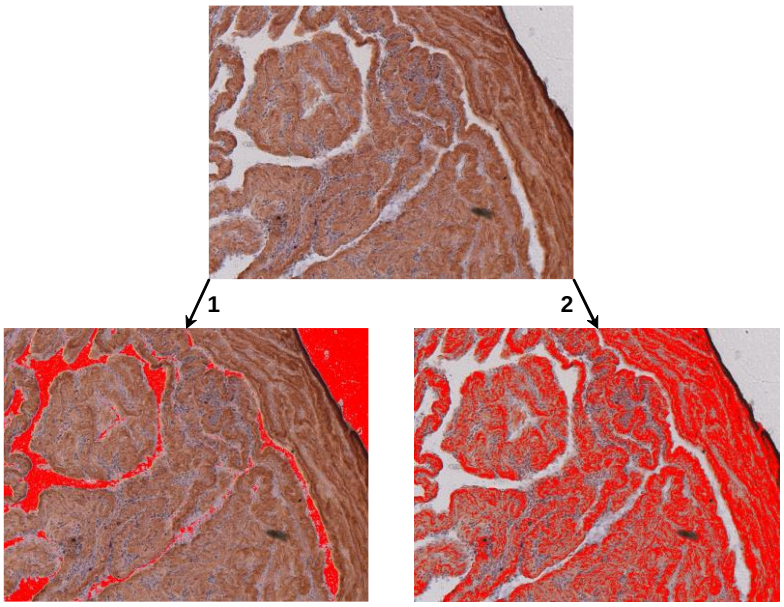

Figure 7: Histomorphometry for immunohistochemistry quantification
100x magnification images of immunohistochemically stained sections were analyzed for relative DAB coverage by (1) identifying the Gap Area (Gp.A.) and (2) the total DAB covered area by using the Color Threshold in ImageJ.

4.2.10 Proteomics – Protein extraction and mass spectrometry

Protein extraction and mass spectrometry were performed at the Berlin Institute of Health (BIH) Proteomics Core Facility by Dr. Marieluise Kirchner who also provided detailed methodological information and critically revised this paragraph. In short, SFCCs samples were cryopulverized and dissolved in 100 µl of 6 M guanidine hydrochloride (pH 5.8) with 20 mM dithiothreitol for protein reduction. Samples were incubated at 95 °C for 10 minutes, sonicated for three times 10 seconds and alkalized with 50 mM chloroacetamide for 30 minutes. 100 µl of 100 mM ammonium bicarbonate buffer (pH 7.8) and 2 µg of the endoproteinase LysC were added, followed by an

incubation for 4 hours at room temperature. After an additional dilution with 100 µl of 100 mM ammonium bicarbonate buffer, 3 µg of sequence-grade trypsin was added to each sample and digestion was performed overnight at room temperature. Samples were acidified using formic acid and the soluble fraction was collected after high speed centrifugation for 15 minutes at 16,000 g. Prior to performing mass spectrometry, peptide samples were desalted and cleaned using the StageTip protocol [159]. For mass spectrometry, 2 µg of sample were used per injection, with two technical replica per sample. Peptides were separated on a 2-meter monolithic column (MonoCap C18 High Resolution 2000) at a flow rate of 300 nl/min on an EASY-nLC II system, using a 404 minute gradient with an increasing Buffer B concentration (from 2% to 60%). Peptides were then measured on a QExactive Plus mass spectrometer. The parameter settings were as follows: full scans were performed at 70K resolution using a $3*10^6$ ion count target and a maximum injection time of 20 milliseconds. MS^2 scans were acquired in Top 10 mode at 17.5K resolution with a $1*10^6$ ion count target, 2 m/z (mass-to-charge ratio) isolation window and maximum injection time of 60 ms. Normalized collision energy was 26 and dynamic exclusion was set to 30 seconds. Data analysis was performed using the MaxQuant software (version 1.5.5.1) [160]. The internal Andromeda search engine was used to search MS^2 spectra against a decoy human Uniprot data base (HUMAN.2017-01) containing forward and reverse sequences. The search included variable modifications of oxidation, N-terminal acetylation and fixed modification of carbamidomethyl cysteine. The minimal peptide length was set to six amino acids and a maximum of three missed cleavages was allowed. The false discovery rate was set to 1% for peptide and protein identifications. Unique and razor peptides were considered for quantification. Copy number calculation and protein abundance in mass / total mass were calculated using the proteomic ruler method by Wiśniewski et al., and based on the total protein amount, average protein concentration (200 g/l) and protein amount per cell (200 pg/cell) [161]. Previous studies on protein analysis of cartilage have shown that standard trypsin preparation prior to mass spectrometry analysis is not sufficient to break up the entire ECM network of cartilage samples [162, 163]. Thus, ECM molecules were excluded, and further quantitative analysis was only performed for the cytokines and proteases that were also analyzed on a gene expression level using qPCR.

4.2.11 Statistical Analysis

The GraphPad Prism V.5 and V.8 software was used for statistical analysis and graph design. For gene expression data, the mean ± standard error of the mean (SEM) and for all other data, the mean ± standard deviation (SD), are shown in the figures. Gaussian distribution could not be presumed due to the small number of samples. No power calculation was performed due to the explorative character of the study and the lack of sufficient preliminary data. Thus, the non-parametric statistical test by Kruskal-Wallis with Dunn's multiple comparison had to be used to statistically analyze for potential differences between experimental groups. Paired analysis was not performed since each SFCC from one donor was assigned one individual replicate on which only one analysis for each outcome was performed. Blind analysis was performed on treatment groups by assigning random numbers to the samples.

CHAPTER 5: RESULTS

5.1 Characterization of SFCCs cultured under normal conditions and evaluation of their cartilage-like phenotype

To evaluate the characteristics of the SFCCs cultured under normal conditions, 4 SFCCs per donor were cultured for three weeks in standard medium without cytokine substitution and samples were taken weekly (d0, d7, d14, d21). Histology, histomorphometry, immunohistochemistry and gene expression analysis were performed on each SFCC (see Fig. 4).

5.1.1 Histological evaluation of SFCCs cultured under normal conditions

HE and AB staining were performed at all timepoints. HE staining showed some structural heterogeneity between the SFCCs; however, no obvious differences were present between the timepoints. Some discontinuities within the ECM could also be observed (Fig. 8, HE). GAGs were identified in all histological sections by AB staining with similar staining intensity at all timepoints, but they were not distributed equally

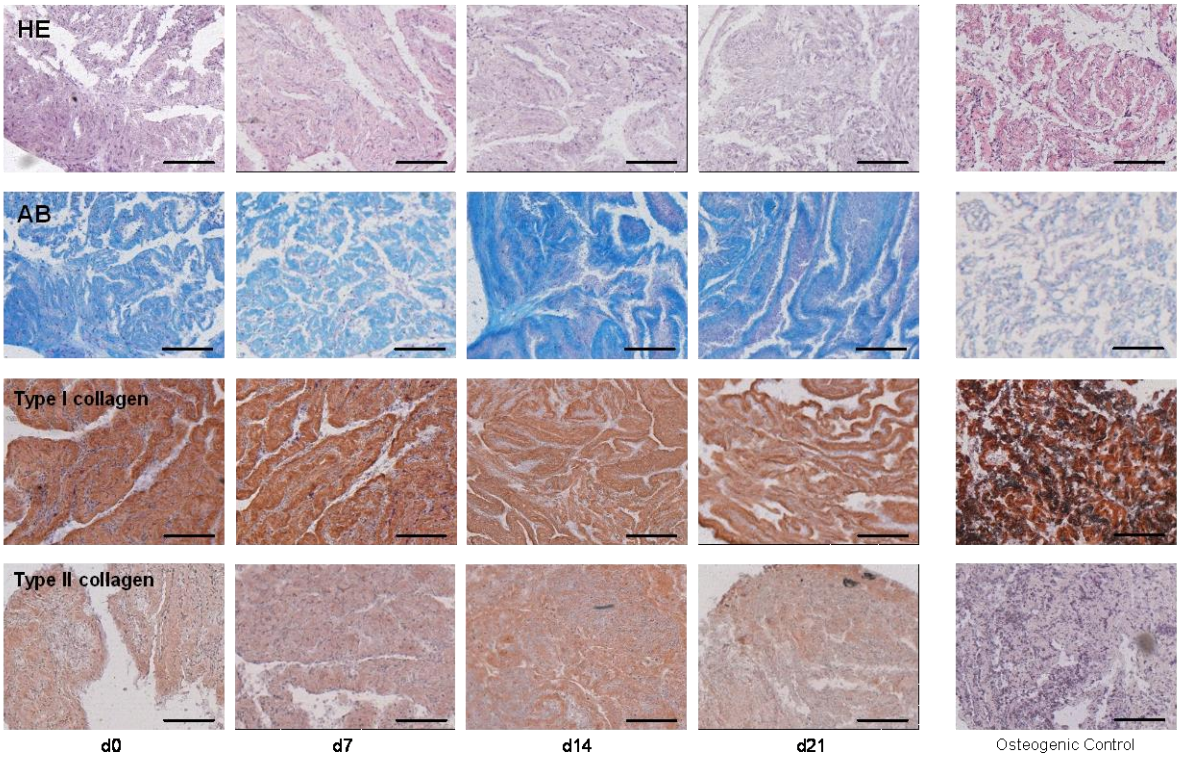

Figure 8: Histological evaluation of SFCCs cultured under normal conditions
Figure and legend reproduced from [1]. Overview over histological sections of SFCCs at d0, d7, d14 and d21. Hematoxylin and Eosin (HE) and Alcian Blue (AB) staining and immunohistochemistry for type I and type II collagen were performed. No obvious microscopic differences could be identified between the timepoints. Comparison with osteogenic controls revealed a lower intensity of AB stain, a higher intensity for type I collagen and no presence of type II collagen in osteogenic controls. Scale bars = 200µm at 100x magnification.

within the ECM, with some areas showing a greater staining intensity than others. When compared to osteogenic controls, AB staining intensity seemed higher in the cartilage-like SFCCs (Fig. 8, AB). Type I and type II collagen were present in all SFCC, with inhomogeneous distribution patterns similar to the AB staining. When compared to osteogenic controls, staining for type I collagen was more prominent, whereas staining for type II collagen was less prominent compared to cartilage-like SFCCs (Fig. 8, Type I/II collagen).

5.1.2 Immunohistochemistry of SFCCs cultured under normal conditions

Both, type I and type II collagen were present within the SFCCs. The intensity and the area covered were higher for type I collagen, with a mean coverage of 50.9 % at d0, 45.6 % at d7, 38.0 % at d14 and 44.5 % at d21. No statistically significant differences between the timepoints was observed (Fig. 9, Table 6). Type II collagen was identified in all SFCCs, with a mean coverage of 24.4 % at d0, 23.6 % at d7, 28.8 % at d14 and 21.1 % at d21. Again, no statistically significant difference was found between the timepoints (Fig. 9, Table 6).

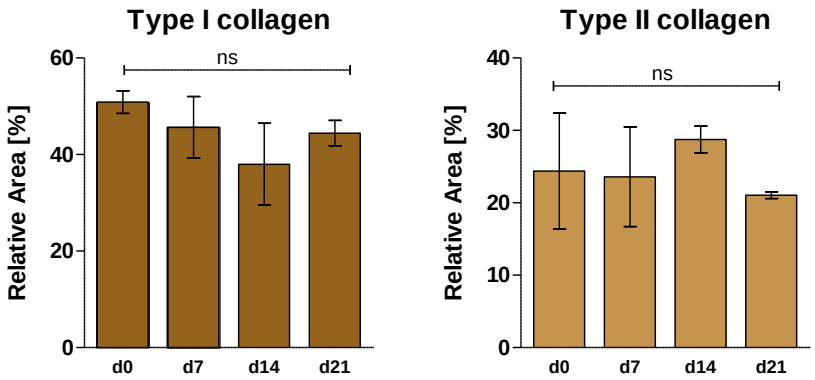

Figure 9: Quantification of immunohistochemical staining for type I and type II collagen in SFCCs cultures under normal conditions
Figure and legend reproduced from [1]. Histomorphometric analysis of immunohistochemical staining for type I and type II collagen. X-axes show timepoints d0, d7, d14 and d21. Y-axes show the relative coverage area in [%]. Bars show mean ± SD. Statistical comparison of groups was performed using the Kruskal-Wallis test and Dunn's multiple comparisons test, ns = $p > 0.05$.

Table 6: Statistical specifications for Figure 9

Specifications	Kruskal-Wallis-Test	
	H	*p*-value
Type I collagen	5.77	*0.12*
Type II collagen	1.97	*0.63*

5.1.3 Histomorphometry of SFCCs cultured under normal conditions

The cell count per area (cell density) was determined from the HE stained section with the histomorphometric method described in Section 4.2.9. The cell density was determined for the Total Area (Tt.A.) and the Outer Area (Ot.A.). The mean cell count per area for the Tt.A. decreased from 1.378 ± 694 cells/mm^2 at d0 to a mean cell count per area of 704 ± 297 cells/mm^2 at d7, 631 ± 28 cells/mm^2 at d14 and 505 ± 268 cells/mm^2 at d21. However, there was no statistically significant difference between timepoints and there was one outlier at d0 (Fig. 10A/B, Table 7). Regarding the cell count per area of the Ot.A., it was generally higher than within the Tt.A., with a mean cell count per area of 1274 ± 734 cells/mm^2 at d0, 883 ± 534 cells/mm^2 at d7, 1122 ± 520 cells/mm^2 at d14 and 1222 ± 384 cells/mm^2 at d21. Again, statistical analysis revealed no difference between the timepoints for cell count per area within the Ot.A. (Fig. 10C/D, Table 7).

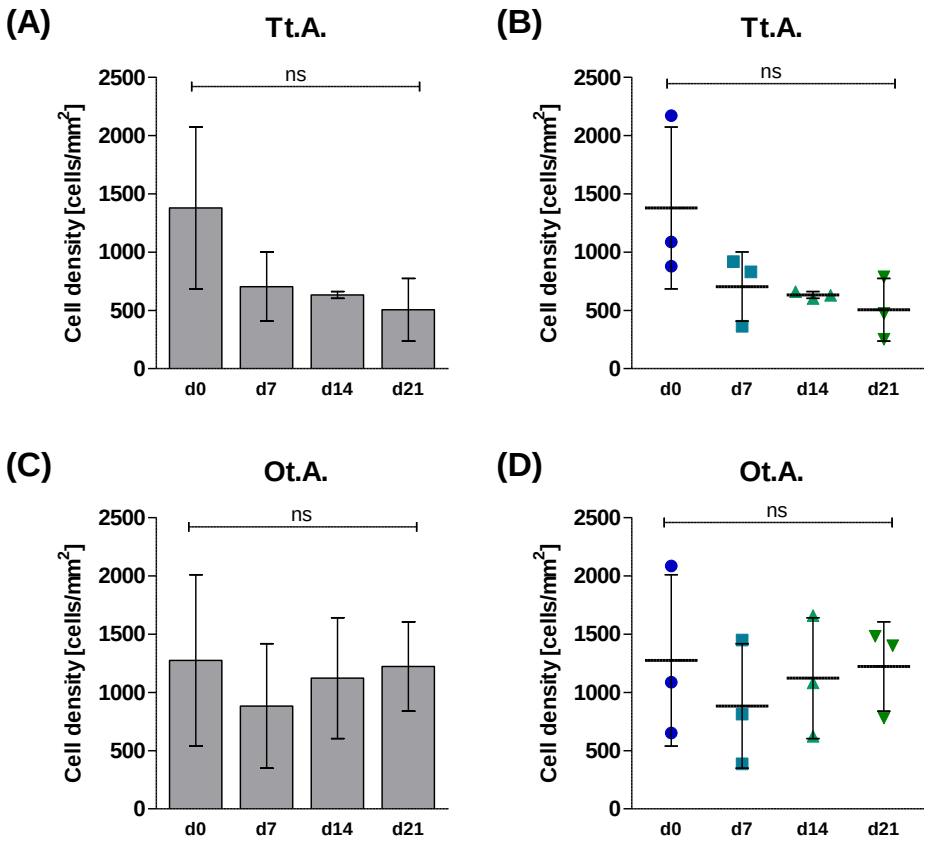

Figure 10: Histomorphometric analysis of SFCCs cultured under normal conditions for cell count per area

(A, C) Figure and legend reproduced from [1]. Cell count per area (cell density) was measured using histomorphometric analysis for the total area (Tt.A.) and the outer area (Ot.A.). X-axes show the timepoints d0, d7, d14 and d21. Y-axes show the relative cell density in [cells/mm^2]. **(A, C)** Bars show mean ± SD. **(B, D)** Single values for each individual sample are depicted to identify outliers. Lines show mean ± SD. Statistical comparison of groups was performed using the Kruskal-Wallis test and Dunn's multiple comparisons test, ns = $p > 0.05$.

Table 7: Statistical specifications for Figure 10

Specifications	Kruskal-Wallis-Test	
	H	*p*-value
Cells – Tt.A.	6.39	*0.79*
Cells – Ot.A.	0.15	*0.9*

5.1.4 Gene expression analysis of SFCCs cultured under normal conditions

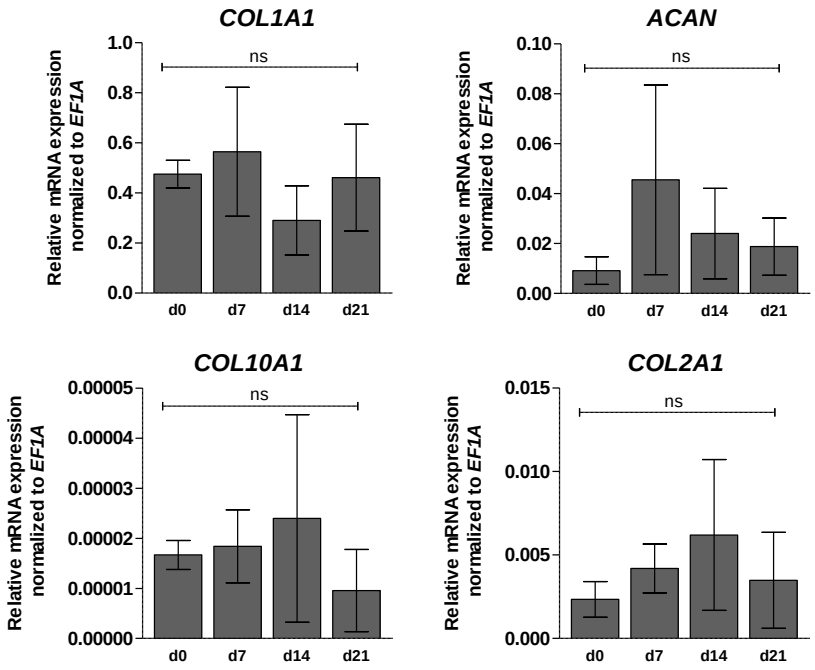

Figure 11: Gene expression analysis of SFCCs cultured under normal conditions
Figure and legend reproduced from [1]. Gene expression analysis was performed by qPCR for *COL1A1, COL2A1, COL10A1* and *ACAN*. X-axes show the timepoints d0, d7, d14 and d21. Y-axes show the relative mRNA expression normalized as 2^-ΔCt to the housekeeper gene *EF1A*. Graph bars show mean ± SEM. Statistical comparison of groups was performed using the Kruskal-Wallis test and Dunn's multiple comparisons test, ns = p > 0.05.

Table 8: Statistical specifications for Figure 11

Specifications	Kruskal-Wallis-Test	
	H	*p*-value
COL1A1	2.93	*0.62*
COL2A1	7.45	*0.09*
ACAN	2.23	*0.74*
COL10A1	4.57	*0.37*

To analyze the gene expression patterns of the SFCC cultured under normal conditions, qPCR was performed for *COL1A1* (collagen type I alpha 1 chain)*, COL2A1* (collagen type II alpha 1 chain)*, ACAN* (aggrecan) and *COL10A1* (collagen type X alpha 1 chain)*.* The data is represented as relative mRNA expression normalized to

the housekeeper gene *EF1A* (eukaryotic translation elongation factor 1 alpha 1). The cartilage specific markers *COL2A1* and *ACAN* were expressed within the SFCCs at all timepoints, with no statistically significant difference between the timepoints. The mean relative expression for *COL2A1* was 0.0023 at d0, 0.0041 at d7, 0.0062 at d14 and 0.0035 at d21. The mean relative expression for *ACAN* was 0.0092 at d0, 0.046 at d7, 0.024 at d14 and 0.019 at d21. However, the expression of *COL1A1* was higher in all SFCCs compared to *COL2A1,* with a mean relative expression of 0.48 at d0, 0.5647 at d7, 0.2903 at d14 and 0.4613 at d21. *COL1A1* is a marker of fibrous cartilage, but not articular cartilage. *COL10A1*, a marker of chondrocyte hypertrophy was expressed in all SFCCs, but at a much lower expression level with a mean relative expression of $1.67*10^{-5}$ at d0, $1.84*10^{-5}$ at d7, $2.40*10^{-5}$ at d14 and $0.95*10^{-5}$ at d21 (Fig. 11, Table 8).

To summarize, the SFCCs showed a stable phenotype over the experimental period of three weeks with cartilage-like features. The cartilage specific markers *COL2A1* and *ACAN* were both expressed, as illustrated by qPCR analysis. On a protein level, type II collagen could be detected using immunohistochemistry. GAGs, one of the main components of the ECM in articular cartilage, were identified by AB staining of histological sections of the SFCCs. However, the expression of *COL1A1* and the high coverage for type I collagen in immunohistochemically stained sections indicate a phenotype similar to fibrous cartilage rather than hyaline cartilage.

5.2 Characterization of SFCCs cultured under pro-inflammatory conditions and evaluation of their OA-like phenotype

After having evaluated the cartilage-like phenotype of the SFCCs when cultured under normal conditions, the feasibility of using SFCCs as an *in vitro* model for the study of OA had to be validated. Thus, the SFCCs were stimulated for three weeks with the two predominant pro-inflammatory and catabolic cytokines in the pathogenesis of OA, IL-1β (50 ng/ml) and TNFα (100 ng/ml). As shown above, the SFCCs show a stable phenotype over the culture period of three weeks. Therefore, samples were only taken at d21 for the control group (CTL) and the cytokine-stimulated group (STIM). A subset of cytokine-treated SFCCs was cultured for three more weeks after d21 in cytokine-free standard medium to evaluate whether changes induced by IL-1β and TNFα could be reversed within the SFCCs. Samples of this group (REG) were thus taken at

d21+21. Histology, histomorphometry, immunohistochemistry, gene expression and proteomics analysis were performed to evaluate phenotypical changes between the treatment groups.

5.2.1 Macroscopic evaluation of SFCCs cultured under pro-inflammatory conditions

Macroscopic evaluation of the SFCCs showed tissue swelling and a volume increase in cytokine stimulated SFCCs (STIM) compared to controls (CTL). This seemed to be reversed after another three weeks of cytokine-free treatment (REG) (Fig. 12A). The wet weight of the SFCCs was measured at d21 (CTL, STIM) and d21+21 (REG) prior to processing of the samples. Cytokine stimulated SFCCs had a higher mean wet weight compared to CTL and REG, with a mean wet weight of 23.6mg for CTL, 39.4mg for STIM and 25.2mg for REG (Fig. 12B). This supports the suggestion that tissue swelling within the SFCCs happened to some degree upon cytokine stimulation. However, the exact volume of the SFCCs was not measured and differences in wet weight between the treatment groups were not statistically significant.

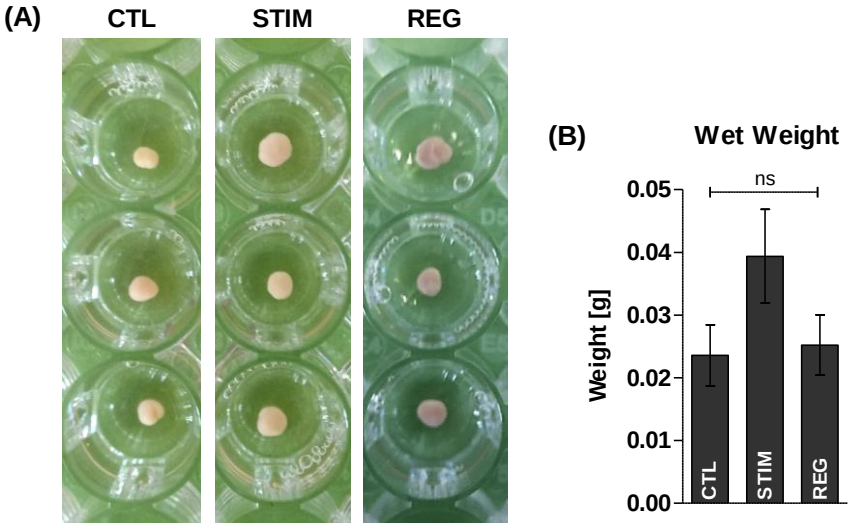

Figure 12: Macroscopic changes and weight changes in SFCCs cultured under pro-inflammatory conditions

Figure and legend reproduced from [1]. **(A)** Macroscopic overview over the SFCCs from one donor with the vertical columns showing the different treatment groups. **(B)** Wet weight of SFCCs prior to processing of samples. X-axis shows weight in [g], y-axis shows treatment groups CTL (control), STIM (pro-inflammatory stimulation) and REG (regeneration). Bars show mean ± SD. Statistical comparison of groups was performed using the Kruskal-Wallis test and Dunn's multiple comparisons test, ns = $p > 0.05$.

5.2.2 Histological evaluation of SFCCs cultured under pro-inflammatory conditions

Histological assessment of HE stained sections of the SFCCs stimulated with IL-1β and TNFα showed morphological changes compared to controls that support the macroscopic observations of tissue swelling in the STIM group. Microscopically, increased water retention and decreased compactness of the ECM was visible. The superficial layer of the SFCCs showed signs of maceration with pronounced discontinuities of the matrix and changes in cell shape (Fig. 13).

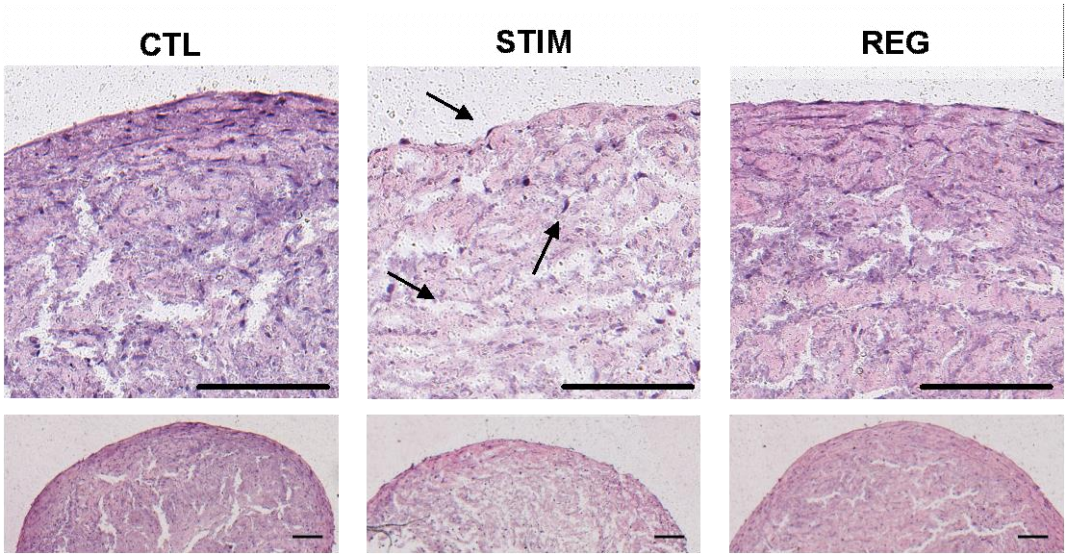

Figure 13: Histological evaluation of SFCCs cultured under pro-inflammatory conditions
Figure and legend reproduced from [1]. HE stained sections of the CTL (control), STIM (pro-inflammatory stimulation) and REG (regeneration), with exemplary images for each condition at 200x magnification (upper row) and 50x magnification (bottom row). Arrows point at morphological changes in the STIM group such as water retention, decreased ECM (extracellular matrix) compactness and changes in cell shape.

5.2.3 Histomorphometry of SFCCs cultured under pro-inflammatory conditions

To quantify the cell count per area and the spatial distribution of cells within the SFCCs, histomorphometry was performed to identify the cell count per area for the Tt.A. (Total Area), as well as the different regions, i.e. the Ot.A. (Outer Area), Ot.C.A. (Outer Core Area) and In.C.A. (Inner Core Area). For all groups, cell count per area was significantly higher in the Ot.A. compared to the Ot.C.A. showing the spatial distribution of cells within the SFCCs. When looking at the different areas, the cell count per area changed between the treatment groups. The cell count per area decreased in the cytokine stimulated group (STIM) compared to CTL in all areas except for the In.C.A. Mean cell

count per area was 533 ± 95 (CTL) and 257 ± 38 (STIM) within the Tt.A., 911 ± 207 (CTL) and 523 ± 160 (STIM) within the Ot.A. and 494 ± 89 (CTL) and 222 ± 28 (STIM) within the Ot.C.A. The cell count per area was also generally lower in the REG group compared to CTL, but differences were only statistically significant in the Ot.C.A., with a mean of 271 ± 99 for REG (Fig. 14, Table 9). The cell count per area (cell density) was defined as relative cell count per total tissue area for all regions (Tt.A., Ot.A., Ot.C.A. and In.C.A.) in order to avoid the interference of changes in the gap area due to water retention on the outcome measurements.

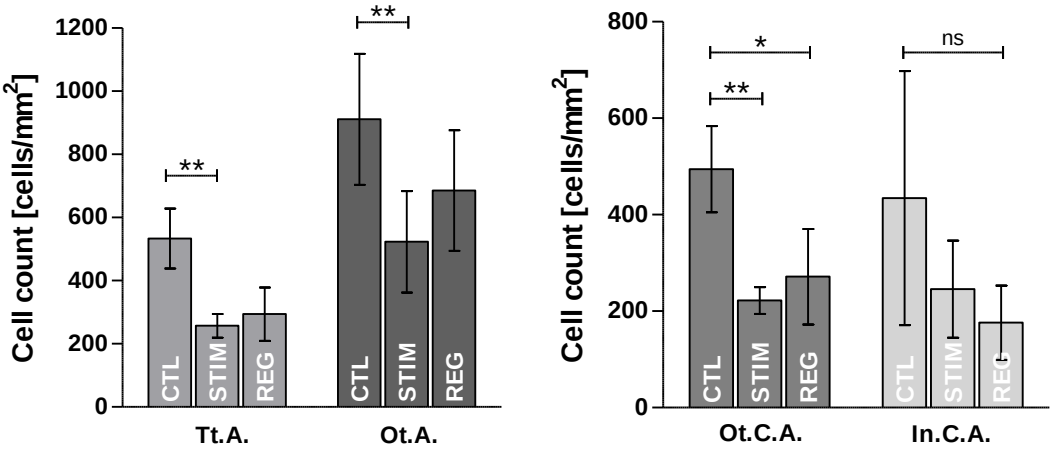

Figure 14: Histomorphometric analysis of SFCCs cultured under pro-inflammatory conditions for cell count per area

Figure and legend reproduced from [1]. Histomorphometry was performed to obtain the cell count per area (cell density) as relative cell count per total tissue area for the regions: total area (Tt.A.), outer area (Ot.A.), outer core area (Ot.C.A.) and inner core area (In.C.A.). X-axes show areas and treatment groups CTL (control), STIM (pro-inflammatory stimulation) and REG (regeneration), y-axes show cell count as [cells/m3], bars indicate mean ± SD. Statistical comparison of groups was performed using the Kruskal-Wallis test and Dunn's multiple comparisons test, ns = $p > 0.05$, * = $p < 0.05$, ** = $p < 0.01$.

Table 9: Statistical specifications for Figure 14

Specifications	**Kruskal-Wallis-Test**	
	H	*p*-value
Tt.A.	10.71	*0.001*
Ot.A.	9.36	*0.004*
Ot.C.A.	10.33	*0.002*
In.C.A.	5.07	*0.075*
Specifications	**Dunn's multiple comparisons test**	
	Comparison	Adjusted *p*-value
Tt.A.	CTL vs. STIM	*0.005*
	STIM vs. REG	*0.99*
	CTL vs. REG	*0.05*
Ot.A.	CTL vs. STIM	*0.007*
	STIM vs. REG	*0.48*
	CTL vs. REG	*0.30*
Ot.C.A.	CTL vs. STIM	*0.008*
	STIM vs. REG	*0.99*
	CTL vs. REG	*0.03*

5.2.4 Immunohistochemistry of SFCCs cultured under pro-inflammatory conditions

Immunohistochemistry was performed for type I and type II collagen and the relative coverage area was determined as described above. Type I collagen coverage was similar in all treatment groups, with a mean coverage of 24.5 ± 5.3 % for CTL, 26.2 ± 4.7 % for STIM and 22.0 % ± 8.4 for REG. No statistically significant difference between groups was observed. Type II collagen coverage was lower after pro-inflammatory stimulation (STIM) and in the REG group compared to controls (CTL), with the difference between CTL and REG being statistically significant. The mean type II collagen coverage was 25.3 ± 4.7 % for CTL, 14.4 ± 5.5 % for STIM and 8.8 ± 5.9 % for REG (Fig. 15, Table 10).

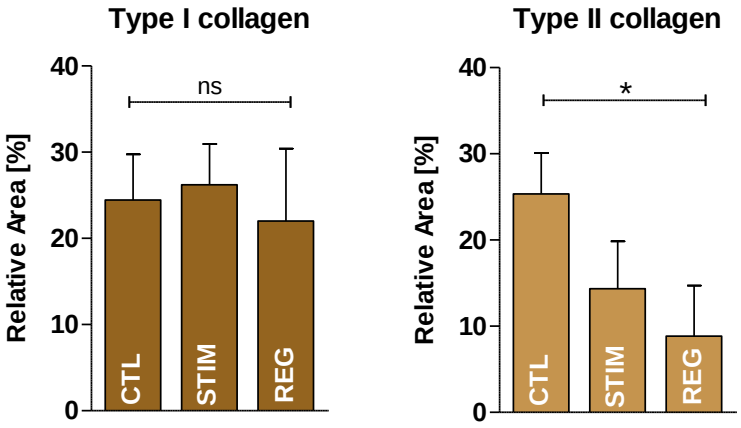

Figure 15: Changes in immunohistochemistry for type I and type II collagen in SFCCs cultures under pro-inflammatory conditions
Figure and legend reproduced from [1]. Relative coverage area for type I and II collagen was determined by immunohistochemistry. X-axes show regions and treatment groups CTL (control), STIM (pro-inflammatory stimulation) and REG (regeneration), y-axes show relative area in [%], bars indicate mean ± SD. Statistical comparison of groups was performed using the Kruskal-Wallis test and Dunn's multiple comparisons test, ns = $p > 0.05$, *$p < 0.05$.

Table 10: Statistical specifications for Figure 15

Specifications	Kruskal-Wallis-Test	
	H	*p*-value
Type I collagen	2.68	*0.27*
Type II collagen	8.59	*0.006*
Specifications	**Dunn's multiple comparisons test**	
	Comparison	Adjusted *p*-value
Type II collagen	CTL vs. STIM	*0.20*
	STIM vs. REG	*0.68*
	CTL vs. REG	*0.01*

5.2.5 Gene expression analysis of SFCCs cultured under pro-inflammatory conditions

Gene expression was performed using qPCR for the ECM components *COL1A1*, *COL2A1*, *ACAN* and *COL10A1*, the proteases *MMP1*, *MMP3* and *MMP13* and the pro-inflammatory cytokines *IL1, IL6, IL8* and *TFN.* The data is represented as relative mRNA expression normalized to the housekeeper gene *EF1A* (Fig. 16, Table 11). *COL1A1* was significantly downregulated in SFCCs cultured under pro-inflammatory stimulation with IL-1β and TNFα (STIM) compared to controls (CTL) with a mean relative expression of 0.718 ± 0.283 for CTL and 0.021 ± 0.005 for STIM. *COL1A1* expression partially recovered after three weeks of cytokine-free culture to a mean relative expression of 0.278 ± 0.067 for REG, although not statistically significant. The gene expression of the cartilage specific markers *COL2A1* and *ACAN* was downregulated in the cytokine-stimulated SFCCs from a mean relative expression of $9.55*10^{-4}$ ± $2.16*10^{-4}$ (*COL2A1*) and 0.020 ± 0.006 (*ACAN*) in the CTL group, to $4.60*10^{-4}$ ± $2.42*10^{-4}$ (*COL2A1*) and $5.7*10^{-4}$ ± $0.4*10^{-4}$ (*ACAN*) in the STIM group. However, the differences were not statistically significant with a *p*-value of 0.1 for *COL2A1* and 0.5 for *ACAN*. The gene expression of *COL10A1*, a marker for chondrocyte hypertrophy, was very low in the STIM group with an absolute Ct-value of 45 for two out of three SFCCs. However, in the REG group the expression of *COL10A1* seemed to be numerically upregulated compared to CTL (Fig. 16A, Table 11). The pro-inflammatory treatment of the SFCCs significantly increased the expression of the cytokines *IL1*, *IL6* and *IL8* in the STIM group compared to untreated controls. The mean relative expression was $1.5*10^{-7}$ ± $0.4*10^{-7}$ (CTL) and 0.033 ± 0.004 (STIM) for *IL1*, $9.0*10^{-4}$ ± $4.2*10^{-4}$ (CTL) and 0.44 ± 0.06 (STIM) for *IL6* and $1.9*10^{-3}$ ± $1.2*10^{-3}$ (CTL) and 4.25 ± 0.96 (STIM) for *IL8*. Although the relative expression of these three cytokines was again numerically lower in the REG group compared to STIM, there was no statistically significant difference (Fig. 16B, Table 11). The relative expression of *TNF* did not differ between the experimental groups. The gene expression of *MMP1* and *MMP3* was also significantly increased in the SFCCs cultured under pro-inflammatory conditions compared to controls, from a mean relative expression of 0.0014 ± 0.0011 (*MMP1*) and $8.6*10^{-6}$ ± $8.4*10^{-6}$ (*MMP3*) in the CTL group to a mean relative expression of 0.0949 ± 0.0378 (*MMP1*) and 0.56 ± 0.25 (*MMP3*) in the STIM group. Similarly to the gene expression patterns of *IL1*, *IL6* and *IL8*, the gene expression of *MMP1* and *MMP3* was numerically lower in the REG group, but with no

statistically significant difference to the STIM group. The expression of *MMP13* did not differ between the treatment groups (Fig. 16C, Table 11).

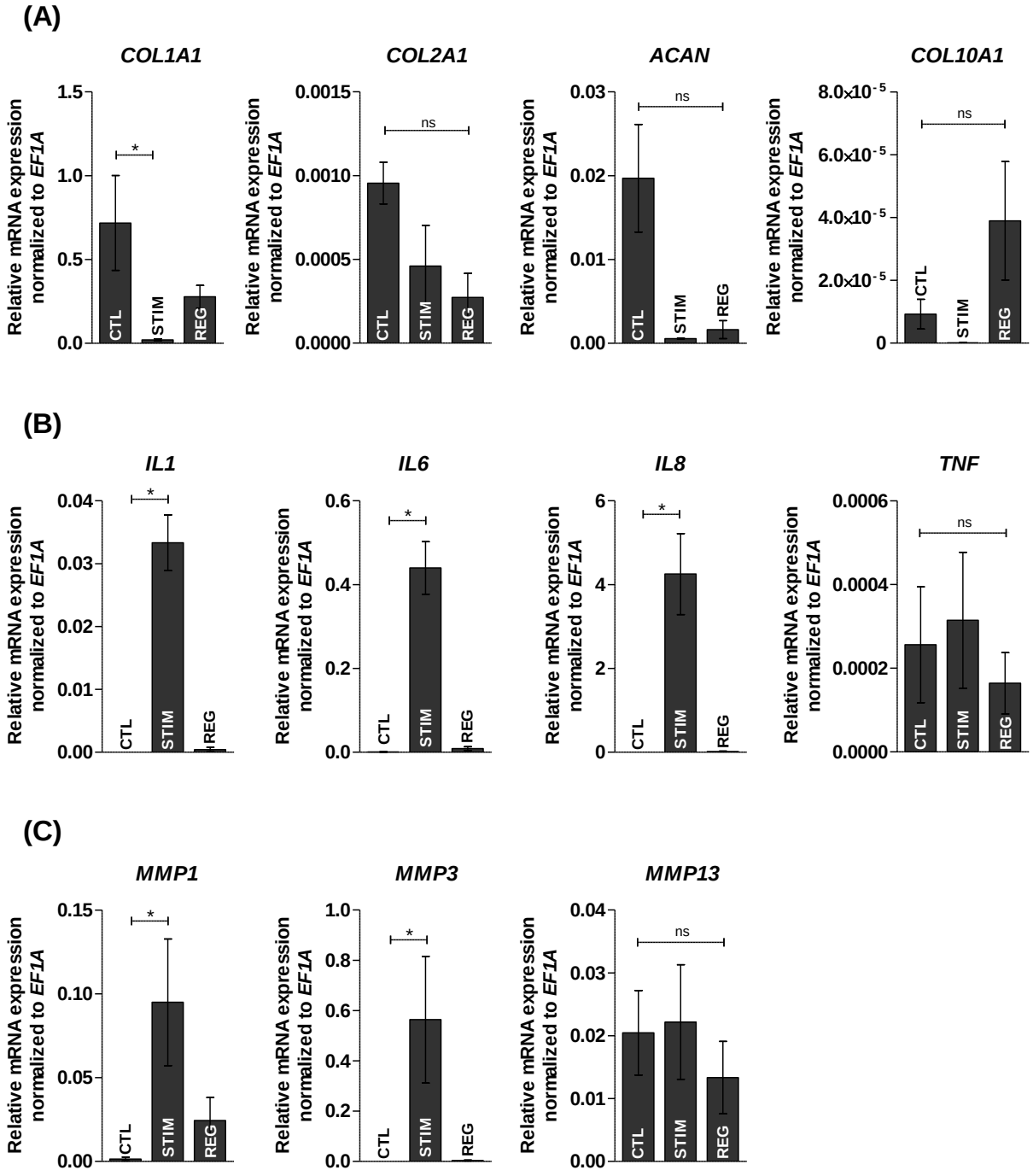

Figure 16: Gene expression analysis of SFCCs cultured under pro-inflammatory conditions
Figure and legend reproduced from [1]. Gene expression analysis was performed by qPCR for (**A**) *COL1A1*, *COL2A1* and *ACAN* **(B)** *IL1*, *IL6*, *IL8* and *TNF* and **(C)** *MMP1*, *MMP3* and *MMP13*. X-axes show the experimental groups for controls (CTL), pro-inflammatory stimulation (STIM) and regeneration (REG). Y-axes show the relative mRNA expression normalized as 2^-ΔCt to the housekeeper gene *EF1A*. Graph bars show mean ± SEM. Statistical comparison of groups was performed using the Kruskal-Wallis test and Dunn's multiple comparisons test, ns = $p > 0.05$, * = $p < 0.05$.

Table 11: Statistical specifications for Figure 16

Specifications	Kruskal-Wallis-Test	
	H	*p*-value
COL1A1	6.49	*0.012*
COL2A1	4.62	*0.1*
ACAN	5.60	*0.05*
COL10A1	5.96	*0.03*
IL1	7.2	*0.004*
IL6	7.2	*0.004*
IL8	0.49	*0.01*
TNF	0.36	*0.88*
MMP1	6.49	*0.01*
MMP3	7.2	*0.004*
MMP13	1.16	*0.63*
Specifications	**Dunn's multiple comparisons test**	
	Comparison	Adjusted *p*-value
COL1A1	CTL vs. STIM	*0.03*
	STIM vs. REG	*0.41*
	CTL vs. REG	*0.89*
IL1	CTL vs. STIM	*0.02*
	STIM vs. REG	*0.54*
	CTL vs. REG	*0.54*
IL6	CTL vs. STIM	*0.02*
	STIM vs. REG	*0.54*
	CTL vs. REG	*0.54*
IL8	CTL vs. STIM	*0.03*
	STIM vs. REG	*0.41*
	CTL vs. REG	*0.89*
MMP1	CTL vs. STIM	*0.03*
	STIM vs. REG	*0.41*
	CTL vs. REG	*0.89*
MMP3	CTL vs. STIM	*0.02*
	STIM vs. REG	*0.54*
	CTL vs. REG	*0.54*

In summary, the pro-inflammatory stimulation of the SFCCs using IL-1β and TNFα led to the significant upregulation of the cytokines *IL1*, *IL6* and *IL8,* as well as the proteases *MMP1* and *MMP3*. In the REG group, these changes were numerically reversed, but not statistically significantly. Additionally, a significant downregulation for *COL1A1* and a trend towards downregulation of *COL2A1* and *ACAN* was observed after pro-inflammatory stimulation. No differences between the experimental groups were observed for the expression of *TNF* and *MMP13*.

5.2.6 Proteomics of SFCCs cultured under pro-inflammatory conditions

Protein expression patterns of the cytokines IL-1β, IL-6, IL-8 and TNF, as well as the proteases MMP-1, -3 and -13 were assessed using the proteomics data set obtained with shot gun mass spectrometry. The protein expression data is presented as relative

abundance in mass/total mass. For IL-1β and IL-8, protein expression was significantly higher in the STIM group compared to the CTL group, with a mean relative abundance of $3.26*10^{-6}$ (CTL) and $28.12*10^{-6}$ (STIM) for IL-1β and $89.49*10^{-6}$ (CTL) and $1813.68*10^{-6}$ (STIM) for IL-8. In the REG group, the protein expression levels of these two cytokines was numerically but not statistically significantly downregulated compared to the STIM group, with a mean relative abundance of $4.06*10^{-6}$ (REG) for IL-1β and $256.40*10^{-6}$ (REG) for IL-8. For IL-6 and TNF, protein expression was significantly upregulated in both the STIM and the REG group compared to controls, with a mean relative protein expression of $16.48*10^{-6}$ (CTL), $249.64*10^{-6}$ (STIM) and $378.99*10^{-6}$ (REG) for IL-6 and 0 (CTL), $56.00*10^{-6}$ (STIM) and $50.03*10^{-6}$ (REG) for TNF (Fig. 17, Table 12). Regarding the proteases MMP-1 and -3, they were both upregulated on a protein level in the SFCCs cultured under pro-inflammatory conditions compared to controls. MMP-3 was numerically but not statistically significantly downregulated in the REG group.

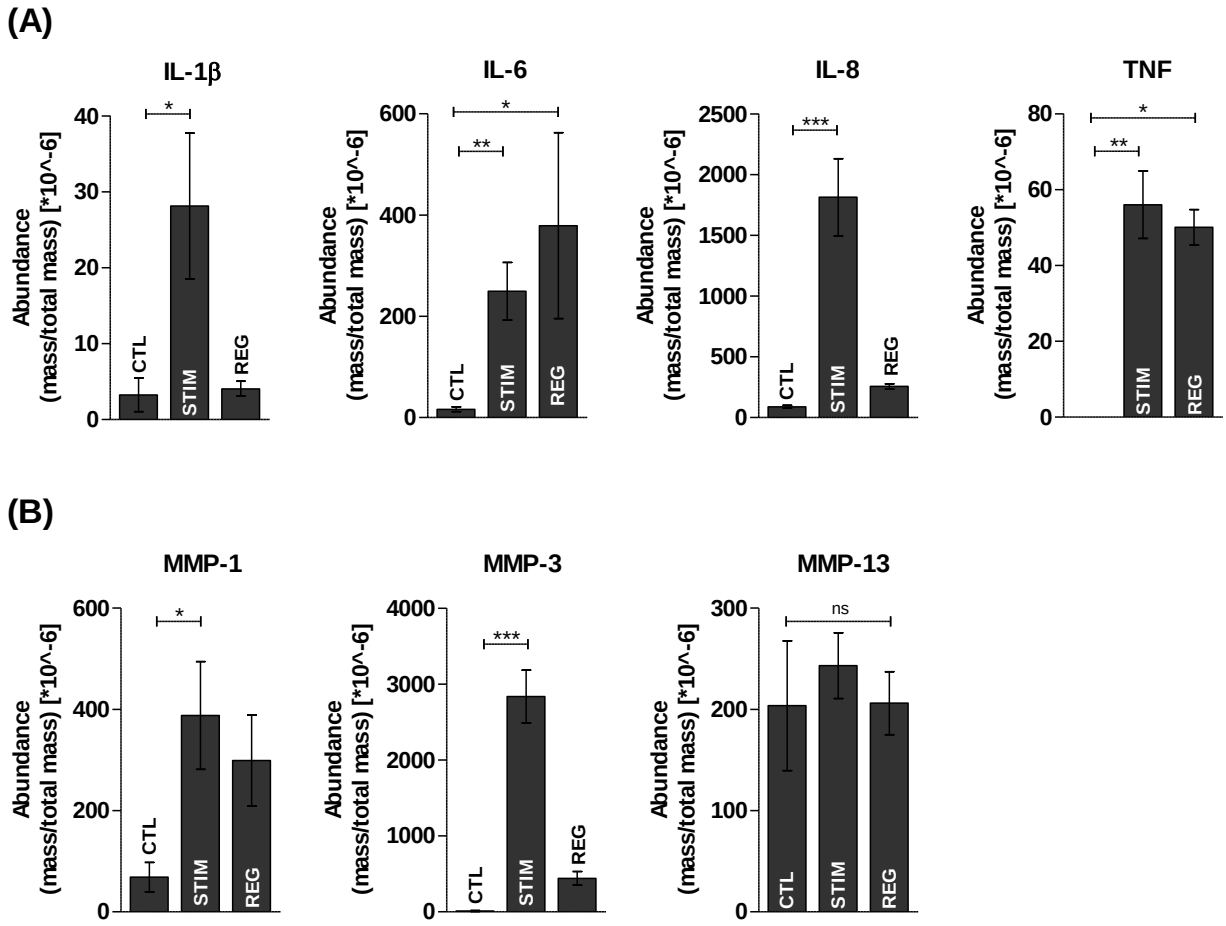

Figure 17: Proteomics of SFCCs cultured under pro-inflammatory conditions
Protein expression analysis was performed using proteomics and analyzed for (**A**) IL-1, IL-6, IL-8 and TNF and **(B)** MMP-1, MMP-3 and MMP-13. X-axes show the experimental groups for controls (CTL), pro-inflammatory stimulation (STIM) and regeneration (REG). Y-axes show protein abundance as mass/total mass * 10^{-6}. Graph bars show mean ± SEM. Statistical comparison of groups was performed using the Kruskal-Wallis test and Dunn's multiple comparisons test, ns = $p > 0.05$, * = $p < 0.05$, ** = $p < 0.01$, *** = $p < 0.001$.

Table 12: Statistical specifications for Figure 17

Specifications	Kruskal-Wallis-Test	
	H	*p*-value
IL-1β	8.25	*0.01*
IL-6	11.38	*0.0006*
IL-8	15.16	*0.0001*
TNF	11.9	*0.0004*
MMP-1	8.78	*0.007*
MMP-3	15.16	*0.0001*
MMP-13	1.84	*0.42*
Specifications	**Dunn's multiple comparisons test**	
	Comparison	Adjusted *p*-value
IL-1β	CTL vs. STIM	*0.02*
	STIM vs. REG	*0.99*
	CTL vs. REG	*0.08*
IL-6	CTL vs. STIM	*0.009*
	STIM vs. REG	*0.01*
	CTL vs. REG	*0.99*
IL-8	CTL vs. STIM	*0.0003*
	STIM vs. REG	*0.15*
	CTL vs. REG	*0.15*
TNF	CTL vs. STIM	*0.005*
	STIM vs. REG	*0.01*
	CTL vs. REG	*0.99*
MMP-1	CTL vs. STIM	*0.01*
	STIM vs. REG	*0.08*
	CTL vs. REG	*0.99*
MMP-3	CTL vs. STIM	*0.0003*
	STIM vs. REG	*0.15*
	CTL vs. REG	*0.15*

The mean relative protein expression was $68.74*10^{-6}$ (CTL), $387.87*10^{-6}$ (STIM) and $299.14*10^{-6}$ (REG) for MMP-1 and $10.82*10^{-6}$ (CTL), $2834.89*10^{-6}$ (STIM) and $440.23*10^{-6}$ (REG) for MMP-3. MMP-13 showed the same protein expression pattern as the gene expression pattern of *MMP13,* with no significant differences between the treatment groups (Fig. 17, Table 12).

Taken together, the SFCCs stimulated with the pro-inflammatory cytokines IL-1β and TNFα show features of the main characteristics of OA cartilage, the breakdown of the ECM, cell loss through apoptosis, and the upregulation of pro-inflammatory cytokines and matrix degrading enzymes. A loss of type II collagen coverage in immunohistochemically stained sections as well as the decrease of cell count per area were demonstrated in cytokine stimulated SFCCs using histological methods. Microscopically, SFCCs of the STIM group also showed morphological features similar to *in vivo* OA cartilage, such as increased water retention and maceration of the outer tissue layer. The upregulation of pro-inflammatory cytokines such as IL-1β, IL-6 and

IL-8 and the proteases MMP-1 and MMP-3 upon stimulation with IL-1β and TNFα within the SFCCs were detected on a gene and protein expression level by qPCR and proteomics.

CHAPTER 6: DISCUSSION

The aim of this thesis was to establish and characterize a human *in vitro* OA model based on 3D tissue-engineered cartilage-like constructs produced from human MSCs without the use of a scaffold. The cartilage-like phenotype of these scaffold-free cartilage-like constructs (SFCCs) was demonstrated using an experimental set-up of culture in cytokine-free standard medium. To show the use of SFCCs as an *in vitro* model for the study of OA, and to show their capacity to attain an OA-like phenotype, they were stimulated with the two main pro-inflammatory cytokines in the pathogenesis of OA, IL-1β and TNFα. Accordingly, OA-like changes in the SFCCs cultured under these pro-inflammatory conditions were demonstrated. The methods used in this study included histology, histomorphometry, immunohistochemistry, gene expression analysis via qPCR and proteomics using mass spectrometry. Thus, it has been shown that tissue-engineered cartilage-like constructs such as the SFCCs can be used as *in vitro* model systems for future studies on OA pathophysiology, with specific focus on cytokine-mediated cartilage degradation and the evaluation of possible therapeutic options. However, several limitations of this study must be considered in future approaches to refine measurement outcomes and further promote translatability of *in vitro* approaches in the study of OA.

6.1 Evaluation of methods and study design

It was shown that the SFCCs express a stable cartilage-like phenotype over a period of three weeks; however, the measurement outcomes for individual SFCCs were variable, especially regarding SFCCs from different donors. This variability of the phenotype can partly be explained by the fact that MSCs from different donors and subpopulations have specific characteristics, especially regarding chondrogenic capacity [164]. To obtain a more homogeneous phenotype of SFCCs, it could be considered to combine MSCs from different donors (pool) or to identify subpopulations of MSCs before expanding the cells for SFCC production.

For histology, the Kawamoto film method was used, which allows the processing of calcified tissue without prior chemical decalcification procedures. This facilitated a better comparability of the cartilage-like tissue engineered constructs to osteogenic controls. However, there was a lack of quantitative information that could be extracted

from the histological sections of the SFCCs. After pro-inflammatory stimulation with IL-1β and TNFα, changes such as an increased water retention and maceration of the superficial layer of the SFCCs were visible, though these changes were only of subjective nature. For studies on OA in *in vivo* animal models and human samples, standardized histological grading scores already exist [60, 165, 166]. It would be useful to also develop such a score for *in vitro* 3D models or tissue engineered cartilage.

In order to obtain information about the spatial distribution of cells within the SFCCs, a histomorphometric method was developed in this thesis to quantify the cell count per area on HE stained sections. The protocol was based on a modified color deconvolution method using the FIJI ImageJ 1.52i open source software that contains vectors to divide RGB (additive color model using red, green and blue) images into their red, green and blue channels. Based on the blue channel that represents the hematoxylin staining for the cell nuclei, a threshold was applied to identify the cell nuclei and obtain the cell count per area (Fig. 5). In the process of establishing this histomorphometric procedure, the use of another method based on the immunofluorescence DAPI stain was also evaluated. 4′,6-Diamidin-2-phenylindol (DAPI) is a fluorescent stain that binds to the DNA and can thus visualize the cell nuclei. It turned out, however, that the quantification of the total tissue area, i.e. the area of the whole section subtracted by the gap area, was not possible in DAPI stained sections, as no accurate thresholds could be deployed. Thus, HE stained sections were used for histomorphometry to obtain the cell count per total tissue area.

Immunohistochemical staining was used to visualize the presence of type I and type II collagen within the SFCCs. Immunohistochemical staining is not stoichiometric, therefore, the amount of the antigen present in the histological sections does not correlate with the amount of DAB staining. Thus, immunohistochemical staining was not suitable for exact quantitative analysis. To overcome this problem, a histomorphometric protocol was established as a semiquantitative method to measure the relative coverage area for type I and type II collagen staining compared to the total tissue area. This was possible as the ECM was distributed homogeneously within the SFCCs, which was previously observed in HE and AB stained sections priorly (see Fig. 8).

In addition, issues occurred concerning the amount of RNA that could be extracted from the SFCCs for qPCR analysis. In the first experimental set-up with SFCCs cultured under normal conditions, only parts of each SFCC sample were used for RNA extraction, limiting the number of PCR reactions and genes that could be analyzed by qPCR (see Fig. 4). In the second experimental set-up with SFCCs cultured under pro-inflammatory conditions, one entire SFCC per treatment group was used for qPCR to be able to perform gene expression analysis for more genes of interest (see Fig. 4).

Mass spectrometry was chosen in order to obtain information about the protein expression patterns of the cytokines and proteases of which gene expression levels were also measured using qPCR. As the sample volumes of the SFCCs were limited, no specific method such as western blot was used to verify the protein expression data obtained from mass spectrometry. Protein expression levels of type I and II collagen as well as aggrecan were not considered, as the standard digestion protocols using trypsin prior to mass spectrometry are not able to break down the highly crosslinked collagen network in cartilage tissues.

6.2 Characterization of SFCCs cultured under normal conditions and evaluation of their cartilage-like phenotype

Bone marrow derived hMSCs were used as cells to form the SFCCs. MSC cell populations have been shown to be able to differentiate into different lineages including the chondrogenic, osteogenic and adipogenic lineage [152]. However, MSCs do not fulfill the stem cell criteria as the capacity of full self-renewal is not present [167]. Thus, to date in the literature it has not been described that MSCs can form human hyaline or articular cartilage *in vitro* that is identical to the *in vivo* equivalent [168]. SFCCs were manufactured by self-organization and the application of repetitive mechanical forces [154, 169]. However, after arrival back in the laboratory after manufacturing, they were cultured for 4 weeks before starting the experiments in order to adapt to the laboratory conditions. In that time period, and during the experimental time of 3-6 weeks, no further mechanical forces were applied to the SFCCs. It is known, however, that mechanical stimulation is necessary to maintain articular cartilage homeostasis *in vivo* and a chondrogenic phenotype *in vitro* [170]. In view of these facts, the expectation was to observe a phenotype of the SFCCs that was not completely identical to articular cartilage.

In order to establish the *in vitro* model for OA based on the SFCCs, the SFCC phenotype and its stability over time were evaluated first. The gene expression of *COL2A1* and *ACAN*, with type II collagen being the predominant collagen and aggrecan being the predominant proteoglycan in articular cartilage, were verified (Fig. 11). On a protein level, type II collagen was visualized by immunohistochemistry and the presence of GAGs was seen in the AB stain (Fig. 8). This indicated a hyaline-like cartilage phenotype of the SFCCs; however, the gene expression of *COL1A1* and the presence of type I collagen shown by immunohistochemistry is not characteristic for articular and hyaline cartilage, but rather for fibrocartilage [171]. In the course of creating the publication for the study presented in this thesis, the gene expression of *COL1A1*, *COL2A1* and *ACAN* was additionally determined from native human articular cartilage [172]. It turned out that the expression of *COL2A1* and *ACAN* was significantly higher, and the expression of *COL1A1* significantly lower, in native articular cartilage compared to the SFCCs [172]. Gene expression analysis within the SFCCs was also performed for *COL10A1*, a marker of chondrocyte hypertrophy [173]. Chondrocyte hypertrophy occurs in the growth plate of long bones during endochondral ossification, in which chondrocytes undergo a programmed differentiation progress towards hypertrophy, calcification and replacement through osteoblasts to form bone [93]. In OA pathophysiology, chondrocyte hypertrophy has been described as an essential process leading to a disturbed cartilage homeostasis and contributing to joint degeneration [174]. Although it was expressed at a very low level within the SFCC, it is usually only present in the region above the subchondral bone in articular cartilage *in vivo* [175].

The phenotypical characteristics of the SFCCs were evaluated over a culture period of three weeks and no significant changes were found between the different timepoints. Thus, they show a stable phenotype, although no mechanical stimulation was applied to the constructs. Taken together, a cartilage-like phenotype could be identified within the SFCC. However, the phenotype was not specific to articular hyaline cartilage but rather fibrocartilage and significant differences remain when compared to human *in vivo* articular cartilage.

6.3 Characterization of SFCCs cultured under pro-inflammatory conditions and evaluation of their OA-like phenotype

The inflammatory environment in OA articular cartilage was simulated *in vitro* using the human recombinant proteins IL-1β and TNFα, which are supposed to be the predominant pro-inflammatory cytokines involved in the pathogenesis of OA [69]. OA-induction through cytokines is a common method for *in vitro* OA models and cytokine concentrations for IL-1β and TNFα range from 100pg/ml to 100ng/ml for IL-1β and 60pg/ml to 100ng/ml for TNFα in the described models [176-179]. However, the cytokine concentration in the synovial fluid of OA joints in humans seem to be much lower. Baseline concentrations of 0.068 and 0.333 pg/ml for IL-1β, and 2.52 and 3.76 pg/ml baseline TNFα concentrations, were found in the knee synovial fluid of OA patients by Vincent et al. [180]. However, a highly aggressive cytokine treatment with IL-1β at 50 ng/ml and TNFα at 100 ng/ml was chosen in this study to achieve high local cytokine concentrations and obtain maximal stimulation and significant phenotypical changes in the SFCCs. OA usually progresses over decades in the human condition and cartilage degradation seems to be a very slow process in OA. Consequently, *in vitro* models must be modified by using shorter experimental time periods and higher cytokine concentrations to achieve experimental results. This must therefore be considered when performing studies, especially with regard to possible therapeutic options.

As mentioned above, no quantitative data could be obtained from HE and AB histologically stained sections of the SFCCs, except for the determination of the cell count per area. Although morphological changes upon pro-inflammatory stimulation were present, they could not be quantified, as no standardized evaluation tool for tissue-engineered cartilage-like constructs has been developed yet. Nevertheless, the increased water retention and maceration of the superficial layers suggests that changes in the integrity of the ECM occurred due to the stimulation with IL-1β and TNFα. A parallel can be drawn to similar morphological changes in early stages of osteoarthritis articular cartilage degradation [60].

Regarding the results from the histomorphometric analysis of the SFCCs cultured under pro-inflammatory conditions, a decrease in cell count per area could be observed in all areas except for the Inner Core Area (In.C.A.) compared to untreated controls.

As the cell count per area was determined as cell count per Total Tissue Area (Tt.T.A.), a bias due to an increased Gap Area (Gp.A.) as a result of increased water retention in the tissue could be excluded. Therefore, the decreased cell density could be a consequence of (I) disintegration of the cells out of the ECM and adherence to plastic surface of the culture dish that was observed during the experimental process or (II) apoptosis of cells due to the upregulation of the NF-κB pathway upon stimulation with IL-1β and TNFα which has been previously described in the literature [181]. The cell count per area did not recover in the REG group. This can be interpreted as a sign for the loss of proliferation potential of the remaining cells within the SFCCs as compared to the MSCs the constructs were generated from.

With respect to the results from immunohistochemical analysis of the SFCCs cultured under pro-inflammatory conditions, two main aspects are important to address. To begin with, the coverage of type I collagen did not change between the treatment groups, although the gene expression of *COL1A1* did significantly decrease after pro-inflammatory stimulation (Fig. 15, 16). This could be due to the fact that the collagen fibrils were protected from proteolytic cleavage through MMPs, and that possible proteolytically cleaved collagen fibrils were not fully degraded and removed from the ECM matrix in the cytokine-treated SFCCs. Thus, collagen fibrils could still be detected by the antibodies used for immunohistochemistry. As immunohistochemical staining is not a stoichiometric staining procedure, only the location of the antigen can be identified by this method, not its quantity. Secondly, the coverage for type II collagen decreased numerically in the STIM group and significantly in the REG group compared to controls. It could be assumed that the type II collagen fibrils were not as tightly incorporated into the ECM within the SFCCs compared to type I collagen fibrils. Consequently, they could be cleaved and removed more easily from the ECM after proteolytic degradation through MMPs. This might have resulted in the decrease of the areas where collagen II could be detected within STIM and REG group (Fig. 16).

When looking at the gene expression analysis for the SFCC cultured with IL-1β and TNFα, the pro-inflammatory stimulation led to the upregulation of pro-inflammatory cytokines and proteases as well as the downregulation of ECM proteins. In the STIM group, gene expression of pro-inflammatory cytokines such as *IL6* and *IL8* was upregulated indicating the induction of a cascade of pro-inflammatory downstream

effects after stimulation with IL-1β and TNFα (Fig. 16B). Regarding the proteomics data, IL-6 and IL-8 were also upregulated on the protein level (Fig. 17A). Both IL-6 and IL-8 have been found to be upregulated in the synovial fluid of OA patients [182]. IL-6 has been shown to be able to contribute to the downregulation of *COL2A1* and *ACAN* expression and the upregulation of *MMP13* in chondrocytes [183, 184]. In SFCCs treated with IL-1β and TNFα, the gene expression of *IL1* but not *TNF* was upregulated compared to controls (Fig. 16B). Some studies have suggested that the upregulation of MMPs and ADAMTs in OA by TNFα is mediated through the upregulation of IL-1, which could explain why the gene expression of *TNF* is not further upregulated in the cytokine-stimulated SFCCs [75, 185]. However, when looking at the protein expression, TNF expression was significantly higher in the STIM group compared to controls, with a relative abundance for TNF of 0 in the CTL group (Fig. 17A). A possible explanation for these results could be that post-transcriptional regulation of TNF occurred within the SFCCs. Several mechanisms have been identified to regulate the post-transcriptional processing of TNF mRNA, such as ligand-binding to a adenosine/uridine-rich element within the mRNA preventing RNA translation [186, 187].

It was therefore shown that the pro-inflammatory stimulation of the SFCCs was able to induce downstream pro-inflammatory pathways and a positive feedback loop that led to a lasting pro-inflammatory environment, as cytokine levels did not fully decrease 3 weeks after pro-inflammatory stimulation in the REG group.

Another main pathophysiological pathway that plays a role in the cartilage destruction in OA is the upregulation of specific proteases of the MMP and ADAMTS family [188]. In SFCCs treated with IL-1β and TNFα, the gene and protein expression of MMP-1 and MMP-3 was upregulated compared to controls (Fig. 16C, 17B). However, MMP-13, which is thought to be the most important MMP in OA pathophysiology as it is specifically able to degrade type II collagen fibrils, showed no differences in gene and protein expression between the experimental groups [189]. Regarding the literature, Bau et al. showed differential expression patterns of MMPs in different stages of OA. They demonstrated that *MMP13* gene expression is only upregulated in late stage OA cartilage, whereas *MMP3* gene expression is downregulated in late stage OA cartilage [190]. These findings were supported by another study by Swingler et al. who

Table 13: Summary of main features of healthy and osteoarthritic cartilage *in vivo* compared to findings from the *in vitro* SFCC model.

	In vivo **Healthy articular cartilage**	***In vitro*** **SFCCs cultured under normal conditions**
Cells	□ **Chondrocytes** → low cell turnover → responsible for steady yet slow matrix turnover → balance between anabolism and catabolism	□ **MSCs** → chondrogenically differentiated
Extracellular matrix components	□ **Proteoglycans** → predominantly aggrecan □ **Glycosaminoglycans** → predominantly hyaluronic acid, chondroitin sulfate □ **Collagens** → predominantly type II collagen	□ **Proteoglycans** → aggrecan (qPCR) □ **Glycosaminoglycans** → non-specific detection (AB staining) □ **Collagens** → type I and type II collagen (qPCR, immunohistochemistry)
	In vivo **Osteoarthritic articular cartilage**	***In vitro*** **SFCCs cultured under pro-inflammatory conditions**
Triggers	□ **Local inflammation** □ Mechanical stress or injury □ Ageing factors □ Systemic inflammation □ Fragments of ECM components + crystals	□ **Local pro-inflammatory stimulation** in form of pro-inflammatory cytokines (IL-1β, TNFα)
Reaction of chondrocytes	□ Induction of NFκB signaling pathway (+ other pathways: BMP, Wnt, etc.) □ **Upregulation of matrix degrading enzymes** (MMPs, ADAMTS, etc.) **and pro-inflammatory cytokines** (TNF, IL-1, -6, -8, etc.) □ **Apoptosis** □ **Chondrocyte hypertrophy**	□ **Upregulation of matrix degrading enzymes (MMP-1, -3) and pro-inflammatory cytokines (IL-1, -6, -8)** (qPCR, proteomics) □ **Apoptosis (?)** (histomorphometry) □ **Chondrocyte hypertrophy (?)** (qPCR)
Extracellular matrix	□ **Partial breakdown of proteoglycan and collagen matrix** □ Increased water content in early stages of OA □ Loss of functional and structural integrity □ Complete degradation of articular cartilage	□ **Loss of type II collagen (?)** (immunohistochemistry, qPCR) □ **Increased water content (?)** (histology, wet weight) □ **Loss of structural integrity** (histology)

showed the same gene expression patterns for *MMP3* and *MMP13* in OA cartilage [191]. Nevertheless, most studies using *in vitro* OA and cartilage models show the induction of *MMP13* gene expression by IL-1β and or TNFα, contradicting the SFCC *in vitro* model presented in this study [192, 193].

Furthermore, IL-1β and or TNFα downregulated the gene expression of ECM proteins within the SFCCs as shown by the downregulation of *COL1A1*, *COL2A1* and *ACAN* in the STIM group, although the downregulation of *COL2A1* and *ACAN* was only numerically relevant but not statistically significant. Interestingly, *COL10A1* was upregulated in the REG group, suggesting that the cells within the SFCC differentiate towards a hypertrophic phenotype as the expression of *COL2A1* did not regenerate either.

Taken together, the main features of osteoarthritic cartilage, inflammation and cartilage matrix breakdown through matrix degrading enzymes such as MMPs were reproduced using SFCCs as an *in vitro* model. In Table 13 the main features of *in vivo* healthy and osteoarthritic cartilage are compared to the findings from the *in vitro* SFCCs model.

6.4 Comparison to other *in vitro* approaches

Preclinical *in vitro* modeling is an important tool in biomedical research and aimed at enhancing translatability of results into clinical practice. With recent advances in tissue engineering methods in regenerative medicine, the use of such engineered tissues and organoids as 3D *in vitro* model systems for the study of various human diseases has emerged [194, 195]. In OA research, tissue engineering is mainly used with focus on regenerative methods creating cartilage-transplants for the repair of cartilage defects in joints [196]. However, tissue-engineered cartilage or osteochondral constructs are also increasingly being used as 3D *in vitro* models for the study of cartilage biology and OA pathophysiology [197]. Most tissue engineering approaches for cartilage generation focus on scaffold-based methods, using a variety of different polymers to provide a predetermined 3D structure to the cells used [198]. In recent years, however, scaffold-free approaches in cartilage tissue engineering have emerged [148]. Scaffold-free approaches are advantageous for *in vitro* models as they only consist of the cells and their own metabolic products and ECM molecules which resemble the *in vivo*

tissue structure more closely, and the influence of the scaffold materials on the cells does not have to be considered.

In this study, the use of tissue engineered scaffold-free cartilage-like constructs, the SFCCs, as an *in vitro* model for the study of OA has been established and validated. The SFCCs presented here were engineered from hMSCs that were first centrifuged to form a pellet culture that was then stimulated with cyclic mechanical stimulation in order to generate the cartilage-like constructs [154]. Other approaches for scaffold-free cartilage tissue engineering include a study by Bhumiratana et al., who demonstrated the regeneration of scaffold-free articular cartilage-like tissue using hMSCs with the substitution of TGFβ in the culture media. Their approach was based on the recapitulation of mesenchymal condensation of hMSCs and the cartilage-like tissue achieved in their study showed a Young's modulus similar to *in vivo* articular cartilage [199]. In another study, Park et al. created scaffold-free cartilage constructs from rabbit chondrocytes that were tested for the repair of cartilage defects in rabbits [200]. Yasui et al. used synovial hMSCs to generate scaffold-free cartilage-like constructs under low oxygen tension to generate tissue engineered constructs for potential application in cartilage repair in humans [201, 202].

Independent of whether they are scaffold-free or scaffold-based, advances in the knowledge of articular cartilage tissue engineering can be used for creating innovative 3D-culture systems that can serve as *in vitro* models for the study of OA, as demonstrated in this study. One main advantage is that human cells can be used in these model systems, which could be a step forward to an improved translatability of preclinical experimental results. Moreover, advances in the development of *in vitro* models for the study of OA could lead towards a better understanding of OA pathophysiology and the reduction of animal models needed in OA research.

6.5 Limitations

Although the model in this study represents a promising approach towards its use as an *in vitro* model for the study of OA, several limitations must be considered. hMSCs that are widely used for cartilage tissue engineering were also the cell source for the SFCCs presented in this study. However, hMSCs have been shown to be inhomogeneous cell populations with different chondrogenic differentiation capacities

when looking at donor sources as well as strain specifics [164]. Consequently, the results presented here also show relatively large variances between the measurement outcomes of individual SFCCs. Along with the small sample size in all experimental set-ups presented, a Gaussian distribution could not be assumed for statistical analysis of the results and non-parametric statistical testing had to be applied. The SFCCs were generated at the Research Center of Medical Technology and Biotechnology in Bad Langensalza using cyclic biomechanical stimulation. However, 4 weeks prior to the start of the experiments as well as during the experimental period, no mechanical forces were applied to the SFCCs. Using a bioreactor system with a continuous media exchange and the ability, to apply repetitive controlled mechanical stimuli onto the SFCCs during the experimental period would mimic the *in vivo* situation more accurately [203]. As OA is considered a whole joint disease, with all joint tissues involved in its pathophysiology, the ideal *in vitro* disease model would not only include cartilage tissue but also subchondral bone and synovium [37]. In this study, very high concentrations of the pro-inflammatory cytokines IL-1β and TNFα were used to stimulate the cartilage-like constructs. However, in the human condition, OA is a long-term and usually slowly progressing degeneration of cartilage, which finally affects the integrity of the entire joint. Using such high cytokine concentrations allows for significant experimental results in a reasonable experimental time frame, however, they could lead to different downstream pathways and results could differ from the *in vivo* condition.

CHAPTER 7: CONCLUSIONS AND FUTURE DIRECTIONS

In this study, a human 3D *in vitro* model for the study of OA was established and evaluated. The model was able to simulate the main features of cartilage destruction in OA - the inflammation and upregulation of matrix degrading enzymes. It has therefore been shown that OA can be simulated using tissue engineered cartilage-like tissue and cytokine-based OA induction. The model system was based on human cells providing advantages regarding the translatability of experimental results. The wide availability of tissue engineered cartilage provides the opportunity for creating sophisticated *in vitro* model systems to gain better understanding in OA pathophysiology and test potential therapeutic options. In particular, with the emerging approaches in scaffold-free cartilage tissue engineering as presented in this study, new insights into matrix degradation and regeneration were obtained. *In vitro* models also have the potential to be an alternative to *in vivo* animal models for some research questions, making them an important tool in the application of 3R research that aims to reduce, refine and replace experiments using animals as model systems.

Mathematical modeling was performed from the collected data in parallel to the study presented in this thesis to create an *in silico* model based on partial differential equations. The *in silico* model was designed to simulate the degradation of type II collagen through MMPs, concentrations of IL-1β within the SFCC and changes in cell density. Such mathematical modeling provides the opportunity to optimize and refine *in vitro* model systems, for example by predicting measurement outcomes when changing parameters such as cytokine-concentrations or time periods [172].

Future steps include (I) generating an osteochondral *in vitro* model extending the current cartilage-like model with a tissue engineered bone-like compartment that simulates the osteochondral unit of the joint, (II) overcoming methodical limitations including the generation of SFCCs in a bioreactor system and mechanical stimulation and testing of the SFCCs, and (III) further extending the osteochondral model towards the ultimate goal of creating a whole joint model using a bioreactor culture system that allows the co-culture of cartilage-, bone- and synovium-like tissues.

A good model system is the foundation of most biomedical research. Consequently, the development of new model systems and the critical evaluation of existing ones is crucial for scientific progress.

REFERENCES

1. Weber MC, Fischer L, Damerau A, Ponomarev I, Pfeiffenberger M, Gaber T, Gotschel S, Lang J, Roblitz S, Buttgereit F, Ehrig R, Lang A. Macroscale mesenchymal condensation to study cytokine-driven cellular and matrix-related changes during cartilage degradation. Biofabrication. 2020;12(4):045016.

2. Glyn-Jones S, Palmer AJ, Agricola R, Price AJ, Vincent TL, Weinans H, Carr AJ. Osteoarthritis. Lancet (London, England). 2015;386(9991):376-87.

3. Kellgren JH, Lawrence JS. Radiological assessment of osteo-arthrosis. Ann Rheum Dis. 1957;16(4):494-502.

4. Mansfield JC, Mandalia V, Toms A, Winlove CP, Brasselet S. Collagen reorganization in cartilage under strain probed by polarization sensitive second harmonic generation microscopy. Journal of the Royal Society, Interface. 2019;16(150):20180611-.

5. Buckwalter JA, Saltzman C, Brown T. The impact of osteoarthritis: implications for research. Clin Orthop Relat Res. 2004(427 Suppl):S6-15.

6. Woolf AD, Pfleger B. Burden of major musculoskeletal conditions. Bulletin of the World Health Organization. 2003;81(9):646-56.

7. Pereira D, Peleteiro B, Araujo J, Branco J, Santos RA, Ramos E. The effect of osteoarthritis definition on prevalence and incidence estimates: a systematic review. Osteoarthritis Cartilage. 2011;19(11):1270-85.

8. Woolf AD, Erwin J, March L. The need to address the burden of musculoskeletal conditions. Best Pract Res Clin Rheumatol. 2012;26(2):183-224.

9. Rabenberg M. Themenheft 54 "Arthrose". Robert Koch-Institut; 2013.

10. Cross M, Smith E, Hoy D, Nolte S, Ackerman I, Fransen M, Bridgett L, Williams S, Guillemin F, Hill CL, Laslett LL, Jones G, Cicuttini F, Osborne R, Vos T, Buchbinder R, Woolf A, March L. The global burden of hip and knee osteoarthritis: estimates from the global burden of disease 2010 study. Annals of the rheumatic diseases. 2014;73(7):1323-30.

11. O'Neill TW, McCabe PS, McBeth J. Update on the epidemiology, risk factors and disease outcomes of osteoarthritis. Best Pract Res Clin Rheumatol. 2018;32(2):312-26.

12. Rahmati M, Nalesso G, Mobasheri A, Mozafari M. Aging and osteoarthritis: Central role of the extracellular matrix. Ageing research reviews. 2017;40:20-30.

13. Yusuf E, Nelissen RG, Ioan-Facsinay A, Stojanovic-Susulic V, DeGroot J, van Osch G, Middeldorp S, Huizinga TW, Kloppenburg M. Association between weight or body mass index and hand osteoarthritis: a systematic review. Ann Rheum Dis. 2010;69(4):761-5.

14. Ding C, Stannus O, Cicuttini F, Antony B, Jones G. Body fat is associated with increased and lean mass with decreased knee cartilage loss in older adults: a prospective cohort study. International journal of obesity (2005). 2013;37(6):822-7.

15. Sharma L, Song J, Dunlop D, Felson D, Lewis CE, Segal N, Torner J, Cooke TD, Hietpas J, Lynch J, Nevitt M. Varus and valgus alignment and incident and progressive knee osteoarthritis. Ann Rheum Dis. 2010;69(11):1940-5.

16. Sharma L, Chmiel JS, Almagor O, Felson D, Guermazi A, Roemer F, Lewis CE, Segal N, Torner J, Cooke TD, Hietpas J, Lynch J, Nevitt M. The role of varus and valgus alignment in the initial development of knee cartilage damage by MRI: the MOST study. Ann Rheum Dis. 2013;72(2):235-40.

17. Morvan J, Bouttier R, Mazieres B, Verrouil E, Pouchot J, Rat AC, Guellec D, Guillemin F, Coste J, Saraux A. Relationship between hip dysplasia, pain, and osteoarthritis in a cohort of patients with hip symptoms. J Rheumatol. 2013;40(9):1583-9.

18. Agricola R, Waarsing JH, Arden NK, Carr AJ, Bierma-Zeinstra SM, Thomas GE, Weinans H, Glyn-Jones S. Cam impingement of the hip: a risk factor for hip osteoarthritis. Nat Rev Rheumatol. 2013;9(10):630-4.

19. Ni GX, Zhou YZ, Chen W, Xu L, Li Z, Liu SY, Lei L, Zhan LQ. Different responses of articular cartilage to strenuous running and joint immobilization. Connect Tissue Res. 2016;57(2):143-51.

20. Reynard LN. Analysis of genetics and DNA methylation in osteoarthritis: What have we learnt about the disease? Seminars in Cell & Developmental Biology. 2017;62:57-66.

21. van Meurs JB. Osteoarthritis year in review 2016: genetics, genomics and epigenetics. Osteoarthritis Cartilage. 2017;25(2):181-9.

22. Thomas AC, Hubbard-Turner T, Wikstrom EA, Palmieri-Smith RM. Epidemiology of Posttraumatic Osteoarthritis. Journal of athletic training. 2017;52(6):491-6.

23. Hunter DJ, McDougall JJ, Keefe FJ. The symptoms of osteoarthritis and the genesis of pain. The Medical clinics of North America. 2009;93(1):83-100, xi.

24. Bedson J, Croft PR. The discordance between clinical and radiographic knee osteoarthritis: a systematic search and summary of the literature. BMC Musculoskelet Disord. 2008;9:116.

25. Neogi T. The epidemiology and impact of pain in osteoarthritis. Osteoarthritis Cartilage. 2013;21(9):1145-53.

26. Steultjens MP, Dekker J, van Baar ME, Oostendorp RA, Bijlsma JW. Range of joint motion and disability in patients with osteoarthritis of the knee or hip. Rheumatology (Oxford). 2000;39(9):955-61.

27. Knoop J, van der Leeden M, van der Esch M, Thorstensson CA, Gerritsen M, Voorneman RE, Lems WF, Roorda LD, Dekker J, Steultjens MPM. Association of lower muscle strength with self-reported knee instability in osteoarthritis of the knee: Results from the Amsterdam Osteoarthritis Cohort. Arthritis care & research. 2012;64(1):38-45.

28. Hunter DJ, Bierma-Zeinstra S. Osteoarthritis. Lancet (London, England). 2019;393(10182):1745-59.

29. Watt FE. Osteoarthritis biomarkers: year in review. Osteoarthritis Cartilage. 2018;26(3):312-8.

30. Demehri S, Guermazi A, Kwoh CK. Diagnosis and Longitudinal Assessment of Osteoarthritis: Review of Available Imaging Techniques. Rheumatic diseases clinics of North America. 2016;42(4):607-20.

31. Altman R, Asch E, Bloch D, Bole G, Borenstein D, Brandt K, Christy W, Cooke TD, Greenwald R, Hochberg M, et al. Development of criteria for the classification and reporting of osteoarthritis. Classification of osteoarthritis of the knee. Diagnostic and Therapeutic Criteria Committee of the American Rheumatism Association. Arthritis Rheum. 1986;29(8):1039-49.

32. Altman R, Alarcon G, Appelrouth D, Bloch D, Borenstein D, Brandt K, Brown C, Cooke TD, Daniel W, Gray R, et al. The American College of Rheumatology criteria for the classification and reporting of osteoarthritis of the hand. Arthritis Rheum. 1990;33(11):1601-10.

33. Altman R, Alarcon G, Appelrouth D, Bloch D, Borenstein D, Brandt K, Brown C, Cooke TD, Daniel W, Feldman D, et al. The American College of Rheumatology criteria for the classification and reporting of osteoarthritis of the hip. Arthritis Rheum. 1991;34(5):505-14.

34. Zhang W, Doherty M, Peat G, Bierma-Zeinstra MA, Arden NK, Bresnihan B, Herrero-Beaumont G, Kirschner S, Leeb BF, Lohmander LS, Mazieres B, Pavelka K, Punzi L, So AK, Tuncer T, Watt I, Bijlsma JW. EULAR evidence-based recommendations for the diagnosis of knee osteoarthritis. Ann Rheum Dis. 2010;69(3):483-9.

35. Zhang W, Doherty M, Leeb BF, Alekseeva L, Arden NK, Bijlsma JW, Dincer F, Dziedzic K, Hauselmann HJ, Kaklamanis P, Kloppenburg M, Lohmander LS, Maheu E, Martin-Mola E, Pavelka K, Punzi L, Reiter S, Smolen J, Verbruggen G, Watt I, Zimmermann-Gorska I. EULAR evidence-based recommendations for the diagnosis of hand osteoarthritis: report of a task force of ESCISIT. Ann Rheum Dis. 2009;68(1):8-17.

36. Crema MD, Watts GJ, Guermazi A, Kim YJ, Kijowski R, Roemer FW. A narrative overview of the current status of MRI of the hip and its relevance for osteoarthritis research - what we know, what has changed and where are we going? Osteoarthritis Cartilage. 2017;25(1):1-13.

37. Martel-Pelletier J, Barr AJ, Cicuttini FM, Conaghan PG, Cooper C, Goldring MB, Goldring SR, Jones G, Teichtahl AJ, Pelletier JP. Osteoarthritis. Nature reviews Disease primers. 2016;2:16072.

38. Richette P, Poitou C, Garnero P, Vicaut E, Bouillot JL, Lacorte JM, Basdevant A, Clement K, Bardin T, Chevalier X. Benefits of massive weight loss on symptoms, systemic inflammation and cartilage turnover in obese patients with knee osteoarthritis. Ann Rheum Dis. 2011;70(1):139-44.

39. Uthman OA, van der Windt DA, Jordan JL, Dziedzic KS, Healey EL, Peat GM, Foster NE. Exercise for lower limb osteoarthritis: systematic review incorporating trial sequential analysis and network meta-analysis. BMJ : British Medical Journal. 2013;347:f5555.

40. Towheed T, Maxwell L, Anastassiades TP, Shea B, Houpt JB, Welch V, Hochberg MC, Wells GA. Glucosamine therapy for treating osteoarthritis. Cochrane Database of Systematic Reviews. 2005(2).

41. Singh JA, Noorbaloochi S, MacDonald R, Maxwell LJ. Chondroitin for osteoarthritis. Cochrane Database of Systematic Reviews. 2015(1).

42. Wasserman A, Matthewson G, MacDonald P. Platelet-Rich Plasma and the Knee-Applications in Orthopedic Surgery. Curr Rev Musculoskelet Med. 2018;11(4):607-15.

43. Hunter DJ. Viscosupplementation for osteoarthritis of the knee. N Engl J Med. 2015;372(11):1040-7.

44. Jüni P, Hari R, Rutjes AWS, Fischer R, Silletta MG, Reichenbach S, da Costa BR. Intra-articular corticosteroid for knee osteoarthritis. The Cochrane database of systematic reviews. 2015(10):CD005328-CD.

45. Chiba K, Yonekura A, Miyamoto T, Osaki M, Chiba G. Tibial condylar valgus osteotomy (TCVO) for osteoarthritis of the knee: 5-year clinical and radiological results. Archives of orthopaedic and trauma surgery. 2017;137(3):303-10.

46. Leunig M, Ganz R. The evolution and concepts of joint-preserving surgery of the hip. Bone Joint J. 2014;96-B(1):5-18.

47. Ferguson RJ, Palmer A, Jr., Taylor A, Porter ML, Malchau H, Glyn-Jones S. Hip replacement. Lancet (London, England). 2018;392(10158):1662-71.

48. Carr AJ, Robertsson O, Graves S, Price AJ, Arden NK, Judge A, Beard DJ. Knee replacement. Lancet (London, England). 2012;379(9823):1331-40.

49. Maffulli N, Longo UG, Locher J, Romeo G, Salvatore G, Denaro V. Outcome of ankle arthrodesis and ankle prosthesis: a review of the current status. Br Med Bull. 2017;124(1):91-112.

50. Sott AH. Minimally Invasive Arthrodesis of 1st Metatarsophalangeal Joint for Hallux Rigidus. Foot Ankle Clin. 2016;21(3):567-76.

51. Fernandes L, Hagen KB, Bijlsma JWJ, Andreassen O, Christensen P, Conaghan PG, Doherty M, Geenen R, Hammond A, Kjeken I, Lohmander LS, Lund H, Mallen CD, Nava T, Oliver S, Pavelka K, Pitsillidou I, da Silva JA, de la Torre J, Zanoli G, Vliet Vlieland TPM, European League Against R. EULAR recommendations for the non-pharmacological core management of hip and knee osteoarthritis. Annals of the rheumatic diseases. 2013;72(7):1125-35.

52. Hochberg MC, Altman RD, April KT, Benkhalti M, Guyatt G, McGowan J, Towheed T, Welch V, Wells G, Tugwell P, American College of R. American College of Rheumatology 2012 recommendations for the use of nonpharmacologic and pharmacologic therapies in osteoarthritis of the hand, hip, and knee. Arthritis care & research. 2012;64(4):465-74.

53. McAlindon TE, Bannuru RR, Sullivan MC, Arden NK, Berenbaum F, Bierma-Zeinstra SM, Hawker GA, Henrotin Y, Hunter DJ, Kawaguchi H, Kwoh K, Lohmander S, Rannou F, Roos EM, Underwood M. OARSI guidelines for the non-surgical management of knee osteoarthritis. Osteoarthritis Cartilage. 2014;22(3):363-88.

54. Decker RS. Articular cartilage and joint development from embryogenesis to adulthood. Seminars in cell & developmental biology. 2017;62:50-6.

55. Benninghoff A, Drenckhahn D. Anatomie. Makroskopische Anatomie, Histologie, Embryologie, Zellbiologie. Band 1: Zelle, Gewebe, Entwicklung, Skelett- und Muskelsystem, Atemsystem, Verdauungssystem, Harn- und Genitalsystem. Urban & Fischer Verlag/Elsevier GmbH; 2008. p. 968.

56. Lüllmann-Rauch R. Taschenlehrbuch Histologie. Georg Thieme Verlag KG, Stuttgart. 2012;4. Auflage.

57. Poole CA. Articular cartilage chondrons: form, function and failure. J Anat. 1997;191 (Pt 1):1-13.

58. Wilusz RE, Sanchez-Adams J, Guilak F. The structure and function of the pericellular matrix of articular cartilage. Matrix biology : journal of the International Society for Matrix Biology. 2014;39:25-32.

59. Carballo CB, Nakagawa Y, Sekiya I, Rodeo SA. Basic Science of Articular Cartilage. Clinics in sports medicine. 2017;36(3):413-25.

60. Pritzker KP, Gay S, Jimenez SA, Ostergaard K, Pelletier JP, Revell PA, Salter D, van den Berg WB. Osteoarthritis cartilage histopathology: grading and staging. Osteoarthritis Cartilage. 2006;14(1):13-29.

61. Sophia Fox AJ, Bedi A, Rodeo SA. The basic science of articular cartilage: structure, composition, and function. Sports health. 2009;1(6):461-8.

62. Heinegard D, Saxne T. The role of the cartilage matrix in osteoarthritis. Nat Rev Rheumatol. 2011;7(1):50-6.

63. Goldring MB, Goldring SR. Osteoarthritis. Journal of cellular physiology. 2007;213(3):626-34.

64. Mononen ME, Tanska P, Isaksson H, Korhonen RK. New algorithm for simulation of proteoglycan loss and collagen degeneration in the knee joint: Data from the osteoarthritis initiative. J Orthop Res. 2018;36(6):1673-83.

65. Hui Mingalone CK, Liu Z, Hollander JM, Garvey KD, Gibson AL, Banks RE, Zhang M, McAlindon TE, Nielsen HC, Georgakoudi I, Zeng L. Bioluminescence and second harmonic generation imaging reveal dynamic changes in the inflammatory and collagen landscape in early osteoarthritis. Lab Invest. 2018;98(5):656-69.

66. Hosseininia S, Lindberg LR, Dahlberg LE. Cartilage collagen damage in hip osteoarthritis similar to that seen in knee osteoarthritis; a case-control study of relationship between collagen, glycosaminoglycan and cartilage swelling. BMC musculoskeletal disorders. 2013;14:18-.

67. Appleyard RC, Burkhardt D, Ghosh P, Read R, Cake M, Swain MV, Murrell GAC. Topographical analysis of the structural, biochemical and dynamic biomechanical properties of cartilage in an ovine model of osteoarthritis. Osteoarthritis and Cartilage. 2003;11(1):65-77.

68. Berenbaum F. Osteoarthritis as an inflammatory disease (osteoarthritis is not osteoarthrosis!). Osteoarthritis Cartilage. 2013;21(1):16-21.

69. Kapoor M, Martel-Pelletier J, Lajeunesse D, Pelletier JP, Fahmi H. Role of proinflammatory cytokines in the pathophysiology of osteoarthritis. Nat Rev Rheumatol. 2011;7(1):33-42.

70. Goldring MB. Osteoarthritis and cartilage: the role of cytokines. Curr Rheumatol Rep. 2000;2(6):459-65.

71. Carames B, Lopez-Armada MJ, Cillero-Pastor B, Lires-Dean M, Vaamonde C, Galdo F, Blanco FJ. Differential effects of tumor necrosis factor-alpha and interleukin-1beta on cell death in human articular chondrocytes. Osteoarthritis Cartilage. 2008;16(6):715-22.

72. Funato S, Yasuhara R, Yoshimura K, Miyamoto Y, Kaneko K, Suzawa T, Chikazu D, Mishima K, Baba K, Kamijo R. Extracellular matrix loss in chondrocytes after exposure to interleukin-1beta in NADPH oxidase-dependent manner. Cell Tissue Res. 2017;368(1):135-44.

73. Henrotin YE, De Groote DD, Labasse AH, Gaspar SE, Zheng SX, Geenen VG, Reginster JY. Effects of exogenous IL-1 beta, TNF alpha, IL-6, IL-8 and LIF on cytokine production by human articular chondrocytes. Osteoarthritis Cartilage. 1996;4(3):163-73.

74. Kobayashi M, Squires GR, Mousa A, Tanzer M, Zukor DJ, Antoniou J, Feige U, Poole AR. Role of interleukin-1 and tumor necrosis factor alpha in matrix degradation of human osteoarthritic cartilage. Arthritis Rheum. 2005;52(1):128-35.

75. Pratta MA, Di Meo TM, Ruhl DM, Arner EC. Effect of interleukin-1-beta and tumor necrosis factor-alpha on cartilage proteoglycan metabolism in vitro. Agents and actions. 1989;27(3-4):250-3.

76. Martel-Pelletier J, McCollum R, DiBattista J, Faure MP, Chin JA, Fournier S, Sarfati M, Pelletier JP. The interleukin-1 receptor in normal and osteoarthritic human articular chondrocytes. Identification as the type I receptor and analysis of binding kinetics and biologic function. Arthritis Rheum. 1992;35(5):530-40.

77. Sadouk MB, Pelletier JP, Tardif G, Kiansa K, Cloutier JM, Martel-Pelletier J. Human synovial fibroblasts coexpress IL-1 receptor type I and type II mRNA. The increased level of the IL-1 receptor in osteoarthritic cells is related to an increased level of the type I receptor. Lab Invest. 1995;73(3):347-55.

78. Palmer G, Guerne PA, Mezin F, Maret M, Guicheux J, Goldring MB, Gabay C. Production of interleukin-1 receptor antagonist by human articular chondrocytes. Arthritis Res. 2002;4(3):226-31.

79. Webb GR, Westacott CI, Elson CJ. Chondrocyte tumor necrosis factor receptors and focal loss of cartilage in osteoarthritis. Osteoarthritis Cartilage. 1997;5(6):427-37.

80. Westacott CI, Atkins RM, Dieppe PA, Elson CJ. Tumor necrosis factor-alpha receptor expression on chondrocytes isolated from human articular cartilage. J Rheumatol. 1994;21(9):1710-5.

81. Rigoglou S, Papavassiliou AG. The NF-kappaB signalling pathway in osteoarthritis. The international journal of biochemistry & cell biology. 2013;45(11):2580-4.

82. Mathiessen A, Conaghan PG. Synovitis in osteoarthritis: current understanding with therapeutic implications. Arthritis research & therapy. 2017;19(1):18-.

83. Goldring SR, Goldring MB. Changes in the osteochondral unit during osteoarthritis: structure, function and cartilage-bone crosstalk. Nature reviews Rheumatology. 2016;12(11):632-44.

84. Rosenberg JH, Rai V, Dilisio MF, Agrawal DK. Damage-associated molecular patterns in the pathogenesis of osteoarthritis: potentially novel therapeutic targets. Molecular and cellular biochemistry. 2017;434(1-2):171-9.

85. Goldring MB, Marcu KB. Cartilage homeostasis in health and rheumatic diseases. Arthritis research & therapy. 2009;11(3):224-.

86. Sanchez C, Bay-Jensen AC, Pap T, Dvir-Ginzberg M, Quasnichka H, Barrett-Jolley R, Mobasheri A, Henrotin Y. Chondrocyte secretome: a source of novel insights and exploratory biomarkers of osteoarthritis. Osteoarthritis and cartilage. 2017;25(8):1199-209.

87. de Hooge AS, van de Loo FA, Bennink MB, Arntz OJ, de Hooge P, van den Berg WB. Male IL-6 gene knock out mice developed more advanced osteoarthritis upon aging. Osteoarthritis Cartilage. 2005;13(1):66-73.

88. Goldring MB, Otero M. Inflammation in osteoarthritis. Current opinion in rheumatology. 2011;23(5):471-8.

89. Wang Q, Rozelle AL, Lepus CM, Scanzello CR, Song JJ, Larsen DM, Crish JF, Bebek G, Ritter SY, Lindstrom TM, Hwang I, Wong HH, Punzi L, Encarnacion A, Shamloo M, Goodman SB, Wyss-Coray T, Goldring SR, Banda NK, Thurman JM, Gobezie R, Crow MK, Holers VM, Lee DM, Robinson WH. Identification of a central role for complement in osteoarthritis. Nature medicine. 2011;17(12):1674-9.

90. Loeser RF, Yammani RR, Carlson CS, Chen H, Cole A, Im H-J, Bursch LS, Yan SD. Articular chondrocytes express the receptor for advanced glycation end products: Potential role in osteoarthritis. Arthritis and rheumatism. 2005;52(8):2376-85.

91. Chang SH, Mori D, Kobayashi H, Mori Y, Nakamoto H, Okada K, Taniguchi Y, Sugita S, Yano F, Chung U-I, Kim-Kaneyama J-R, Yanagita M, Economides A, Canalis E, Chen D, Tanaka S, Saito T. Excessive mechanical loading promotes osteoarthritis through the gremlin-1-NF-κB pathway. Nature communications. 2019;10(1):1442-.

92. Xu B, Xing R, Huang Z, Yin S, Li X, Zhang L, Ding L, Wang P. Excessive mechanical stress induces chondrocyte apoptosis through TRPV4 in an anterior cruciate ligament-transected rat osteoarthritis model. Life sciences. 2019;228:158-66.

93. Sun MM-G, Beier F. Chondrocyte hypertrophy in skeletal development, growth, and disease. Birth defects research Part C, Embryo today : reviews. 2014;102(1):74-82.

94. Loeser RF, Collins JA, Diekman BO. Ageing and the pathogenesis of osteoarthritis. Nat Rev Rheumatol. 2016;12(7):412-20.

95. McCulloch K, Litherland GJ, Rai TS. Cellular senescence in osteoarthritis pathology. Aging cell. 2017;16(2):210-8.

96. Philipot D, Guerit D, Platano D, Chuchana P, Olivotto E, Espinoza F, Dorandeu A, Pers YM, Piette J, Borzi RM, Jorgensen C, Noel D, Brondello JM. p16INK4a and its regulator miR-24 link senescence and chondrocyte terminal differentiation-associated matrix remodeling in osteoarthritis. Arthritis Res Ther. 2014;16(1):R58.

97. Martin JA, Buckwalter JA. Telomere erosion and senescence in human articular cartilage chondrocytes. The journals of gerontology Series A, Biological sciences and medical sciences. 2001;56(4):B172-9.

98. Greene MA, Loeser RF. Aging-related inflammation in osteoarthritis. Osteoarthritis Cartilage. 2015;23(11):1966-71.

99. Li G, Yin J, Gao J, Cheng TS, Pavlos NJ, Zhang C, Zheng MH. Subchondral bone in osteoarthritis: insight into risk factors and microstructural changes. Arthritis Research & Therapy. 2013;15(6):223.

100. Sanchez C, Pesesse L, Gabay O, Delcour JP, Msika P, Baudouin C, Henrotin YE. Regulation of subchondral bone osteoblast metabolism by cyclic compression. Arthritis Rheum. 2012;64(4):1193-203.

101. Culemann S, Gruneboom A, Nicolas-Avila JA, Weidner D, Lammle KF, Rothe T, Quintana JA, Kirchner P, Krljanac B, Eberhardt M, Ferrazzi F, Kretzschmar E, Schicht M, Fischer K, Gelse K, Faas M, Pfeifle R, Ackermann JA, Pachowsky M, Renner N, Simon D, Haseloff RF, Ekici AB, Bauerle T,

Blasig IE, Vera J, Voehringer D, Kleyer A, Paulsen F, Schett G, Hidalgo A, Kronke G. Locally renewing resident synovial macrophages provide a protective barrier for the joint. Nature. 2019;572(7771):670-5.

102. Mathiessen A, Conaghan PG. Synovitis in osteoarthritis: current understanding with therapeutic implications. Arthritis Res Ther. 2017;19(1):18.

103. Sellam J, Berenbaum F. The role of synovitis in pathophysiology and clinical symptoms of osteoarthritis. Nat Rev Rheumatol. 2010;6(11):625-35.

104. Scanzello CR, Goldring SR. The role of synovitis in osteoarthritis pathogenesis. Bone. 2012;51(2):249-57.

105. Saklatvala J. Tumour necrosis factor α stimulates resorption and inhibits synthesis of proteoglycan in cartilage. Nature. 1986;322(6079):547-9.

106. Chadjichristos C, Ghayor C, Kypriotou M, Martin G, Renard E, Ala-Kokko L, Suske G, de Crombrugghe B, Pujol J-P, Galéra P. Sp1 and Sp3 Transcription Factors Mediate Interleukin-1β Down-regulation of Human Type II Collagen Gene Expression in Articular Chondrocytes. Journal of Biological Chemistry. 2003;278(41):39762-72.

107. Goldring MB, Fukuo K, Birkhead JR, Dudek E, Sandell LJ. Transcriptional suppression by interleukin-1 and interferon-γ of type II collagen gene expression in human chondrocytes. Journal of cellular biochemistry. 1994;54(1):85-99.

108. Séguin CA, Bernier SM. TNFα suppresses link protein and type II collagen expression in chondrocytes: Role of MEK1/2 and NF-κB signaling pathways. Journal of cellular physiology. 2003;197(3):356-69.

109. Stöve J, Huch K, Günther KP, Scharf HP. Interleukin-1β Induces Different Gene Expression of Stromelysin, Aggrecan and Tumor-Necrosis-Factor-Stimulated Gene 6 in Human Osteoarthritic Chondrocytes in vitro. Pathobiology. 2000;68(3):144-9.

110. Wu H, Du J, Zheng Q. Expression of MMP-1 in cartilage and synovium of experimentally induced rabbit ACLT traumatic osteoarthritis: immunohistochemical study. Rheumatology International. 2008;29(1):31.

111. Fernandes JC, Martel-Pelletier J, Lascau-Coman V, Moldovan F, Jovanovic D, Raynauld JP, Pelletier JP. Collagenase-1 and collagenase-3 synthesis in normal and early experimental osteoarthritic canine cartilage: an immunohistochemical study. J Rheumatol. 1998;25(8):1585-94.

112. Shlopov BV, Lie WR, Mainardi CL, Cole AA, Chubinskaya S, Hasty KA. Osteoarthritic lesions: involvement of three different collagenases. Arthritis Rheum. 1997;40(11):2065-74.

113. Verma P, Dalal K. ADAMTS-4 and ADAMTS-5: key enzymes in osteoarthritis. Journal of cellular biochemistry. 2011;112(12):3507-14.

114. Glasson SS, Askew R, Sheppard B, Carito B, Blanchet T, Ma HL, Flannery CR, Peluso D, Kanki K, Yang Z, Majumdar MK, Morris EA. Deletion of active ADAMTS5 prevents cartilage degradation in a murine model of osteoarthritis. Nature. 2005;434(7033):644-8.

115. Nagase H, Kashiwagi M. Aggrecanases and cartilage matrix degradation. Arthritis Res Ther. 2003;5(2):94-103.

116. Deveza LA, Nelson AE, Loeser RF. Phenotypes of osteoarthritis: current state and future implications. Clin Exp Rheumatol. 2019;37 Suppl 120(5):64-72.

117. McCoy AM. Animal Models of Osteoarthritis: Comparisons and Key Considerations. Veterinary pathology. 2015;52(5):803-18.

118. Bapat S, Hubbard D, Munjal A, Hunter M, Fulzele S. Pros and cons of mouse models for studying osteoarthritis. Clinical and translational medicine. 2018;7(1):36.

119. Thysen S, Luyten FP, Lories RJU. Targets, models and challenges in osteoarthritis research. Disease models & mechanisms. 2015;8(1):17-30.

120. Gregory MH, Capito N, Kuroki K, Stoker AM, Cook JL, Sherman SL. A review of translational animal models for knee osteoarthritis. Arthritis. 2012;2012:764621.

121. Innes JF, Clegg P. Comparative rheumatology: what can be learnt from naturally occurring musculoskeletal disorders in domestic animals? Rheumatology (Oxford). 2010;49(6):1030-9.

122. McIlwraith CW, Frisbie DD, Kawcak CE. The horse as a model of naturally occurring osteoarthritis. Bone & joint research. 2012;1(11):297-309.

123. Veronesi F, Della Bella E, Cepollaro S, Brogini S, Martini L, Fini M. Novel therapeutic targets in osteoarthritis: Narrative review on knock-out genes involved in disease development in mouse animal models. Cytotherapy. 2016;18(5):593-612.

124. Jeong J, Bae K, Kim SG, Kwak D, Moon YJ, Choi CH, Kim YR, Na CS, Kim SJ. Anti-osteoarthritic effects of ChondroT in a rat model of collagenase-induced osteoarthritis. BMC complementary and alternative medicine. 2018;18(1):131.

125. Boudenot A, Presle N, Uzbekov R, Toumi H, Pallu S, Lespessailles E. Effect of interval-training exercise on subchondral bone in a chemically-induced osteoarthritis model. Osteoarthritis Cartilage. 2014;22(8):1176-85.

126. Barrachina L, Remacha AR, Romero A, Vitoria A, Albareda J, Prades M, Roca M, Zaragoza P, Vazquez FJ, Rodellar C. Assessment of effectiveness and safety of repeat administration of proinflammatory primed allogeneic mesenchymal stem cells in an equine model of chemically induced osteoarthritis. BMC Vet Res. 2018;14(1):241.

127. Glasson SS, Blanchet TJ, Morris EA. The surgical destabilization of the medial meniscus (DMM) model of osteoarthritis in the 129/SvEv mouse. Osteoarthritis Cartilage. 2007;15(9):1061-9.

128. Chang JC, Sebastian A, Murugesh DK, Hatsell S, Economides AN, Christiansen BA, Loots GG. Global molecular changes in a tibial compression induced ACL rupture model of post-traumatic osteoarthritis. J Orthop Res. 2017;35(3):474-85.

129. Dias IR, Viegas CA, Carvalho PP. Large Animal Models for Osteochondral Regeneration. Adv Exp Med Biol. 2018;1059:441-501.

130. Teeple E, Jay GD, Elsaid KA, Fleming BC. Animal models of osteoarthritis: challenges of model selection and analysis. Aaps j. 2013;15(2):438-46.

131. Johnson CI, Argyle DJ, Clements DN. In vitro models for the study of osteoarthritis. Veterinary journal (London, England : 1997). 2016;209:40-9.

132. Russell WMS, Burch RL, Hume CW. The principles of humane experimental technique: Methuen London; 1959.

133. Yao Y, Wang Y. ATDC5: an excellent in vitro model cell line for skeletal development. Journal of cellular biochemistry. 2013;114(6):1223-9.

134. Gosset M, Berenbaum F, Thirion S, Jacques C. Primary culture and phenotyping of murine chondrocytes. Nat Protoc. 2008;3(8):1253-60.

135. Baker BM, Chen CS. Deconstructing the third dimension: how 3D culture microenvironments alter cellular cues. Journal of cell science. 2012;125(Pt 13):3015-24.

136. Cope PJ, Ourradi K, Li Y, Sharif M. Models of osteoarthritis: the good, the bad and the promising. Osteoarthritis and cartilage. 2019;27(2):230-9.

137. Alexander PG, Gottardi R, Lin H, Lozito TP, Tuan RS. Three-dimensional osteogenic and chondrogenic systems to model osteochondral physiology and degenerative joint diseases. Experimental biology and medicine (Maywood, NJ). 2014;239(9):1080-95.

138. Hendriks J, Riesle J, van Blitterswijk CA. Co-culture in cartilage tissue engineering. Journal of Tissue Engineering and Regenerative Medicine. 2007;1(3):170-8.

139. Shahin K, Doran PM. Shear and Compression Bioreactor for Cartilage Synthesis. Methods in molecular biology (Clifton, NJ). 2015;1340:221-33.

140. Jorgensen AEM, Kjaer M, Heinemeier KM. The Effect of Aging and Mechanical Loading on the Metabolism of Articular Cartilage. J Rheumatol. 2017;44(4):410-7.

141. Hoff P, Buttgereit F, Burmester G-R, Jakstadt M, Gaber T, Andreas K, Matziolis G, Perka C, Röhner E. Osteoarthritis synovial fluid activates pro-inflammatory cytokines in primary human chondrocytes. International orthopaedics. 2013;37(1):145-51.

142. Bhattacharjee M, Coburn J, Centola M, Murab S, Barbero A, Kaplan DL, Martin I, Ghosh S. Tissue engineering strategies to study cartilage development, degeneration and regeneration. Adv Drug Deliv Rev. 2015;84:107-22.

143. Doran PM. Cartilage Tissue Engineering: What Have We Learned in Practice? Methods in molecular biology (Clifton, NJ). 2015;1340:3-21.

144. Kwon H, Brown WE, Lee CA, Wang D, Paschos N, Hu JC, Athanasiou KA. Surgical and tissue engineering strategies for articular cartilage and meniscus repair. Nature reviews Rheumatology. 2019;15(9):550-70.

145. Rai V, Dilisio MF, Dietz NE, Agrawal DK. Recent strategies in cartilage repair: A systemic review of the scaffold development and tissue engineering. Journal of biomedical materials research Part A. 2017;105(8):2343-54.

146. Shimomura K, Ando W, Fujie H, Hart DA, Yoshikawa H, Nakamura N. Scaffold-free tissue engineering for injured joint surface restoration. Journal of experimental orthopaedics. 2018;5(1):2-.

147. Hall BK, Miyake T. All for one and one for all: condensations and the initiation of skeletal development. BioEssays : news and reviews in molecular, cellular and developmental biology. 2000;22(2):138-47.

148. DuRaine GD, Brown WE, Hu JC, Athanasiou KA. Emergence of scaffold-free approaches for tissue engineering musculoskeletal cartilages. Ann Biomed Eng. 2015;43(3):543-54.

149. Mayer-Wagner S, Schiergens TS, Sievers B, Docheva D, Schieker M, Betz OB, Jansson V, Müller PE. Membrane-based cultures generate scaffold-free neocartilage in vitro: influence of growth factors. Tissue engineering Part A. 2010;16(2):513-21.

150. Anderson DE, Johnstone B. Dynamic Mechanical Compression of Chondrocytes for Tissue Engineering: A Critical Review. Frontiers in bioengineering and biotechnology. 2017;5:76-.

151. Pfeiffenberger M, Bartsch J, Hoff P, Ponomarev I, Barnewitz D, Thöne-Reineke C, Buttgereit F, Gaber T, Lang A. Hypoxia and mesenchymal stromal cells as key drivers of initial fracture healing in an equine in vitro fracture hematoma model. PLOS ONE. 2019;14(4):e0214276.

152. Dominici M, Le Blanc K, Mueller I, Slaper-Cortenbach I, Marini FC, Krause DS, Deans RJ, Keating A, Prockop DJ, Horwitz EM. Minimal criteria for defining multipotent mesenchymal stromal cells. The International Society for Cellular Therapy position statement. Cytotherapy. 2006;8(4):315-7.

153. Ponomarev I. A New Technology in Cartilage Tissue Engineering: Scaffold - Free Cartilage Transplantats (Sfct). Biomed Tech (Berl). 2013;58 Suppl 1.

154. Ponomarev IV, Kochneva LM, Barnewitz D. Effect of 3D chondrocyte culturing conditions on the formation of extracellular matrix in cartilage tissue-engineering constructs. Bulletin of experimental biology and medicine. 2014;156(4):548-55.

155. Kawamoto T, Kawamoto K. Preparation of thin frozen sections from nonfixed and undecalcified hard tissues using Kawamot's film method (2012). Methods Mol Biol. 2014;1130:149-64.

156. Schneider CA, Rasband WS, Eliceiri KW. NIH Image to ImageJ: 25 years of image analysis. Nat Methods. 2012;9(7):671-5.

157. Schindelin J, Arganda-Carreras I, Frise E, Kaynig V, Longair M, Pietzsch T, Preibisch S, Rueden C, Saalfeld S, Schmid B, Tinevez JY, White DJ, Hartenstein V, Eliceiri K, Tomancak P, Cardona A. Fiji: an open-source platform for biological-image analysis. Nat Methods. 2012;9(7):676-82.

158. Vayrynen JP, Vornanen JO, Sajanti S, Bohm JP, Tuomisto A, Makinen MJ. An improved image analysis method for cell counting lends credibility to the prognostic significance of T cells in colorectal cancer. Virchows Arch. 2012;460(5):455-65.

159. Rappsilber J, Ishihama Y, Mann M. Stop and go extraction tips for matrix-assisted laser desorption/ionization, nanoelectrospray, and LC/MS sample pretreatment in proteomics. Analytical chemistry. 2003;75(3):663-70.

160. Tyanova S, Temu T, Cox J. The MaxQuant computational platform for mass spectrometry-based shotgun proteomics. Nat Protoc. 2016;11(12):2301-19.

161. Wiśniewski JR, Hein MY, Cox J, Mann M. A "proteomic ruler" for protein copy number and concentration estimation without spike-in standards. Mol Cell Proteomics. 2014;13(12):3497-506.

162. Müller C, Khabut A, Dudhia J, Reinholt FP, Aspberg A, Heinegård D, Önnerfjord P. Quantitative proteomics at different depths in human articular cartilage reveals unique patterns of protein distribution. Matrix Biology. 2014;40:34-45.

163. Önnerfjord P, Khabut A, Reinholt FP, Svensson O, Heinegård D. Quantitative proteomic analysis of eight cartilaginous tissues reveals characteristic differences as well as similarities between subgroups. The Journal of biological chemistry. 2012;287(23):18913-24.

164. Stüdle C, Occhetta P, Geier F, Mehrkens A, Barbero A, Martin I. Challenges Toward the Identification of Predictive Markers for Human Mesenchymal Stromal Cells Chondrogenic Potential. Stem cells translational medicine. 2019;8(2):194-204.

165. Gerwin N, Bendele AM, Glasson S, Carlson CS. The OARSI histopathology initiative - recommendations for histological assessments of osteoarthritis in the rat. Osteoarthritis Cartilage. 2010;18 Suppl 3:S24-34.

166. Glasson SS, Chambers MG, Van Den Berg WB, Little CB. The OARSI histopathology initiative - recommendations for histological assessments of osteoarthritis in the mouse. Osteoarthritis Cartilage. 2010;18 Suppl 3:S17-23.

167. Kuroda Y, Kitada M, Wakao S, Dezawa M. Bone marrow mesenchymal cells: how do they contribute to tissue repair and are they really stem cells? Arch Immunol Ther Exp (Warsz). 2011;59(5):369-78.

168. Caplan AI. Mesenchymal Stem Cells: Time to Change the Name! Stem cells translational medicine. 2017;6(6):1445-51.

169. Athanasiou KA, Eswaramoorthy R, Hadidi P, Hu JC. Self-organization and the self-assembling process in tissue engineering. Annu Rev Biomed Eng. 2013;15:115-36.

170. Fahy N, Alini M, Stoddart MJ. Mechanical stimulation of mesenchymal stem cells: Implications for cartilage tissue engineering. J Orthop Res. 2018;36(1):52-63.

171. Benjamin M, Ralphs JR. Biology of Fibrocartilage Cells. International Review of Cytology. 233: Academic Press; 2004. p. 1-45.

172. Weber M-C, Fischer L, Damerau A, Ponomarev I, Pfeiffenberger M, Gaber T, Götschel S, Lang J, Röblitz S, Buttgereit F, Ehrig R, Lang A. In vitro and in silico modeling of cellular and matrix-related changes during the early phase of osteoarthritis. bioRxiv. 2019:725317.

173. Ionescu A, Kozhemyakina E, Nicolae C, Kaestner KH, Olsen BR, Lassar AB. FoxA family members are crucial regulators of the hypertrophic chondrocyte differentiation program. Developmental cell. 2012;22(5):927-39.

174. Lian C, Wang X, Qiu X, Wu Z, Gao B, Liu L, Liang G, Zhou H, Yang X, Peng Y, Liang A, Xu C, Huang D, Su P. Collagen type II suppresses articular chondrocyte hypertrophy and osteoarthritis progression by promoting integrin β1−SMAD1 interaction. Bone Research. 2019;7(1):8.

175. Eyre D. Collagen of articular cartilage. Arthritis research. 2002;4(1):30-5.

176. Afif H, Benderdour M, Mfuna-Endam L, Martel-Pelletier J, Pelletier J-P, Duval N, Fahmi H. Peroxisome proliferator-activated receptor gamma1 expression is diminished in human osteoarthritic cartilage and is downregulated by interleukin-1beta in articular chondrocytes. Arthritis research & therapy. 2007;9(2):R31-R.

177. Macrory L, Vaughan-Thomas A, Clegg PD, Innes JF. An exploration of the ability of tepoxalin to ameliorate the degradation of articular cartilage in a canine in vitro model. BMC Vet Res. 2009;5:25.

178. Kaneva MK, Kerrigan MJP, Grieco P, Curley GP, Locke IC, Getting SJ. Chondroprotective and anti-inflammatory role of melanocortin peptides in TNF-α activated human C-20/A4 chondrocytes. British journal of pharmacology. 2012;167(1):67-79.

179. Fukui N, Zhu Y, Maloney WJ, Clohisy J, Sandell LJ. Stimulation of BMP-2 expression by pro-inflammatory cytokines IL-1 and TNF-alpha in normal and osteoarthritic chondrocytes. J Bone Joint Surg Am. 2003;85-A Suppl 3:59-66.

180. Vincent HK, Percival SS, Conrad BP, Seay AN, Montero C, Vincent KR. Hyaluronic Acid (HA) Viscosupplementation on Synovial Fluid Inflammation in Knee Osteoarthritis: A Pilot Study. Open Orthop J. 2013;7:378-84.

181. Choi M-C, Jo J, Park J, Kang HK, Park Y. NF-κB Signaling Pathways in Osteoarthritic Cartilage Destruction. Cells. 2019;8(7):734.

182. Kaneko S, Satoh T, Chiba J, Ju C, Inoue K, Kagawa J. Interleukin-6 and interleukin-8 levels in serum and synovial fluid of patients with osteoarthritis. Cytokines Cell Mol Ther. 2000;6(2):71-9.

183. Zanotti S, Canalis E. Interleukin 6 mediates selected effects of Notch in chondrocytes. Osteoarthritis and cartilage. 2013;21(11):1766-73.

184. Porée B, Kypriotou M, Chadjichristos C, Beauchef G, Renard E, Legendre F, Melin M, Gueret S, Hartmann D-J, Malléin-Gerin F, Pujol J-P, Boumediene K, Galéra P. Interleukin-6 (IL-6) and/or soluble IL-6 receptor down-regulation of human type II collagen gene expression in articular chondrocytes requires a decrease of Sp1.Sp3 ratio and of the binding activity of both factors to the COL2A1 promoter. The Journal of biological chemistry. 2008;283(8):4850-65.

185. Zwerina J, Redlich K, Polzer K, Joosten L, Krönke G, Distler J, Hess A, Pundt N, Pap T, Hoffmann O, Gasser J, Scheinecker C, Smolen JS, van den Berg W, Schett G. TNF-induced structural joint damage is mediated by IL-1. Proceedings of the National Academy of Sciences of the United States of America. 2007;104(28):11742-7.

186. Carballo E, Lai WS, Blackshear PJ. Feedback inhibition of macrophage tumor necrosis factor-alpha production by tristetraprolin. Science (New York, NY). 1998;281(5379):1001-5.

187. Clark A. Post-transcriptional regulation of pro-inflammatory gene expression. Arthritis Research & Therapy. 2000;2(3):172.

188. Troeberg L, Nagase H. Proteases involved in cartilage matrix degradation in osteoarthritis. Biochim Biophys Acta. 2012;1824(1):133-45.

189. Goldring MB, Otero M, Plumb DA, Dragomir C, Favero M, El Hachem K, Hashimoto K, Roach HI, Olivotto E, Borzi RM, Marcu KB. Roles of inflammatory and anabolic cytokines in cartilage metabolism: signals and multiple effectors converge upon MMP-13 regulation in osteoarthritis. Eur Cell Mater. 2011;21:202-20.

190. Bau B, Gebhard PM, Haag J, Knorr T, Bartnik E, Aigner T. Relative messenger RNA expression profiling of collagenases and aggrecanases in human articular chondrocytes in vivo and in vitro. Arthritis and rheumatism. 2002;46(10):2648-57.

191. Swingler TE, Waters JG, Davidson RK, Pennington CJ, Puente XS, Darrah C, Cooper A, Donell ST, Guile GR, Wang W, Clark IM. Degradome expression profiling in human articular cartilage. Arthritis research & therapy. 2009;11(3):R96-R.

192. Cortial D, Gouttenoire J, Rousseau CF, Ronzière MC, Piccardi N, Msika P, Herbage D, Mallein-Gerin F, Freyria AM. Activation by IL-1 of bovine articular chondrocytes in culture within a 3D collagen-based scaffold. An in vitro model to address the effect of compounds with therapeutic potential in osteoarthritis. Osteoarthritis and Cartilage. 2006;14(7):631-40.

193. Liacini A, Sylvester J, Li WQ, Huang W, Dehnade F, Ahmad M, Zafarullah M. Induction of matrix metalloproteinase-13 gene expression by TNF-alpha is mediated by MAP kinases, AP-1, and NF-kappaB transcription factors in articular chondrocytes. Experimental cell research. 2003;288(1):208-17.

194. Benam KH, Dauth S, Hassell B, Herland A, Jain A, Jang K-J, Karalis K, Kim HJ, MacQueen L, Mahmoodian R, Musah S, Torisawa Y-s, van der Meer AD, Villenave R, Yadid M, Parker KK, Ingber DE. Engineered in vitro disease models. Annu Rev Pathol. 2015;10:195-262.

195. Li M, Izpisua Belmonte JC. Organoids - Preclinical Models of Human Disease. N Engl J Med. 2019;380(6):569-79.

196. Makris EA, Gomoll AH, Malizos KN, Hu JC, Athanasiou KA. Repair and tissue engineering techniques for articular cartilage. Nature reviews Rheumatology. 2015;11(1):21-34.

197. Bhattacharjee M, Coburn J, Centola M, Murab S, Barbero A, Kaplan DL, Martin I, Ghosh S. Tissue engineering strategies to study cartilage development, degeneration and regeneration. Advanced drug delivery reviews. 2015;84:107-22.

198. Armiento AR, Stoddart MJ, Alini M, Eglin D. Biomaterials for articular cartilage tissue engineering: Learning from biology. Acta Biomater. 2018;65:1-20.

199. Bhumiratana S, Eton RE, Oungoulian SR, Wan LQ, Ateshian GA, Vunjak-Novakovic G. Large, stratified, and mechanically functional human cartilage grown in vitro by mesenchymal condensation. Proc Natl Acad Sci U S A. 2014;111(19):6940-5.

200. Park IS, Jin RL, Oh HJ, Truong MD, Choi BH, Park SH, Park DY, Min BH. Sizable Scaffold-Free Tissue-Engineered Articular Cartilage Construct for Cartilage Defect Repair. Artif Organs. 2018.

201. Yasui Y, Chijimatsu R, Hart DA, Koizumi K, Sugita N, Shimomura K, Myoui A, Yoshikawa H, Nakamura N. Preparation of Scaffold-Free Tissue-Engineered Constructs Derived from Human Synovial Mesenchymal Stem Cells Under Low Oxygen Tension Enhances Their Chondrogenic Differentiation Capacity. Tissue engineering Part A. 2016;22(5-6):490-500.

202. Yasui Y, Ando W, Shimomura K, Koizumi K, Ryota C, Hamamoto S, Kobayashi M, Yoshikawa H, Nakamura N. Scaffold-free, stem cell-based cartilage repair. Journal of clinical orthopaedics and trauma. 2016;7(3):157-63.

203. Mabvuure N, Hindocha S, Khan WS. The role of bioreactors in cartilage tissue engineering. Current stem cell research & therapy. 2012;7(4):287-92.

STATUTORY DECLARATION

“I, Marie-Christin Weber, by personally signing this document in lieu of an oath, hereby affirm that I prepared the submitted dissertation on the topic “Establishment and evaluation of a human three-dimensional *in vitro* model for the study of osteoarthritis“ / “Etablierung und Evaluation eines humanen dreidimensionalen *in vitro* Arthrose-Modells“, independently and without the support of third parties, and that I used no other sources and aids than those stated.

All parts which are based on the publications or presentations of other authors, either in letter or in spirit, are specified as such in accordance with the citing guidelines. The sections on methodology (in particular regarding practical work, laboratory regulations, statistical processing) and results (in particular regarding figures, charts and tables) are exclusively my responsibility.

Furthermore, I declare that I have correctly marked all of the data, the analyses, and the conclusions generated from data obtained in collaboration with other persons, and that I have correctly marked my own contribution and the contributions of other persons (cf. declaration of contribution). I have correctly marked all texts or parts of texts that were generated in collaboration with other persons.

My contributions to any publications to this dissertation correspond to those stated in the below joint declaration made together with the supervisor. All publications created within the scope of the dissertation comply with the guidelines of the ICMJE (International Committee of Medical Journal Editors; www.icmje.org) on authorship. In addition, I declare that I shall comply with the regulations of Charité – Universitätsmedizin Berlin on ensuring good scientific practice.

I declare that I have not yet submitted this dissertation in identical or similar form to another Faculty.

The significance of this statutory declaration and the consequences of a false statutory declaration under criminal law (Sections 156, 161 of the German Criminal Code) are known to me.”

Date Signature

DECLARATION OF CONTRIBUTION

Marie-Christin Weber contributed to the following publications:

***(1) Weber MC**, Fischer L, Damerau A, Ponomarev I, Pfeiffenberger M, Gaber T, Gotschel S, Lang J, Roblitz S, Buttgereit F, Ehrig R, Lang A. Macroscale mesenchymal condensation to study cytokine-driven cellular and matrix-related changes during cartilage degradation. Biofabrication. 2020;12(4):045016.*
***(2) Weber MC**, Fischer L, Damerau A, Ponomarev I, Pfeiffenberger M, Gaber T, Götschel S, Lang J, Röblitz S, Buttgereit F, Ehrig R, Lang A. In vitro and in silico modeling of cellular and matrix-related changes during the early phase of osteoarthritis. bioRxiv. 2019:725317. (Preprint)*

Marie-Christin Weber

- performed experiments and data analysis, and created the tables and figures for **(1)** Table 1, 2, A1 and Figure 2, 3, A1-4 and **(2)** Table 1-3 and Figure 2-4.
- processed and provided the data for the mathematical *in silico* modelling.
- interpreted the results and created the manuscripts in cooperation with Lisa Fischer (*in silico* model) and Dr. Annemarie Lang.

The hMSC culture was performed by Marie-Christin Weber in cooperation with Alexandra Damerau und Moritz Pfeiffenberger. The characterization of hMSCs was performed by Moritz Pfeiffenberger. The SFCCs were produced by Igor Ponomarev at the Research Center of Medical Technology and Biotechnology in Bad Langensalza as described in the methods chapter of this monography.
Analysis of RNA integrity using the BioAnalyzer was performed by the service facility at the German Rheumatism Research Centre Berlin.

Signature, date and stamp of first supervising university professor / lecturer

Signature of doctoral candidate

CURRICULUM VITAE

Mein Lebenslauf wird aus datenschutzrechtlichen Gründen in der elektronischen Version meiner Arbeit nicht veröffentlicht.

Mein Lebenslauf wird aus datenschutzrechtlichen Gründen in der elektronischen Version meiner Arbeit nicht veröffentlicht.

PUBLICATIONS

1. PEER-REVIEWED ARTICLES

- **Weber MC**, Fischer L, Damerau A, Ponomarev I, Pfeiffenberger M, Gaber T, Gotschel S, Lang J, Roblitz S, Buttgereit F, Ehrig R, Lang A. Macroscale mesenchymal condensation to study cytokine-driven cellular and matrix-related changes during cartilage degradation. Biofabrication. 2020;12(4):045016.

- Gasparini SJ, Swarbrick MM, Kim S, Thai LJ, Henneicke H, Cavanagh LL, Tu J, **Weber MC**, et al. *Androgens sensitise mice to glucocorticoid-induced insulin resistance and fat accumulation*. Diabetologia. 2019.

- Ohrndorf S, **Weber MC**, Hermann S, Aupperle K, Follendorf B, Krahl D, Kücük A, Schmittat G, et al. *Patient Reported Outcomes (PROs) im rheumatologischen Praxisalltag – App hat sich bewährt.* Akt Rheumatol. 2019;44(01):52-6.

- Lang A, Kirchner M, Stefanowski J, Durst M, **Weber MC**, Pfeiffenberger M, Damerau A, Hauser AE, et al. *Collagen I-based scaffolds negatively impact fracture healing in a mouse-osteotomy-model although used routinely in research and clinical application.* Acta Biomater. 2019;86:171-84.

- Gasparini SJ, **Weber MC**, Henneicke H, Kim S, Zhou H, Seibel MJ. *Continuous corticosterone delivery via the drinking water or pellet implantation: A comparative study in mice.* Steroids. 2016;116:76-82.

2. PRE-PRINT ARTICLES

- **Weber MC**, Fischer L, Damerau A, Ponomarev I, Pfeiffenberger M, Gaber T, et al. In vitro and in silico modeling of cellular and matrix-related changes during the early phase of osteoarthritis. bioRxiv. 2019:725317

3. CONFERENCE ABSTRACTS

- **Weber MC**, Ponomarev I, Gaber T, Buttgereit F, Lang A. *Simulating osteoarthritis in vitro with human scaffold-free 3D cartilage transplants.* Osteoarthritis and Cartilage. 2018;26:S103.

ACKNOWLEDGEMENTS

I would like to thank my supervisor Professor Frank Buttgereit for his guidance and support throughout the preparation of this thesis and my time in his research group. I especially wish to express my gratitude to Dr. Annemarie Lang for her constant support in the lab, for teaching me the methods used in my research and for her constant feedback on my abstracts, posters and finally this thesis. A special thanks is also dedicated to the Buttgereit Lab, especially to Dr. Timo Gabor for his critical advise throughout this project, to Alexandra Damerau and Moritz Pfeiffenberger for the great collaboration and the support in the lab and to all other members of our research group, particularly to Manuela Jakstadt, Dr. Cindy Strehl, Pierre-Louis Krauß and Yuling Chen.

I would like to express my thanks to Igor Ponomarev for the fabrication of the SFCCs and to Dr. Marieluise Kirchner for performing the protein extraction and mass spectrometry.

Thank you also to the mathematical team from the Zuse Institute Berlin, especially to Dr. Rainald Ehrig and Lisa Fischer for the great collaboration.

I would like to express my deepest gratitude to my family and friends and especially to Simon for their support, patience, and encouragement.